UNIVERSITY OF BIRMINGHAM
University of Birmingham Research at Birmingham

Measurement of jet activity in top quark events using the $eμ$ final state with two b-tagged jets in pp collisions at $\sqrt{s}=8$ TeV with the ATLAS detector

ATLAS Collaboration

DOI:
10.1007/JHEP09(2016)074

License:
Creative Commons: Attribution (CC BY)

Document Version
Peer reviewed version

Citation for published version (Harvard):
ATLAS Collaboration 2016, 'Measurement of jet activity in top quark events using the $eμ$ final state with two b-tagged jets in pp collisions at $\sqrt{s}=8$ TeV with the ATLAS detector', *Journal of High Energy Physics*, vol. 2016, pp. 74. https://doi.org/10.1007/JHEP09(2016)074

Link to publication on Research at Birmingham portal

Publisher Rights Statement:
Eligibility for repository: Checked on 2/2/2017

General rights
Unless a licence is specified above, all rights (including copyright and moral rights) in this document are retained by the authors and/or the copyright holders. The express permission of the copyright holder must be obtained for any use of this material other than for purposes permitted by law.

•Users may freely distribute the URL that is used to identify this publication.
•Users may download and/or print one copy of the publication from the University of Birmingham research portal for the purpose of private study or non-commercial research.
•User may use extracts from the document in line with the concept of ‘fair dealing’ under the Copyright, Designs and Patents Act 1988 (?)
•Users may not further distribute the material nor use it for the purposes of commercial gain.

Where a licence is displayed above, please note the terms and conditions of the licence govern your use of this document.

When citing, please reference the published version.

Take down policy
While the University of Birmingham exercises care and attention in making items available there are rare occasions when an item has been uploaded in error or has been deemed to be commercially or otherwise sensitive.

If you believe that this is the case for this document, please contact UBIRA@lists.bham.ac.uk providing details and we will remove access to the work immediately and investigate.

Download date: 29. Mar. 2024

EUROPEAN ORGANISATION FOR NUCLEAR RESEARCH (CERN)

Submitted to: JHEP

CERN-EP-2016-122
1st July 2016

arXiv:1606.09490v1 [hep-ex] 30 Jun 2016

Measurement of jet activity in top quark events using the $e\mu$ final state with two b-tagged jets in pp collisions at $\sqrt{s} = 8$ TeV with the ATLAS detector

The ATLAS Collaboration

Abstract

Measurements of the jet activity in $t\bar{t}$ events produced in proton–proton collisions at $\sqrt{s} = 8$ TeV are presented, using 20.3 fb^{-1} of data collected by the ATLAS experiment at the Large Hadron Collider. The events were selected in the dilepton $e\mu$ decay channel with two identified b-jets. The numbers of additional jets for various jet transverse momentum (p_{T}) thresholds, and the normalised differential cross-sections as a function of p_{T} for the five highest-p_{T} additional jets, were measured in the jet pseudorapidity range $|\eta| < 4.5$. The gap fraction, the fraction of events which do not contain an additional jet in a central rapidity region, was measured for several rapidity intervals as a function of the minimum p_{T} of a single jet or the scalar sum of p_{T} of all additional jets. These fractions were also measured in different intervals of the invariant mass of the $e\mu b\bar{b}$ system. All measurements were corrected for detector effects, and found to be mostly well-described by predictions from next-to-leading-order and leading-order $t\bar{t}$ event generators with appropriate parameter choices. The results can be used to further optimise the parameters used in such generators.

© 2016 CERN for the benefit of the ATLAS Collaboration.
Reproduction of this article or parts of it is allowed as specified in the CC-BY-4.0 license.

1 Introduction

The top quark plays a special role in the Standard Model and in some theories of physics beyond the Standard Model. The large top quark mass and large $t\bar{t}$ pair-production cross-section in pp collisions (242 ± 10 pb at $\sqrt{s} = 8$ TeV [1]) make top quark production at the Large Hadron Collider (LHC) a unique laboratory for studying the behaviour of QCD at the highest accessible energy scales. The decays of top quarks to charged leptons, neutrinos and b-quarks also make such events a primary source of background in many searches for new physics. Therefore, the development of accurate modelling for events involving top quark production forms an important part of the LHC physics programme. Measurements of the activity of *additional jets* in $t\bar{t}$ events, *i.e.* jets not originating from the decay of the top quark and antiquark, but arising from quark and gluon radiation produced in association with the $t\bar{t}$ system, have been made by ATLAS [2, 3] and CMS [4] using pp data at $\sqrt{s} = 7$ TeV, and by CMS [5] at $\sqrt{s} = 8$ TeV. These data are typically presented as particle-level results in well-defined fiducial regions, corrected to remove detector efficiency and resolution effects, and compared to the predictions of Monte Carlo (MC) generators through tools such as the Rivet framework [6]. Such comparisons indicate that some state-of-the-art generators have difficulties in reproducing the data, whilst for others agreement with data can be improved with an appropriate choice of generator parameter values or 'tune', including those controlling QCD factorisation and renormalisation scales, and matching to the parton shower [7–11].

This paper presents two studies of the additional jet activity in $t\bar{t}$ events collected with the ATLAS detector in pp collisions at a centre-of-mass energy of $\sqrt{s} = 8$ TeV. Top quark pairs are selected in the same way in both measurements, using the dilepton $e\mu$ final state with two jets identified ('tagged') as likely to contain b-hadrons. Distributions of the properties of additional jets in these events are normalised to the cross-section ($\sigma_{e\mu b\bar{b}}$) for events passing this initial selection, requiring the electron, muon and two b-tagged jets to have transverse momentum $p_{\mathrm{T}} > 25$ GeV and pseudorapidity[1] $|\eta| < 2.5$.

In the first study, the normalised particle-level cross-sections for additional jets with $|\eta| < 4.5$ and $p_{\mathrm{T}} > 25$ GeV are measured differentially in jet rank and p_{T};

$$\frac{1}{\sigma}\frac{\mathrm{d}\sigma_i}{\mathrm{d}p_{\mathrm{T}}} \equiv \frac{1}{\sigma_{e\mu b\bar{b}}}\frac{\mathrm{d}\sigma_{\mathrm{jet},i}}{\mathrm{d}p_{\mathrm{T}}}\,, \tag{1}$$

with rank $i = 1$ to 5, where $i = 1$ denotes the leading (highest p_{T}) additional jet. These normalised differential cross-sections are then used to obtain the multiplicity distributions for additional jets as a function of the minimum p_{T} threshold for such extra jets.

The additional-jet differential cross-section measurements are complemented by a second study measuring the jet 'gap fraction', *i.e.* the fraction of events where no additional jet is present in a given detector rapidity region Δy. The gap fraction is measured as a function of the jet p_{T} threshold, Q_0;

$$f(Q_0) \equiv \frac{\sigma(Q_0)}{\sigma_{e\mu b\bar{b}}}\,, \tag{2}$$

starting from a minimum Q_0 of 25 GeV, where $\sigma(Q_0)$ is the cross-section for events having no additional jets with $p_{\mathrm{T}} > Q_0$, within the rapidity interval Δy. The gap fraction is also measured as a function of

[1] ATLAS uses a right-handed coordinate system with its origin at the nominal interaction point in the centre of the detector, and the z axis along the beam line. Pseudorapidity is defined in terms of the polar angle θ as $\eta = -\ln\tan\theta/2$, and transverse momentum and energy are defined relative to the beamline as $p_{\mathrm{T}} = p\sin\theta$ and $E_{\mathrm{T}} = E\sin\theta$. The azimuthal angle around the beam line is denoted by ϕ, and distances in (η, ϕ) space by $\Delta R = \sqrt{(\Delta\eta)^2 + (\Delta\phi)^2}$. The rapidity is defined as $y = \frac{1}{2}\ln\left(\frac{E+p_z}{E-p_z}\right)$, where p_z is the z-component of the momentum and E is the energy of the relevant object.

a threshold Q_{sum} placed on the scalar sum of the p_{T} of all additional jets with $p_{\text{T}} > 25\,\text{GeV}$ within the rapidity interval Δy:

$$f(Q_{\text{sum}}) \equiv \frac{\sigma(Q_{\text{sum}})}{\sigma_{e\mu b\bar{b}}} \,. \tag{3}$$

The gap fraction measured as a function of Q_0 is sensitive to the leading p_{T} emission accompanying the $t\bar{t}$ system, whereas the gap fraction based on Q_{sum} is sensitive to all accompanying hard emissions. To facilitate comparisons with the corresponding measurement at $\sqrt{s} = 7\,\text{TeV}$ [2], $f(Q_0)$ and $f(Q_{\text{sum}})$ are determined using the same jet fiducial requirements, namely $|y| < 2.1$ and $p_{\text{T}} > 25$ GeV, in contrast to the normalised jet cross-sections, which are measured over the wider angular range $|\eta| < 4.5$. The gap fraction is measured for multiple values of Q_0 and Q_{sum} and for four jet rapidity intervals Δy. In addition, the gap fraction is measured in four intervals of the invariant mass of the $e\mu b\bar{b}$ system $m_{e\mu b\bar{b}}$, which is related to the invariant mass of the produced $t\bar{t}$ system and is on average higher if produced from quark–antiquark rather than gluon–gluon initial states.

This paper is organised as follows. Section 2 describes the ATLAS detector and the data sample used for these measurements. Section 3 provides information about the Monte Carlo simulated samples used to model signal and background processes, and to compare with the measured results. The common object and event selection criteria are presented in Section 4, and sources of systematic uncertainty are discussed in Section 5. The measurement of the normalised jet differential cross-sections by rank and p_{T} is described in Section 6 and the measurement of the gap fraction is presented in Section 7, in both cases including comparisons with the predictions of various $t\bar{t}$ event generators. Section 8 gives a summary and conclusions.

2 Detector and data sample

The ATLAS detector [12] at the LHC covers almost the full solid angle around the collision point, and consists of an inner tracking detector surrounded by a thin superconducting solenoid magnet producing a 2 T axial magnetic field, electromagnetic and hadronic calorimeters, and an external muon spectrometer incorporating three large toroidal magnet systems. The inner detector consists of a high-granularity silicon pixel detector and a silicon microstrip tracker, together providing precision tracking in the pseudorapidity range $|\eta| < 2.5$, complemented by a transition radiation tracker providing tracking and electron identification information for $|\eta| < 2.0$. A lead/liquid-argon (LAr) electromagnetic calorimeter covers the region $|\eta| < 3.2$, and hadronic calorimetry is provided by steel/scintillator tile calorimeters for $|\eta| < 1.7$ and copper/LAr hadronic endcap calorimeters covering $1.5 < |\eta| < 3.2$. The calorimeter system is completed by forward LAr calorimeters with copper and tungsten absorbers which extend the coverage to $|\eta| = 4.9$. The muon spectrometer consists of precision tracking chambers covering the region $|\eta| < 2.7$, and separate trigger chambers covering $|\eta| < 2.4$. A three-level trigger system, using custom hardware followed by two software-based levels, is used to reduce the event rate to about 400 Hz for offline storage.

The analyses were performed on the 2012 ATLAS proton–proton collision data sample, corresponding to an integrated luminosity of $20.3\,\text{fb}^{-1}$ at $\sqrt{s} = 8\,\text{TeV}$ after the application of detector status and data quality requirements. The integrated luminosity was measured using the methodology described in Ref. [13] applied to beam separation scans performed in November 2012, and has a relative uncertainty of 2.8 %. Events were required to pass either a single-electron or single-muon trigger, with thresholds chosen such that the efficiency plateau is reached for leptons with $p_{\text{T}} > 25\,\text{GeV}$ passing offline selections. Each

triggered event also includes the signals from an average of 20 additional inelastic pp collisions in the same bunch crossing (referred to as pile-up).

3 Simulated event samples

Monte Carlo simulated event samples were used to evaluate signal efficiencies and backgrounds, and to estimate and correct for resolution effects. The samples were processed either through the full ATLAS detector simulation [14] based on GEANT4 [15], or through a faster simulation making use of parameterised showers in the calorimeters [16]. Additional simulated inelastic pp collisions, generated with Pythia8.1 [17] using the MSTW2008 LO [18] parton distribution functions (PDFs) and the A2 tune [19], were overlaid to simulate the effects of both in- and out-of-time pile-up, from additional activity in the same and nearby bunch crossings. The resulting simulated events were processed using the same reconstruction algorithms and analysis chains as the data. The effects of pile-up were also studied with data recorded from randomly selected bunch crossings (zero-bias data) as discussed in Section 5.

The baseline $t\bar{t}$ full simulation sample was produced using the next-to-leading-order (NLO) QCD matrix-element generator Powheg-Box v1.0 [20–22] using the CT10 PDFs [23] and interfaced to Pythia6 (version 6.426) [24] with the CTEQ6L1 PDF set [25] and the Perugia 2011C (P2011C) tune [26] for the parton shower, fragmentation and underlying event modelling. The renormalisation and factorisation scales were set to the generator default value of $\sqrt{m_t^2 + p_{\mathrm{T}}^2}$, the sum in quadrature of the top quark mass m_t and transverse momentum p_{T}, the latter evaluated for the underlying Born configuration before radiation. The Powheg parameter h_{damp}, used in the damping function that limits the resummation of higher-order effects incorporated into the Sudakov form factor, was set to infinity, corresponding to no damping. The top quark mass was set to 172.5 GeV. The total $t\bar{t}$ production cross-section, used when comparing predictions from simulation with data, was taken to be 253^{+13}_{-15} pb, based on the next-to-next-to-leading-order (NNLO) calculation including the resummation of next-to-next-to-leading logarithmic soft gluon terms as described in Refs. [27–31] and implemented in the Top++ 2.0 program [32]. The quoted uncertainties include PDF and α_{s} uncertainties based on the PDF4LHC prescription [33] applied to the MSTW2008 NNLO [18, 34], CT10 NNLO [23, 35] and NNPDF2.3 5f FFN [36] PDF sets, added in quadrature to the QCD scale uncertainty.

Alternative $t\bar{t}$ simulation samples were used to evaluate systematic uncertainties, and were compared with the data measurements after unfolding for detector effects. Samples were produced with Powheg with $h_{\mathrm{damp}} = \infty$ interfaced to Herwig (version 6.520) [37, 38] with the ATLAS AUET2 tune [39] and Jimmy (version 4.31) [40] for underlying-event modelling. Samples with $h_{\mathrm{damp}} = m_t$, which softens the $t\bar{t}$ p_{T} spectrum, improving the agreement between data and simulation at $\sqrt{s} = 7$ TeV [7], were generated by combining Powheg with either Pythia6 with the P2011C tune or Pythia8 (version 8.186) with the A14 tune [41]. Samples were also produced with MC@NLO (version 4.01) [42, 43] interfaced to Herwig and Jimmy, with the generator's default renormalisation and factorisation scales of $\sqrt{m_t^2 + (p_{\mathrm{T},t}^2 + p_{\mathrm{T},\bar{t}}^2)/2}$ where $p_{\mathrm{T},t}$ and $p_{\mathrm{T},\bar{t}}$ are the transverse momenta of the top quark and antiquark. Several leading-order 'multi-leg' generators were also studied. The Alpgen generator (version 2.13) [44] was used with leading-order matrix elements for $t\bar{t}$ production accompanied by up to three additional light partons, and dedicated matrix elements for $t\bar{t}$ plus $b\bar{b}$ or $c\bar{c}$ production, interfaced to Herwig and Jimmy. An alternative sample was generated with Alpgen interfaced to Pythia6 with the P2011C tune, including up to four additional

light partons. The MLM parton–jet matching scheme [44] was applied to avoid double-counting of configurations generated by both the parton shower and the matrix-element calculation. A further sample was generated using MadGraph (version 2.1.1) [45] with up to three additional partons and using MLM matching, interfaced to Pythia6 with the P2011C tune. Finally, three pairs of samples with matching scale and parton shower parameters tuned to explicitly vary the amount of additional radiation in $t\bar{t}$ events were used, generated using AcerMC (version 3.8) [46], Alpgen or MadGraph, each interfaced to Pythia6 with either the RadLo or RadHi P2011C tunes [26]. The parameters of these samples were tuned to span the variations in radiation compatible with the ATLAS $t\bar{t}$ gap fraction measurements at $\sqrt{s} = 7$ TeV [2] as discussed in detail in Ref. [7].

After the $e\mu b\bar{b}$ event selection, the expected non-$t\bar{t}$ contribution is dominated by Wt, the associated production of a W boson and a single top quark. This process is distinct from $t\bar{t}$ production when considered at leading order. But at NLO in QCD the two processes cannot be separated once the top quarks decay to Wb: the resulting $WbW\bar{b}$ final state can appear for example through both $gg \to t\bar{t} \to WbW\bar{b}$ and $gg \to Wt\bar{b} \to WbW\bar{b}$, and the two processes interfere to an extent depending on the kinematics of the final state. However, the currently available generators do not allow a full treatment of this interference; instead they consider $t\bar{t}$ and Wt production as separate processes. Within this approximation, the 'diagram removal' and 'diagram subtraction' schemes have been proposed as alternatives for approximately handling the interference between the $t\bar{t}$ and Wt processes [47, 48]. For this paper, Wt production was simulated as a process separate from $t\bar{t}$, using Powheg + Pythia6 with the CT10 PDFs and the P2011C tune. The diagram removal scheme was used as the baseline and the diagram subtraction scheme was used to assess systematic uncertainties. A cross-section of 22.4 ± 1.5 pb was assumed for Wt production, determined by using the approximate NNLO prediction described in Ref. [49].

Other backgrounds with two prompt leptons arise from diboson production (WW, WZ and ZZ) accompanied by b-tagged jets, modelled using Alpgen + Herwig + Jimmy with CTEQ6L1 PDFs and with total cross-sections calculated using MCFM [50]; and $Z \to \tau\tau(\to e\mu)$+jets, modelled using Alpgen + Pythia6 with CTEQ6L1 PDFs, and including leading-order matrix elements for $Zb\bar{b}$ production. The normalisation of this background was determined from data using $Z \to ee/\mu\mu$ events with two b-tagged jets as described in Ref. [1]. The remaining background originates from events with one prompt and one misidentified lepton, *e.g.* a non-prompt lepton from the decay of a bottom or charm hadron, an electron from a photon conversion, hadronic jet activity misidentified as an electron, or a muon produced from an in-flight decay of a pion or kaon. Such events can arise from $t\bar{t}$ production with one hadronically decaying W, modelled as for dileptonic $t\bar{t}$ production with Powheg + Pythia6; W+jets production, modelled as for Z+jets; and t-channel single-top production, modelled using AcerMC + Pythia6 with CTEQ6L1 PDFs. Previous studies have shown that these simulation samples provide a good model of the rate and kinematic distributions of $e\mu b\bar{b}$ events with one real and one misidentified lepton [1]. The expected contributions to the additional-jet distributions from $t\bar{t}$ production in association with a W, Z or Higgs boson are below the percent level. Other backgrounds, including processes with two misidentified leptons, are negligible.

4 Object and event selection

The two analyses use the same object and event selection as employed in the ATLAS inclusive $t\bar{t}$ cross-section analysis at $\sqrt{s} = 8$ TeV [1]. Electrons were identified as described in Ref. [51], required to have transverse energy $E_{\mathrm{T}} > 25$ GeV and pseudorapidity $|\eta| < 2.47$, and to be isolated to reduce backgrounds from non-prompt and misidentified electrons. Electron candidates within the transition region between

the barrel and endcap electromagnetic calorimeters, $1.37 < |\eta| < 1.52$, were removed. Muons were identified as described in Ref. [52], required to have $p_{\mathrm{T}} > 25\,\mathrm{GeV}$ and $|\eta| < 2.5$, and also required to be isolated.

Jets were reconstructed using the anti-k_t algorithm [53, 54] with radius parameter $R = 0.4$, starting from clusters of energy deposits in the calorimeters, calibrated using the local cluster weighting method [55]. Jets were calibrated using an energy- and η-dependent simulation-based scheme, with the effects of pile-up on the jet energy measurement being reduced using the jet-area method described in Ref. [56]. After the application of in situ corrections based on data [57], jets were required to satisfy $p_{\mathrm{T}} > 25\,\mathrm{GeV}$ and $|\eta| < 4.5$. To suppress the contribution from low-p_{T} jets originating from pile-up interactions, a jet vertex fraction (JVF) requirement was applied to jets with $p_{\mathrm{T}} < 50\,\mathrm{GeV}$ and $|\eta| < 2.4$ [58]. Such jets were required to have at least 50 % of the scalar sum of the p_{T} of tracks associated with the jet originating from tracks associated with the event primary vertex, the latter being defined as the reconstructed vertex with the highest sum of associated track p_{T}^2. Jets with no associated tracks were also selected. To prevent double-counting of electron energy deposits as jets, jets within $\Delta R = 0.2$ of a reconstructed electron were removed. Finally, to further suppress non-isolated leptons from heavy-flavour decays inside jets, electrons and muons within $\Delta R = 0.4$ of selected jets were also discarded.

Jets containing b-hadrons were tagged using the MV1 algorithm, a multivariate discriminant making use of track impact parameters and reconstructed secondary vertices [59]. Jets were defined to be b-tagged if the MV1 discriminant value was larger than a threshold corresponding to a 70 % efficiency for tagging b-quark jets in $t\bar{t}$ events, giving a rejection factor of about 140 against light-quark and gluon jets, and about five against jets originating from charm quarks.

Events were required to have a reconstructed primary vertex with at least five associated tracks. Events with any jets failing jet quality and timing requirements [57], or with any muons compatible with cosmic-ray interactions or suffering substantial energy loss through bremsstrahlung in the detector material, were removed. An event preselection was then applied, requiring exactly one electron and one muon selected as described above, with opposite-sign electric charges. At least one of the leptons was required to be matched to an electron or muon object triggering the event. Finally, selected events were required to have at least two b-tagged jets. The resulting $e\mu b\bar{b}$ event selection is similar to that of the $\sqrt{s} = 8\,\mathrm{TeV}$ sample with two b-tagged jets used in Ref. [1], except that events with three or more b-tagged jets are also accepted.[2] The numbers of preselected opposite-sign $e\mu$ and selected $e\mu b\bar{b}$ events are shown in Table 1. The observed event count after requiring at least two b-tagged jets is in good agreement with the prediction from the baseline simulation.

Additional jets were defined as those other than the two b-tagged jets used to select the event. For the jet normalised differential cross-section measurements, in the 3 % of selected events with three or more b-tagged jets, the jets with the two highest MV1 b-tagging weight values were taken to be the b-jets from the top quark decays, and any other b-tagged jets were considered as additional jets, along with all untagged jets. Distributions of the number of additional jets are shown for various jet p_{T} thresholds in Figure 1. The p_{T} distributions for reconstructed additional jets are shown in Figure 2, with the estimated contribution from 'unmatched jets' (defined in Section 4.2 below) shown separately. In both cases, the data are shown compared to the predictions from simulation with the baseline Powheg + Pythia6 ($h_{\mathrm{damp}} = \infty$) $t\bar{t}$ sample plus backgrounds, and the predictions from alternative $t\bar{t}$ simulation samples generated with Powheg + Pythia6 and Powheg + Pythia8 with $h_{\mathrm{damp}} = m_t$, Powheg + Herwig with $h_{\mathrm{damp}} = \infty$

[2] The event counts differ from those in Ref. [1] as updated object calibrations were used in this analysis, in particular for the jet energy scale.

	$e\mu$	[%]	≥ 2 b-jets	[%]
Data	70854		12437	
Total simulation	66200	100.0	12400	100.0
$t\bar{t}$	40300	60.8	11900	96.3
Wt single top	3840	5.8	360	2.9
$Z(\rightarrow \tau\tau \rightarrow e\mu)$+jets	12800	19.4	6	0.1
Dibosons	8030	12.3	2	0.0
Misidentified leptons	1200	1.8	96	0.8

Table 1: Selected numbers of events with an opposite-sign $e\mu$ pair, and with an opposite-sign $e\mu$ pair and at least two b-tagged jets in data, compared with the predictions from the baseline simulation, broken down into contributions from $t\bar{t}$, Wt and minor background processes. The predictions are normalised to the same integrated luminosity as the data.

and MC@NLO + Herwig. The jet multiplicity distributions and p_{T} spectra in the simulation samples are generally in reasonable agreement with those from data, except for MC@NLO + Herwig, which underestimates the number of events with three or more extra jets, and also predicts significantly softer jet p_{T} spectra.

The gap fraction measurements use the same basic $e\mu b\bar{b}$ event selection, but restricting the additional jets to the central rapidity region, $|y| < 2.1$. If three or more jets were b-tagged, the two highest-p_{T} jets were considered as the b-jets from the top quark decays, and the others as additional jets. This definition follows the p_{T}-ordered selection used at particle level, and is different from that used in the differential cross-section analysis, as discussed in Sections 4.1 and 4.2 below. Distributions of the p_{T} and $|y|$ of the leading additional jet according to this definition are shown in Figure 3. The predictions generally describe the data well, and the trends seen are similar to those seen for the leading jet over the full rapidity region in Figure 2(a).

4.1 Particle-level selection

To facilitate comparisons with theoretical predictions, the measured jet differential cross-sections and gap fractions were corrected to correspond to the particle level in simulation, thus removing reconstruction efficiency and resolution effects. At particle level, electrons and muons were defined as those originating from W decays, including via the leptonic decay of a τ lepton ($W \rightarrow \tau \rightarrow e/\mu$). The electron and muon four-momenta were defined after final-state radiation, and 'dressed' by adding the four-momenta of all photons within a cone of size $\Delta R = 0.1$ around the lepton direction, excluding photons from hadron decays or interactions with detector material. Jets were reconstructed using the anti-k_t algorithm with radius parameter $R = 0.4$ from all final-state particles with mean lifetime greater than 3×10^{-11} s, excluding dressed leptons and neutrinos not originating from the decays of hadrons. Particles from the underlying event were included, but those from overlaid pile-up collisions were not. Selected jets were required to have $p_{\mathrm{T}} > 25$ GeV and $|\eta| < 4.5$, and those within $\Delta R = 0.2$ of a particle-level electron were removed. Particle-level jets containing b-hadrons were identified using a ghost-matching procedure [60], where the four-momenta of b-hadrons were scaled to a negligible magnitude and included in the set of particles on which the jet clustering algorithm was run. Jets whose constituents included b-hadrons after this procedure were labelled as b-jets.

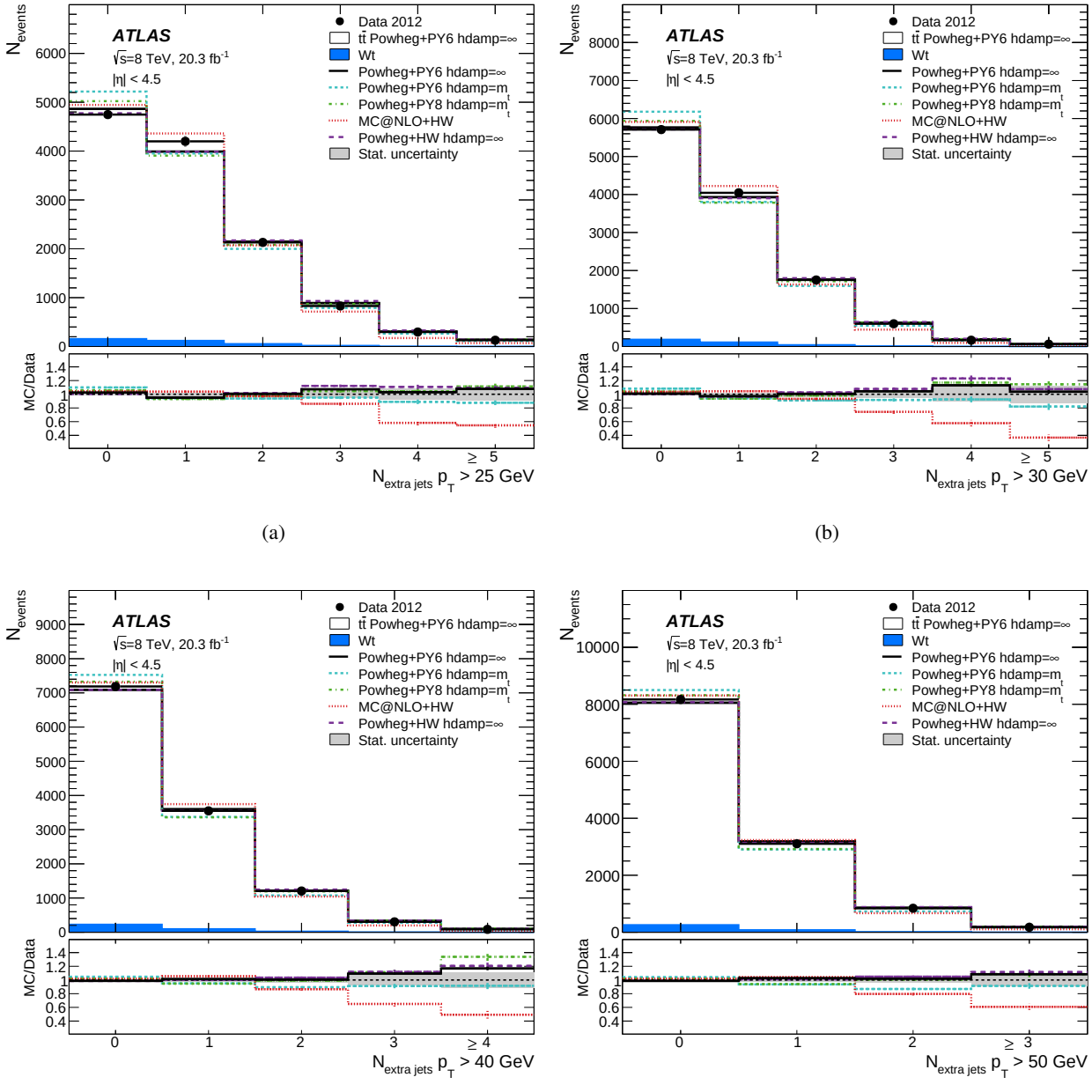
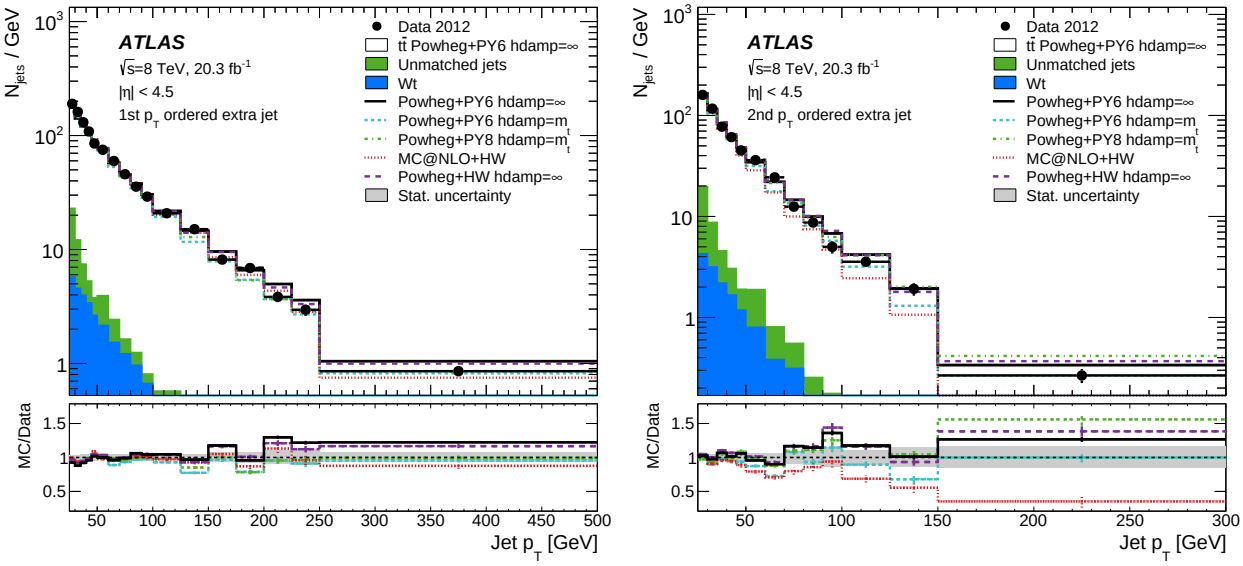
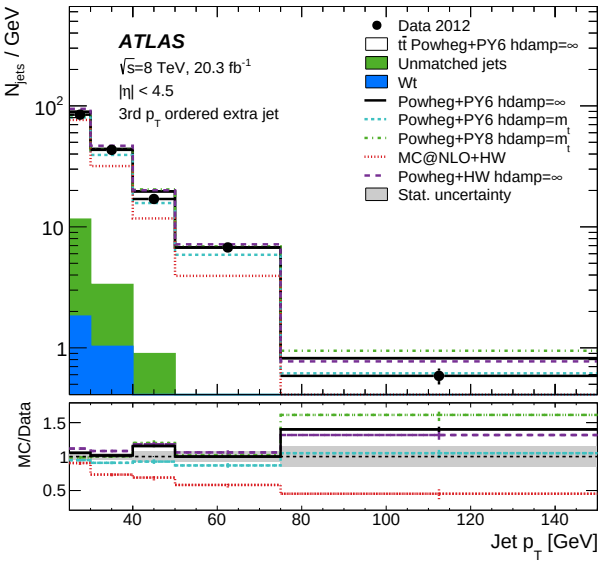


Figure 1: Distributions of the number of reconstructed extra jets with $|\eta| < 4.5$ and $p_{\mathrm{T}} >$ (a) 25, (b) 30, (c) 40 and (d) 50 GeV in selected $e\mu b\bar{b}$ events in data and in simulation, normalised to the same number of events as the data. The simulation predictions for $t\bar{t}$ and Wt single-top production are shown separately, and the contributions from other backgrounds are negligible. The ratios of different MC samples to data are shown with error bars corresponding to the simulation statistical uncertainty and a shaded band corresponding to the data statistical uncertainty. Systematic uncertainties are not shown.

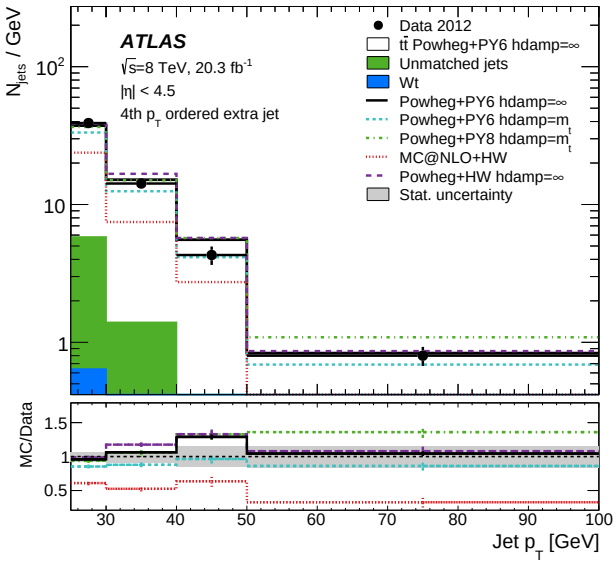


(a)

(b)

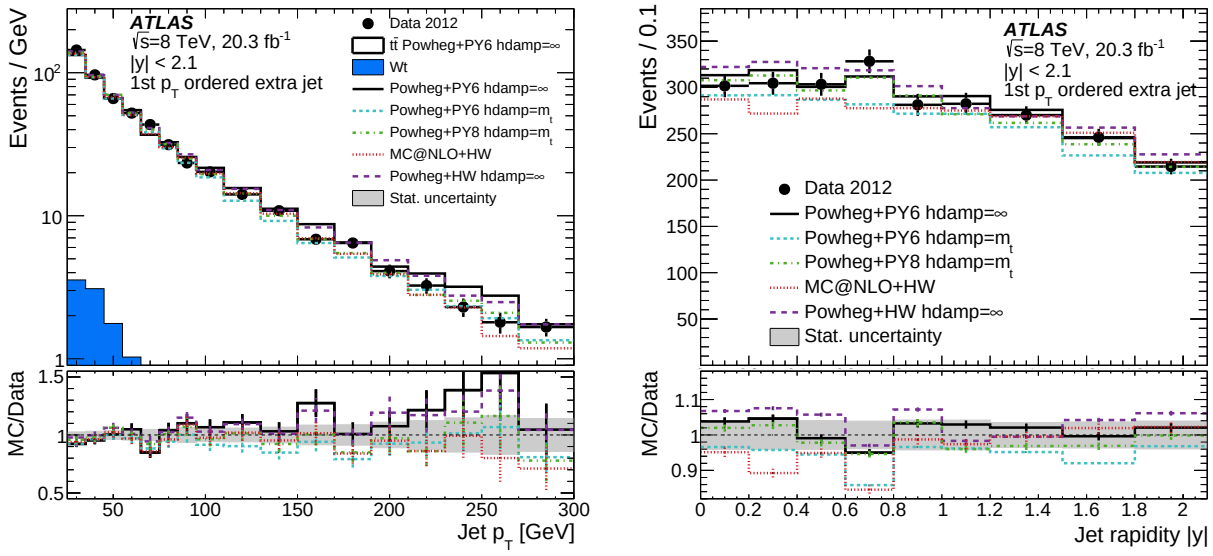


(c)



(d)

Figure 2: Distributions of reconstructed jet p_{T} for the (a) first to (d) fourth additional jet in selected $e\mu b\bar{b}$ events. The data are compared to simulation normalised to the same number of $e\mu b\bar{b}$ events as the data. Backgrounds from Wt single-top and unmatched jets are estimated using the baseline POWHEG + PYTHIA6 samples and shown separately. The contributions from other backgrounds are negligible. The ratios of different MC samples to data are shown with error bars corresponding to the simulation statistical uncertainty and a shaded band corresponding to the data statistical uncertainty. Systematic uncertainties are not shown.



(a) (b)

Figure 3: Distributions of leading additional reconstructed jet (a) p_{T} and (b) $|y|$ in $e\mu b\bar{b}$ events as used in the gap fraction measurement. The data are shown compared to simulation predictions using several $t\bar{t}$ generators, with the Wt background shown separately (not visible in (b)). Other backgrounds are negligible. The ratios of different MC samples to data are shown with error bars corresponding to the simulation statistical uncertainty and a shaded band corresponding to the data statistical uncertainty. Systematic uncertainties are not shown.

The particle-level $e\mu b\bar{b}$ event selection was defined by requiring one electron and one muon with $p_{\mathrm{T}} > 25\,\mathrm{GeV}$ and $|\eta| < 2.5$, each separated from the nearest jet by $\Delta R > 0.4$, and at least two b-jets with $p_{\mathrm{T}} > 25\,\mathrm{GeV}$ and $|\eta| < 2.5$. This closely matches the event selection used at reconstruction level. At particle level, if three or more b-jets were found, the two highest-p_{T} jets were considered to be the b-jets from the top decays, and all other jets were considered to be additional jets, whether labelled b-jets or not.

4.2 Jet matching

The differential jet cross-section measurements require an explicit matching of particle-level to reconstructed jets. This was achieved by first calculating the ΔR between each particle-level jet passing a looser requirement of $p_{\mathrm{T}} > 10\,\mathrm{GeV}$ and each reconstructed b-tagged jet, considering the two with highest MV1 weight if more than two reconstructed jets were b-tagged. Ordering the b-tagged jets by MV1 weight was found to give a greater fraction of correct matches than the jet p_{T} ordering used for the gap fraction measurements, where no jet matching is needed. If the closest reconstructed b-tagged jet was within $\Delta R < 0.4$, the particle-level and reconstructed jets were considered matched. The procedure was then repeated with the remaining particle-level and reconstructed jets, allowing each particle-level and reconstructed jet to be matched only once. Reconstructed jets which remained unassociated with particle-level jets after this procedure are referred to as 'unmatched' jets; these originate from single particle-level jets which are split in two at reconstruction level (only one of which is matched), and from pile-up (since

particles from pile-up collisions are not considered in the particle-level jet clustering). The contributions from such unmatched jets are shown separately in Figure 2.

5 Evaluation of systematic uncertainties

Monte Carlo simulation was used to determine selection efficiencies, detector resolution effects and backgrounds. The corresponding systematic uncertainties were evaluated as discussed in detail below, and propagated through the jet differential cross-section and gap fraction measurements.

$t\bar{t}$ modelling: The uncertainty due to the modelling of $t\bar{t}$ events in simulation was assessed by comparing samples from the different generator configurations described in Section 3. In the differential cross-section measurement, which is sensitive to the modelling of multiple additional jets, the uncertainty due to the choice of matrix-element generator was determined by comparing the NLO generator Powheg with the leading-order multi-leg generator MadGraph, both interfaced to Pythia6. In the gap fraction measurements, which are more sensitive to an accurate modelling of the first additional jet, the corresponding uncertainty was assessed by comparing the NLO generators Powheg and MC@NLO, both interfaced to Herwig. The choice of parton shower and hadronisation model was studied for both analyses by comparing samples with Powheg interfaced either to Pythia6 or to Herwig. In all these cases, the full difference between the predictions from the two compared samples was assigned as the corresponding systematic uncertainty. The uncertainty due to the modelling of additional radiation was calculated as half the difference between the results using MadGraph + Pythia6 (differential cross-section) or Alpgen + Pythia6 (gap fraction) samples with tunes giving more or less parton shower radiation, spanning the results from the $\sqrt{s} = 7$ TeV gap fraction measurement [2]. These three systematic components were added in quadrature to give the total $t\bar{t}$ modelling uncertainty.

Simulation statistical uncertainty: In addition to the modelling uncertainties discussed above, the size of the $t\bar{t}$ simulation samples was also taken into account.

Parton distribution functions: The uncertainties due to limited knowledge of the proton PDFs were evaluated by reweighting the MC@NLO + Herwig simulated $t\bar{t}$ sample based on the x and Q^2 values of the partons participating in the hard scattering in each event. The samples were reweighted using the eigenvector variations of the CT10 [23], MSTW2008 [18] and NNPDF 2.3 [36] NLO PDF sets. The final uncertainty was calculated as half the envelope encompassing the predictions from all three PDF sets along with their associated uncertainties, following the PDF4LHC recommendations [33].

Jet energy scale: The uncertainty due to the jet energy scale (JES) was evaluated by varying it in simulation using a model with 23 separate orthogonal uncertainty components [57]. These components cover in situ measurement uncertainties, the cross-calibration of different η regions, and the dependence on pile-up and the flavour of the jets. The total jet energy scale uncertainty varies in the range 1–6 % with a dependence on both jet p_{T} and $|\eta|$.

Jet energy resolution/efficiency: The jet energy resolution (JER) was found to be well-modelled in simulation [61], and residual uncertainties were assessed by applying additional smearing to the simulated jet energies. The calorimeter jet reconstruction efficiency was measured in data using track-based jets, and found to be generally well-described by the simulation. Residual uncertainties were

assessed by discarding 2 % of jets with $p_{\mathrm{T}} < 30\,\mathrm{GeV}$; the uncertainties for higher-momentum jets are negligible. Both these uncertainties were symmetrised about the nominal value.

Unmatched jets modelling: The modelling of the component of unmatched jets from pile-up collisions was checked by comparing the predictions from simulated $t\bar{t}$ events combined with either Powheg+Pythia8 pile-up simulation or 'zero-bias' data. The latter were recorded from randomly triggered bunch crossings throughout the data-taking period, and reweighted to match the instantaneous luminosity distribution in the simulated $t\bar{t}$ sample. The estimated number of additional jets per event from pile-up is 0.017 ± 0.002 in the central region used by the gap fraction measurements ($|y| < 2.1$) and 0.038 ± 0.005 over the full region used by the differential cross-section measurements ($|\eta| < 4.5$). The uncertainties represent the full difference between the rate in zero-bias data and simulation. The rate of unmatched jets in simulation was varied by these uncertainties in order to determine the effect on the results. In the differential cross-section measurements, the full rate of particle-level jets that were split in two at reconstruction level in the baseline simulation was taken as an additional uncertainty on the rate of unmatched jets.

Jet vertex fraction: In both measurements, the contribution of jets from pile-up within $|\eta| < 2.4$ was reduced by the JVF requirement described in Section 4. The uncertainties in the efficiency on non-pile-up jets of the JVF requirement were assessed by varying the cut value in simulation, based on studies of $Z \to ee$ and $Z \to \mu\mu$ events [56].

Other detector uncertainties: The modelling of the electron and muon trigger and identification efficiencies, energy scales and resolutions were studied using $Z \to ee/\mu\mu$, $J/\psi \to ee/\mu\mu$ and $W \to e\nu$ events in data and simulation, using the techniques described in Refs. [51, 62, 63]. The uncertainties in the efficiencies for b-tagging b, c and light-flavour jets were assessed using studies of b-jets containing muons, jets containing D^* mesons, and inclusive jet events [59]. The resulting uncertainties in the measured normalised differential jet distributions and gap fractions are very small, since these uncertainties typically affect the numerators and denominators in a similar way.

Backgrounds: As shown in Table 1, the most significant background comes from Wt single-top events. The uncertainty due to this background was assessed by conservatively doubling and removing the estimated Wt contribution, taking half the difference in the result between these extreme variations. The sensitivity to the modelling of Wt single-top events was also assessed by using a sample simulated with Powheg + Pythia6 using the diagram subtraction scheme [47, 48] instead of the baseline diagram removal scheme. The uncertainty due to Z+jets and diboson background is negligible in comparison. In the gap fraction measurements, the additional background uncertainty from events with a misidentified lepton was also assessed by doubling and removing it, a conservative range according to the studies of Ref. [1]. In the jet differential cross-section measurements, the misidentification of jets as leptons induces migration in the additional-jet rank distributions, and is corrected for as part of the unfolding procedure. The resulting effects on the unfolding corrections are significantly smaller than the uncertainties from considering different $t\bar{t}$ generators, and no additional uncertainty was included.

Each independent uncertainty was evaluated according to the prescription above and then added in quadrature to obtain the total systematic uncertainty in the final measurements. Since both measurements are effectively ratios of cross-sections, normalised to the total number of selected $e\mu b\bar{b}$ events, many of the systematic uncertainties that typically contribute to a $t\bar{t}$ cross-section measurement cancel, such as those in the integrated luminosity, lepton trigger and identification efficiencies, lepton momentum scales and resolution, and b-jet energy scale and tagging efficiency. Instead, the significant systematic uncertainties

are those that directly affect the measured additional-jet activity, *i.e.* systematic uncertainties in the jet energy scale and resolution, and the modelling of unmatched jets.

6 Measurement of jet multiplicities and p_{T} spectra

The normalised differential cross-sections for additional jets, corrected to the particle level, were measured as a function of jet multiplicity and p_{T} as defined in Equation (1). The fiducial requirements for event and object selection are defined in Section 4.1, and include additional jets in the range $|\eta| < 4.5$. As discussed in Section 3, the fiducial region receives contributions from both the $t\bar{t}$ and Wt processes. Although the requirement for two b-tagged jets ensures that $t\bar{t}$ is dominant, once the Wt process is considered at NLO, the two processes cannot in principle be cleanly separated. Therefore the results are presented both with the Wt contribution subtracted, to allow comparison with the $t\bar{t}$ generators discussed in Section 3, and for the combined $t\bar{t} + Wt$ final state, which may be compared with future NLO calculations treating $t\bar{t}$ and Wt concurrently. In practice, since the results are normalised to the number of selected $e\mu b\bar{b}$ events, from $t\bar{t}$ or $t\bar{t} + Wt$ as appropriate in each case, and the predicted additional-jet distributions in simulated $t\bar{t}$ and Wt events are rather similar, the results from the two definitions are very close.

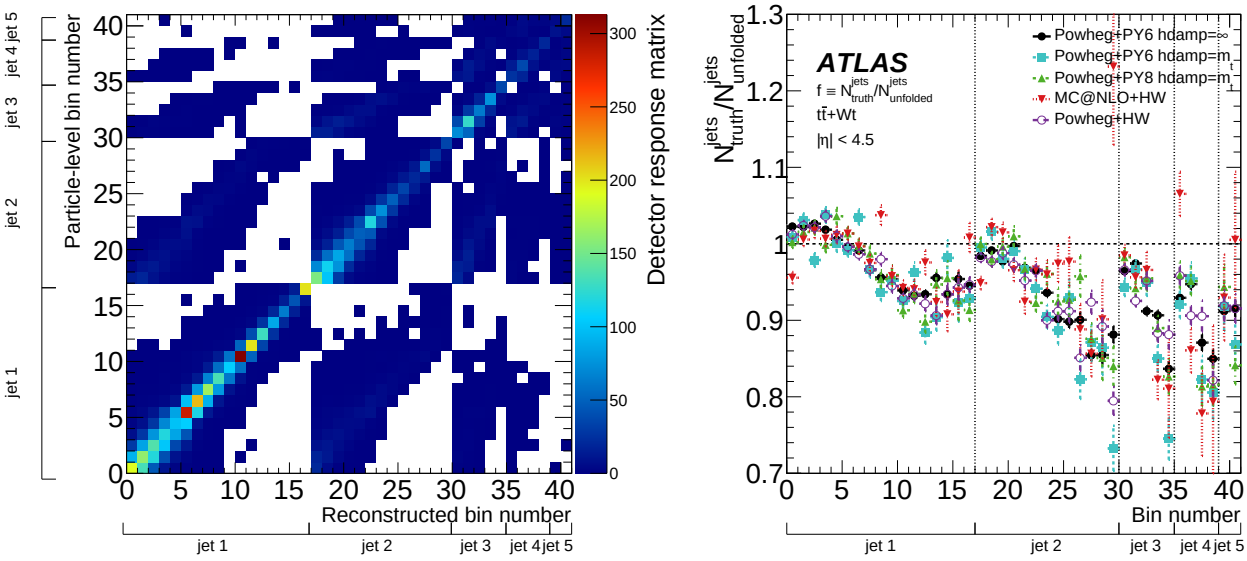
6.1 Correction to particle level

The correction procedure transforms the measured spectra shown in Figure 2, after background subtraction, to the particle-level spectra for events that pass the fiducial requirements. The unfolding was performed using a one-dimensional distribution encoding both the rank and p_{T} of each additional jet in each selected $e\mu b\bar{b}$ event, as shown in Table 2 and graphically in Figure 4. The integral of the input (measured) distribution is the number of measured jets in the $e\mu b\bar{b}$ sample and the integral of the output (unfolded) distribution is the number of particle-level jets passing the fiducial requirements. This procedure involves several steps, as defined in the equation:

$$\frac{1}{\sigma_{e\mu b\bar{b}}}\frac{\mathrm{d}\sigma_{\mathrm{jet},i}}{\mathrm{d}p_{\mathrm{T}}} = \frac{1}{N_{\mathrm{events}}}\frac{1}{\Delta^i}\, f^i \sum_j \left(\mathbf{M}^{-1}\right)^{\mathrm{unfolded},\, i}_{\mathrm{reco},\, j} g^j \left(\mathscr{N}^j_{\mathrm{reco}} - \mathscr{N}^j_{\mathrm{bkgd}}\right) . \tag{4}$$

The bin indices i and j are functions of both jet p_{T} and rank. The raw data event count reconstructed in bin j is represented by $\mathscr{N}^j_{\mathrm{reco}}$. The estimated additional-jet background, $\mathscr{N}^j_{\mathrm{bkgd}}$, is subtracted from this raw distribution. The factor g^j corrects for migration across the fiducial boundaries in p_{T} and η (*e.g.* cases where the reconstructed jet has $p_{\mathrm{T}} > 25\,\mathrm{GeV}$ but the particle-level jet has $p_{\mathrm{T}} < 25\,\mathrm{GeV}$). The expression $\left(\mathbf{M}^{-1}\right)^{\mathrm{unfolded},\, i}_{\mathrm{reco},\, j}$ represents the application of an unfolding procedure mapping the number of jets reconstructed in bin j to the number of jets in bin i at particle level in events which pass both the reconstruction- and particle-level selections. The correction factor f^i removes the bias in the unfolded additional-jet spectrum coming from the reconstruction-level selection, as discussed further below. The number of events in data passing the $e\mu b\bar{b}$ selection requirements is represented by N_{events}, and $\frac{1}{\sigma_{e\mu b\bar{b}}}\frac{\mathrm{d}\sigma_{\mathrm{jet},i}}{\mathrm{d}p_{\mathrm{T}}}$ represents the final number of corrected jets per event in each bin i divided by Δ^i, the width of the p_{T} bin in units of GeV.

The response matrix $\mathbf{M}^{\mathrm{unfolded},\, i}_{\mathrm{reco},\, j}$ encodes the fractions of jets in particle-level bin i which get reconstructed in bin j, with both i and j being obtained from the corresponding jet p_{T} and rank. The matrix is filled from



(a) (b)

Figure 4: (a) Migration matrix between the particle-level and reconstructed number of additional jets in each bin, determined from the baseline $t\bar{t}+Wt$ simulation. Jets are binned according to both p_{T} value and rank; (b) bin-by-bin correction factor f^i for the bias due to the $e\mu b\bar{b}$ event selection, evaluated using both the baseline POWHEG + PYTHIA6 sample and various alternatives.

simulated events that pass both the reconstructed and particle-level selection requirements. Figure 4(a) provides a graphical representation of $\mathbf{M}^{\text{unfolded},\,i}_{\text{reco},\,j}$. The matrix is largely diagonal, showing that jets are most likely to be reconstructed with the correct p_{T} and rank. However, there are significant numbers of particle-level subleading jets reconstructed as leading jets and particle-level leading jets reconstructed as subleading jets, particularly when several jets in the event have similar low p_{T} values. This type of migration motivates the simultaneous binning in both rank and p_{T}.

A Bayesian iterative unfolding method [64] implemented in the RooUnfold [65] software package was used. The response matrix $\mathbf{M}$ is not unitary because in mapping from particle to reconstruction level, some events and objects are lost due to inefficiencies and some are gained due to misreconstruction or migration of objects from outside the fiducial acceptance into the reconstructed distribution. This results in the response matrix being almost singular, and it is therefore not possible to obtain stable unfolded results by inverting the response matrix and applying it to the measured data. Instead, an assumed particle-level distribution (the 'prior') was chosen, the response matrix applied and the resulting trial reconstruction set was compared to the observed reconstruction set. A new prior was then constructed from the old prior and the difference between the trial and the observed distributions. The procedure was iterated until the result became stable. For this analysis, two iterations were found to be sufficient, based on studies of the unfolding performance in simulated samples with reweighted jet p_{T} distributions and from different generators.

This unfolding procedure gives unbiased additional-jet distributions for events passing both the particle-level and reconstruction-level event selections. However, the reconstruction-level selection results in the unfolded distributions differing from those obtained using the particle-level selection alone. An additional contribution to the bias results from events where one of the two reconstructed b-tagged

jets is actually a mistagged light jet. These biases were corrected using a bin-by-bin correction factor $f^i = \mathcal{N}^i_{\text{truth}}/\mathcal{N}^i_{\text{unfolded}}$, where $\mathcal{N}^i_{\text{truth}}$ is the number of jets in bin i at particle level without the application of the reconstruction-level event selection. The correction was applied after the unfolding, as shown in Equation (4). Figure 4(b) shows the values of f for both the baseline and some alternative $t\bar{t}$ generators. The corresponding systematic uncertainty was assessed as part of the $t\bar{t}$ modelling uncertainty as discussed in Section 5.

The procedure described above provides the absolute numbers of additional jets in the number of events passing the $e\mu b\bar{b}$ fiducial requirements (N_{events}). This result was then normalised relative to N_{events} to obtain the final distribution $\frac{1}{\sigma_{e\mu b\bar{b}}}\frac{\mathrm{d}\sigma_{\text{jet},i}}{\mathrm{d}p_{\text{T}}}$, which was finally integrated over jet p_{T} to obtain the jet multiplicity distributions.

6.2 Determination of systematic uncertainties

All systematic uncertainties were evaluated as full covariance matrices including bin-to-bin correlations. The majority of uncertainties from Section 5 are defined in terms of an RMS width, with the assumption that the true distribution is Gaussian with a mean at the nominal value. In these cases, the covariance matrix was calculated from pseudo-experiments drawn from this distribution. Each pseudo-experiment was constructed by choosing the size of the systematic uncertainty randomly according to a Gaussian distribution, calculating the resulting effect at the reconstruction level and propagating it through the unfolding procedure. The covariance was then given by

$$C_{ij} \equiv \frac{1}{N_{\text{pseudo}}} \sum_{x=1}^{N_{\text{pseudo}}} \left(\mathcal{N}^i_x - \left\langle \mathcal{N}^i \right\rangle\right)\left(\mathcal{N}^j_x - \left\langle \mathcal{N}^j \right\rangle\right), \tag{5}$$

where N_{pseudo} is the number of pseudo-experiments (typically 1000), $\langle \mathcal{N}^i \rangle$ is the nominal number of jets in bin i, and $\mathcal{N}^i_x$ is the number of jets in bin i for pseudo-experiment x. Some systematic uncertainties were evaluated by comparing an alternative model to the baseline. In these cases, the covariance was approximated by

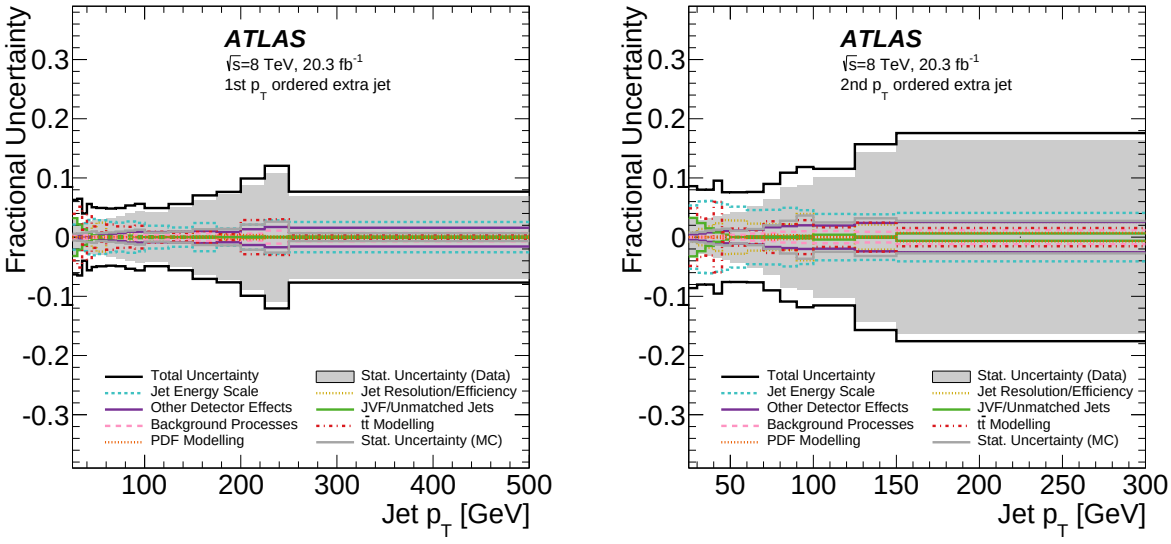
$$C_{ij} \equiv \delta_i \delta_j, \tag{6}$$

where δ_i is the bias in bin i. This bias was determined by analysing the alternative model using Equation (4), with the response matrix and correction factors taken from the baseline.

The uncertainties calculated using Equation (5) include all detector modelling effects (*e.g.* jet energy scale and resolution), PDFs, the Wt cross-section and statistical uncertainties associated with the simulated samples. Uncertainties evaluated using Equation (6) include generator, radiation, parton shower and hadronisation contributions to the $t\bar{t}$ modelling uncertainty, and modelling of the unmatched jet background. Figure 5 shows the fractional uncertainties in the corrected jet distributions. In most bins, the statistical uncertainty dominates, with the largest systematic uncertainty coming from the jet energy scale.

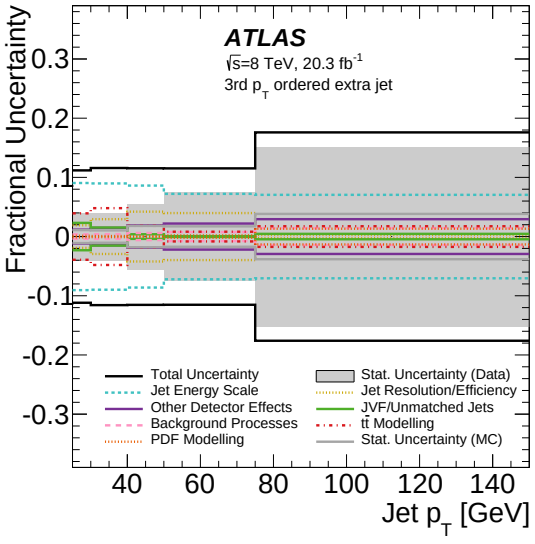
6.3 Jet multiplicity and p_{T} spectra results

Figures 6–7 show normalised distributions of the additional-jet multiplicity for different jet p_{T} thresholds, and compare the data to the NLO generator configurations Powheg + Pythia6 with $h_{\text{damp}} = \infty$ or m_t,

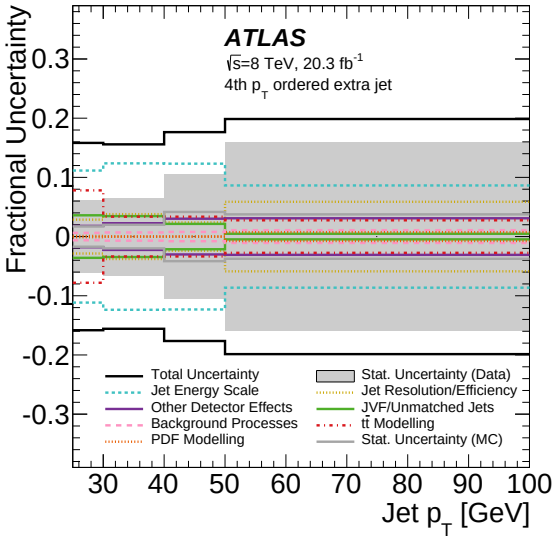


(a)

(b)



(c)



(d)

Figure 5: Envelope of fractional uncertainties in the first (a) to the fourth (d) additional-jet normalised differential cross-sections, as functions of the corresponding jet p_{T}. The total uncertainties are shown, together with the separate contributions from the data statistical uncertainty and various categories of systematic uncertainty.

Powheg + Pythia8, MC@NLO + Herwig and Powheg + Herwig. Figures 8–9 show the normalised differential cross-sections $\frac{1}{\sigma_{e\mu b\bar{b}}}\frac{\mathrm{d}\sigma_{\mathrm{jet},i}}{\mathrm{d}p_{\mathrm{T}}}$ for jets of rank i from one to four. In both cases, the expected contributions from Wt events were subtracted from the event counts before normalising the distributions, based on the baseline Powheg+Pythia6 Wt simulation sample. The same data are presented numerically in Table 2, both with and without subtraction of the Wt contribution, and including two p_{T} bins for the fifth jet. The highest p_{T} bin for each jet rank includes overflows, but the differential cross-sections are normalised using the Δ^i bin widths derived from the upper p_{T} bin limits listed in Table 2 and shown in Figures 8 and 9.

Table 2: Normalised particle-level differential jet cross-sections as a function of jet rank and p_{T}, both without ($\sigma^{t\bar{t}+Wt}$) and with ($\sigma^{t\bar{t}}$) the Wt contribution subtracted. The additional jets are required to have $|\eta| < 4.5$, corresponding to the full pseudorapidity range . The boundaries of each bin are given, together with the mean jet p_{T} in each bin. The last bin for every jet rank includes overflows, but the differential cross-section values are determined using the upper bin limit given for that bin.

Bin	Rank	p_{T} range [GeV]	Avg. p_{T} [GeV]	$\frac{1}{\sigma_{e\mu b\bar{b}}}\frac{\mathrm{d}\sigma^{t\bar{t}+Wt}_{\mathrm{jet},i}}{\mathrm{d}p_{\mathrm{T}}}$ ±(stat.)±(syst.) [10^{-4} GeV^{-1}]	$\frac{1}{\sigma_{e\mu b\bar{b}}}\frac{\mathrm{d}\sigma^{t\bar{t}}_{\mathrm{jet},i}}{\mathrm{d}p_{\mathrm{T}}}$ ±(stat.)±(syst.) [10^{-4} GeV^{-1}]
1	1	25–30	27.4	144.7 ± 4.3 ± 8.0	144.5 ± 4.4 ± 8.2
2	1	30–35	32.4	122.7 ± 3.0 ± 7.3	122.8 ± 3.1 ± 7.5
3	1	35–40	37.4	101.8 ± 2.6 ± 3.1	101.9 ± 2.6 ± 3.2
4	1	40–45	42.5	84.0 ± 2.3 ± 4.1	84.0 ± 2.4 ± 4.2
5	1	45–50	47.4	70.2 ± 2.0 ± 2.9	70.3 ± 2.1 ± 3.0
6	1	50–60	54.8	58.0 ± 1.7 ± 2.3	58.1 ± 1.8 ± 2.3
7	1	60–70	64.8	46.3 ± 1.5 ± 1.6	46.5 ± 1.6 ± 1.7
8	1	70–80	74.8	35.3 ± 1.3 ± 1.2	35.4 ± 1.3 ± 1.2
9	1	80–90	84.8	27.2 ± 1.1 ± 1.0	27.3 ± 1.1 ± 1.0
10	1	90–100	94.8	21.9 ± 0.9 ± 0.8	22.0 ± 1.0 ± 0.8
11	1	100–125	111.5	16.2 ± 0.7 ± 0.4	16.3 ± 0.7 ± 0.5
12	1	125–150	136.7	11.18 ± 0.56 ± 0.29	11.26 ± 0.58 ± 0.30
13	1	150–175	161.8	6.53 ± 0.41 ± 0.22	6.56 ± 0.42 ± 0.22
14	1	175–200	186.7	5.24 ± 0.38 ± 0.13	5.29 ± 0.39 ± 0.14
15	1	200–225	211.9	3.02 ± 0.27 ± 0.14	3.04 ± 0.28 ± 0.14
16	1	225–250	236.8	2.17 ± 0.23 ± 0.12	2.18 ± 0.24 ± 0.12
17	1	250–500+	344.4	0.66 ± 0.05 ± 0.02	0.67 ± 0.05 ± 0.02
18	2	25–30	27.4	110.6 ± 3.5 ± 8.8	110.6 ± 3.6 ± 9.1
19	2	30–35	32.4	80.3 ± 2.3 ± 6.0	80.4 ± 2.3 ± 6.2
20	2	35–40	37.4	59.2 ± 1.9 ± 4.4	59.5 ± 1.9 ± 4.5
21	2	40–45	42.4	44.8 ± 1.6 ± 4.0	44.9 ± 1.6 ± 4.1
22	2	45–50	47.4	35.4 ± 1.4 ± 2.4	35.5 ± 1.4 ± 2.4
23	2	50–60	54.6	26.6 ± 1.1 ± 1.7	26.8 ± 1.2 ± 1.8
24	2	60–70	64.6	17.1 ± 0.9 ± 1.0	17.3 ± 0.9 ± 1.0
25	2	70–80	74.6	9.8 ± 0.6 ± 0.7	9.9 ± 0.6 ± 0.7
26	2	80–90	84.7	5.88 ± 0.50 ± 0.43	5.92 ± 0.51 ± 0.45
27	2	90–100	94.7	3.81 ± 0.34 ± 0.33	3.84 ± 0.34 ± 0.34
28	2	100–125	110.9	2.43 ± 0.25 ± 0.15	2.44 ± 0.25 ± 0.15
29	2	125–150	136.0	1.30 ± 0.19 ± 0.09	1.32 ± 0.19 ± 0.10

Continued on next page

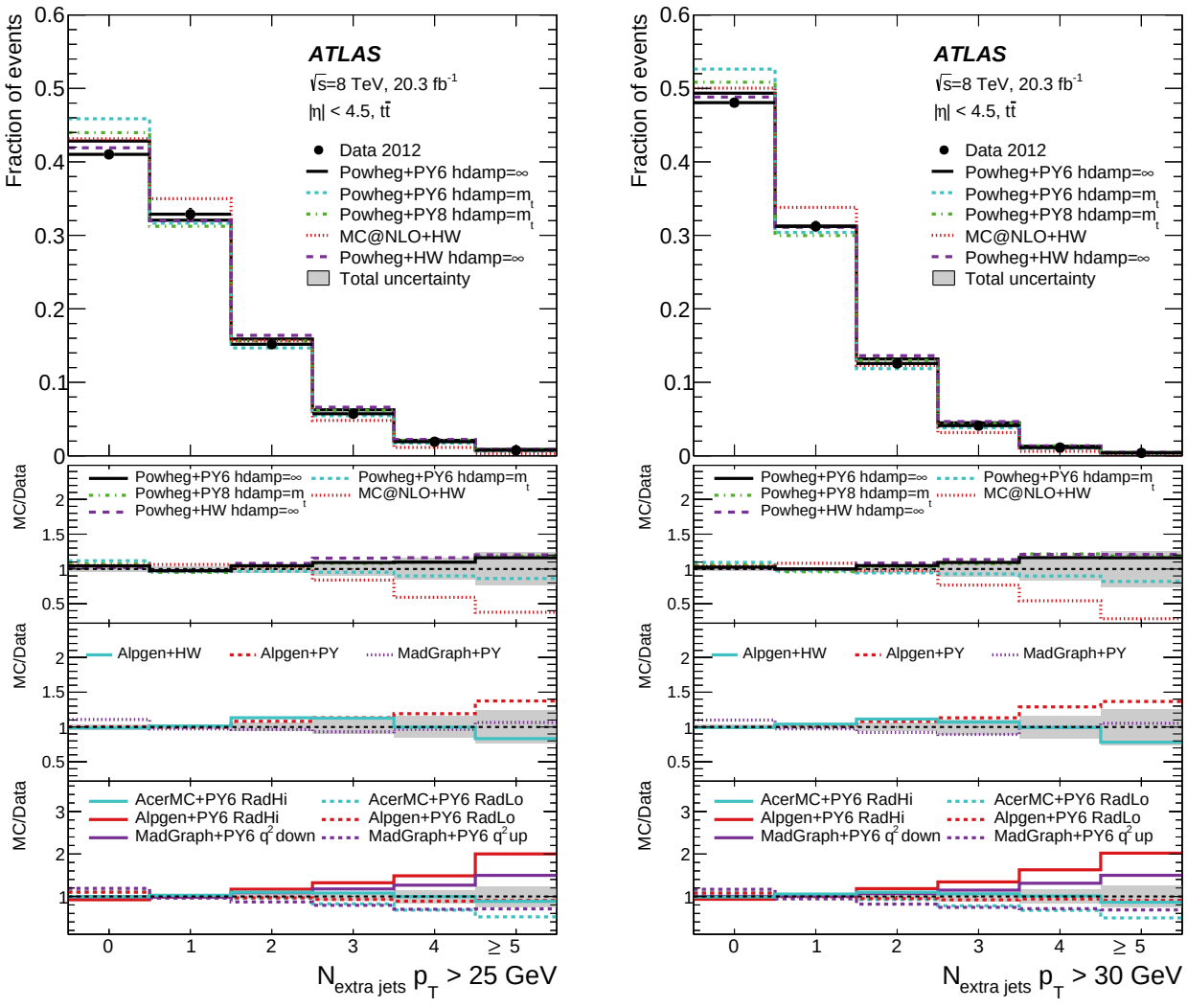
Table 2 –*Continued from previous page*

Bin	Rank	p_{T} range [GeV]	Avg. p_{T} [GeV]	$\frac{1}{\sigma_{e\mu b\bar{b}}}\frac{\mathrm{d}\sigma^{t\bar{t}+Wt}_{\mathrm{jet},i}}{\mathrm{d}p_{\mathrm{T}}}$ ±(stat.)±(syst.) [10^{-4} GeV^{-1}]	$\frac{1}{\sigma_{e\mu b\bar{b}}}\frac{\mathrm{d}\sigma^{t\bar{t}}_{\mathrm{jet},i}}{\mathrm{d}p_{\mathrm{T}}}$ ±(stat.)±(syst.) [10^{-4} GeV^{-1}]
30	2	150–300+	194.2	0.20 ± 0.03 ± 0.01	0.20 ± 0.03 ± 0.01
31	3	25–30	27.3	56.7 ± 2.3 ± 6.0	56.9 ± 2.3 ± 6.2
32	3	30–40	34.3	29.6 ± 1.2 ± 3.3	29.8 ± 1.2 ± 3.4
33	3	40–50	44.4	12.7 ± 0.7 ± 1.4	12.8 ± 0.7 ± 1.4
34	3	50–75	59.3	4.68 ± 0.35 ± 0.45	4.74 ± 0.36 ± 0.47
35	3	75–150+	97.9	0.40 ± 0.06 ± 0.04	0.41 ± 0.06 ± 0.04
36	4	25–30	27.3	23.5 ± 1.4 ± 3.6	23.7 ± 1.5 ± 3.7
37	4	30–40	34.1	9.4 ± 0.6 ± 1.4	9.5 ± 0.6 ± 1.4
38	4	40–50	44.2	3.07 ± 0.32 ± 0.50	3.10 ± 0.33 ± 0.51
39	4	50–100+	64.1	0.55 ± 0.09 ± 0.08	0.55 ± 0.09 ± 0.08
40	5	25–30	27.2	7.3 ± 0.9 ± 1.6	7.4 ± 0.9 ± 1.6
41	5	30–50+	38.8	1.95 ± 0.29 ± 0.40	1.97 ± 0.30 ± 0.41

All the NLO generators provide a reasonable description of the leading jet, which might be expected since they include one additional jet in the matrix-element calculation of the $t\bar{t}$ process. Differences among the generators become larger with increasing jet rank, where the prediction from the NLO generators is determined mainly by the parton shower. In this region, the generators predict significantly different rates of additional-jet production. They also predict some differences in the shapes of the jet p_{T} spectra. The MC@NLO + Herwig sample predicts the lowest rate of additional-jet production and underestimates the number of events with at least four additional jets by 40 %.

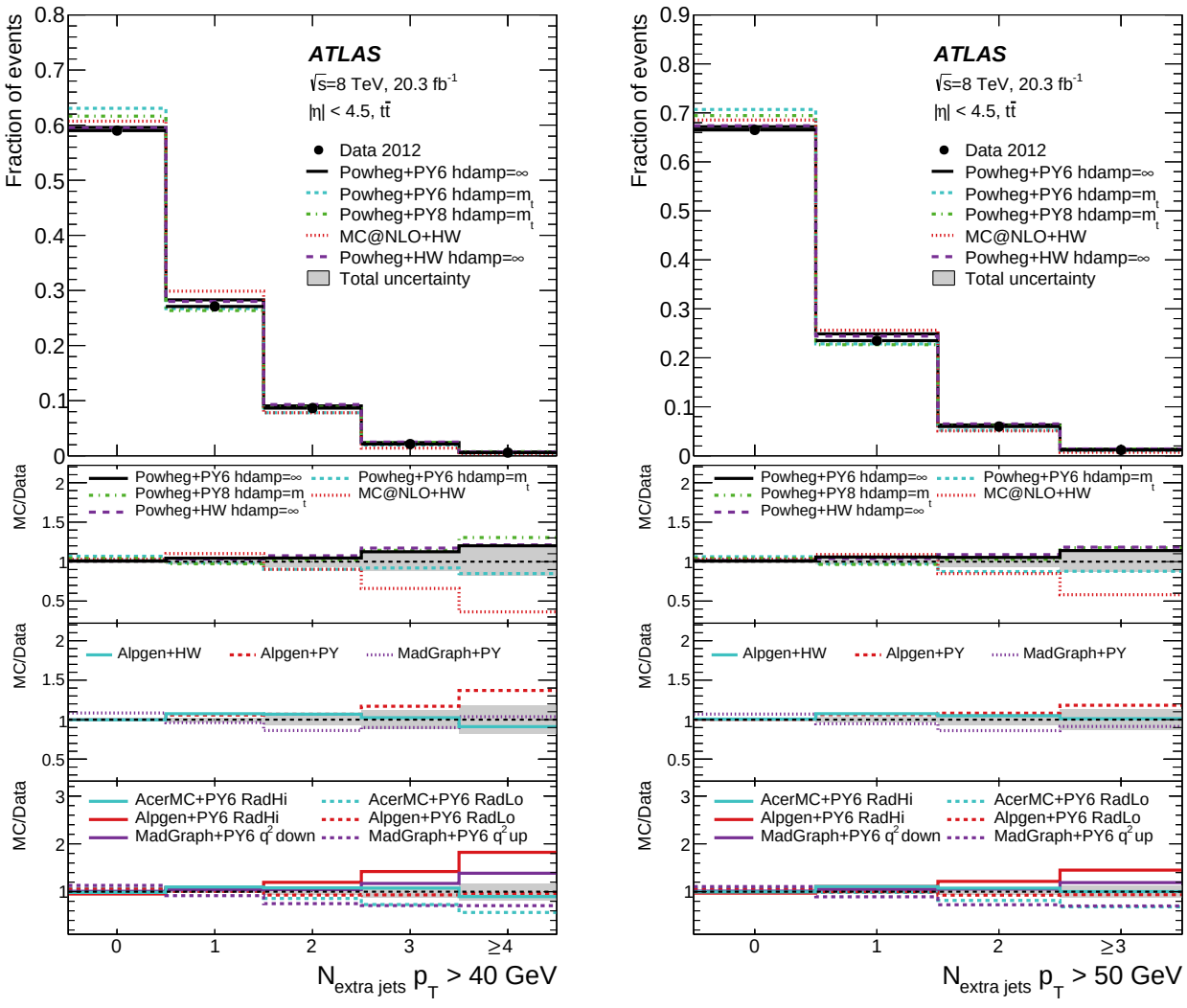
The same fully corrected data are compared to the leading-order multi-leg generators Alpgen + Pythia6, Alpgen + Herwig and MadGraph + Pythia6 in the second set of ratio plots in Figures 6–9. In all cases, the renormalisation and factorisation scales are set to the defaults provided by the code authors. For leading-order generators, the predicted cross-section can depend strongly on the choice of QCD scales and parton shower parameters; Figures 6–9 also show the effects of the variations discussed in Section 3 for samples generated with AcerMC + Pythia6, Alpgen + Pythia6 and MadGraph + Pythia6. The measurement gives an uncertainty in the differential cross-sections that is smaller than the range spanned by these variations in the leading-order generators.

The level of agreement between the generator predictions and the data was assessed quantitatively using a χ^2 test taking into account all bins of the measured jet p_{T} distributions with rank one to five. Since the systematic uncertainties and unfolding corrections induce large correlations between bins, the χ^2 was calculated from the full covariance matrix. Table 3 presents the resulting χ^2 values. Among the NLO generators, Powheg+Herwig, and Powheg + Pythia6 with $h_{\mathrm{damp}} = \infty$ or m_t, agree reasonably well with the data. Powheg+Pythia8 is disfavoured and MC@NLO+Herwig gives a very poor description of the data. The leading-order multi-leg generators Alpgen + Pythia6 and MadGraph+Pythia6 agree reasonably well with data, whilst Alpgen+Herwig is slightly disfavoured. Of the three variations of Alpgen + Pythia6, the 'RadLo' variation with less radiation agrees best with data, suggesting that the scale used in the baseline ATLAS tune predicts too much radiation in the fiducial region of this measurement. For MadGraph+Pythia6 the opposite is true, and the 'q^2 down' tune, which corresponds to more radiation than



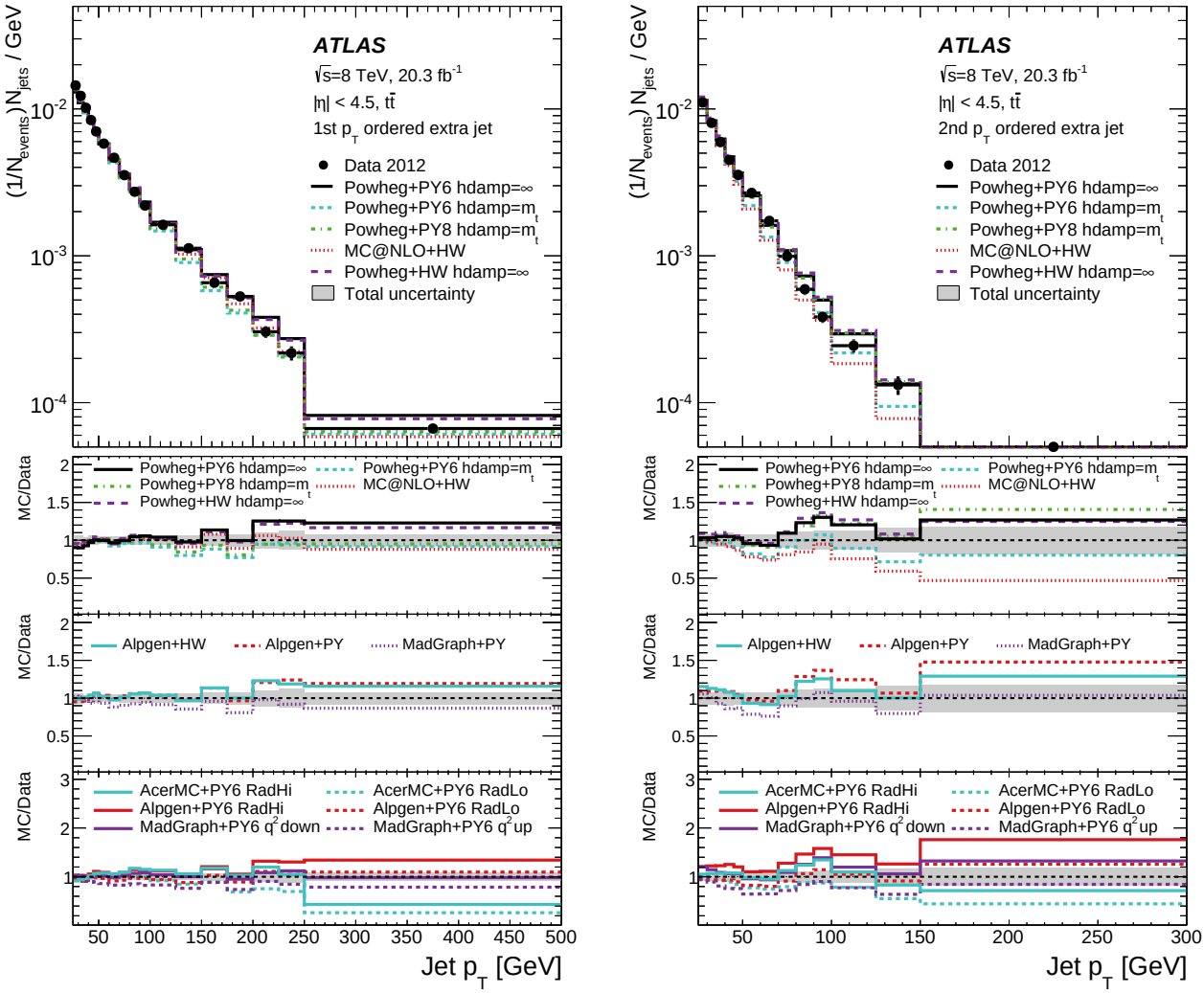
(a) (b)

Figure 6: Unfolded normalised distributions of particle-level additional-jet multiplicity with $p_{\mathrm{T}} >$ (a) 25 GeV and (b) 30 GeV in selected $e\mu b\bar{b}$ events. The data are shown as points with error bars indicating the statistical uncertainty, and are compared to simulation from several NLO $t\bar{t}$ generator configurations. The Wt contribution taken from POWHEG + PYTHIA6 is subtracted from the data. The lower plots show the ratios of the different simulation predictions to data, with the shaded bands including both the statistical and systematic uncertainties of the data.



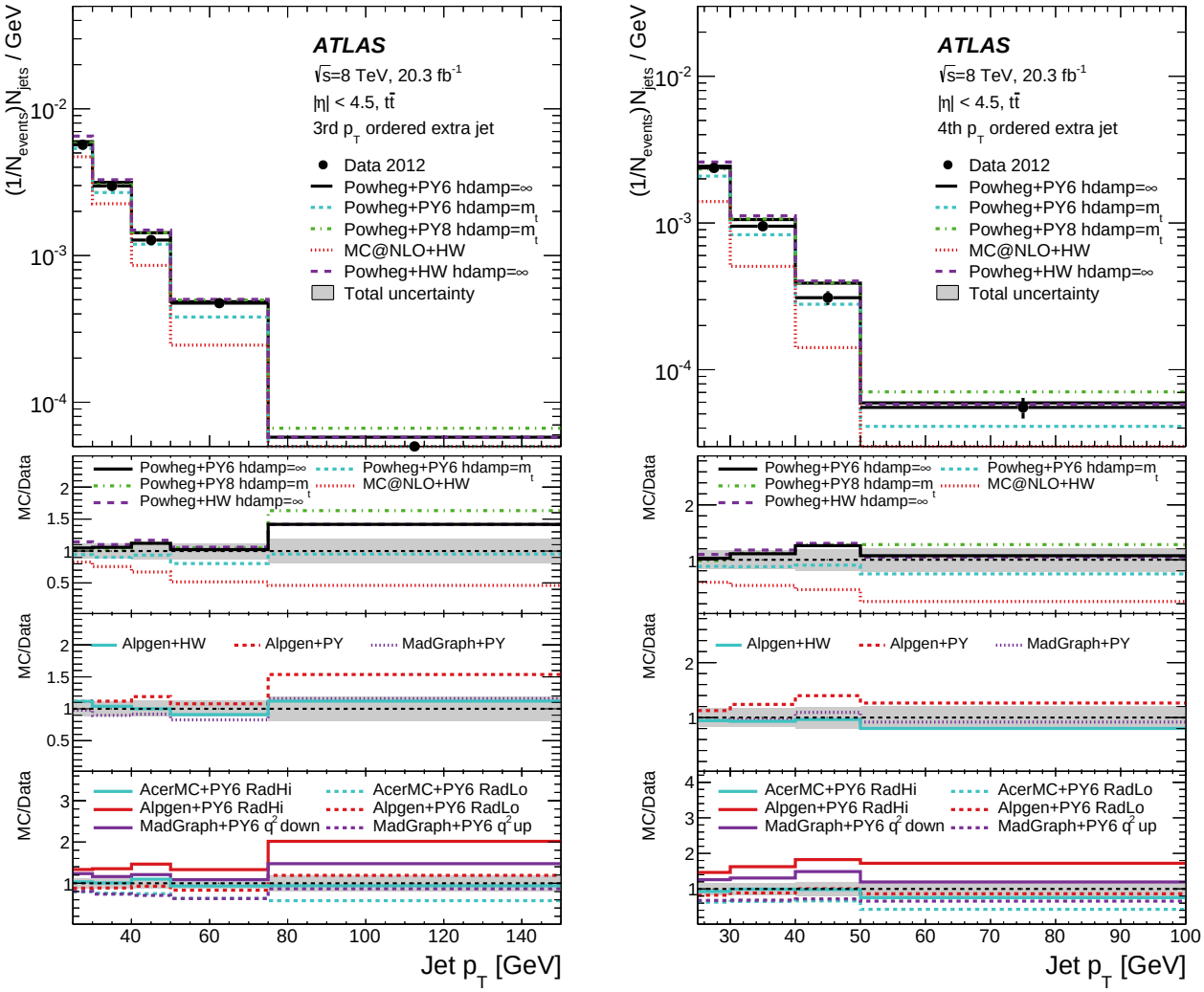
(a) (b)

Figure 7: Unfolded normalised distributions of particle-level additional-jet multiplicity with $p_{\mathrm{T}} >$ (a) 40 GeV and (b) 50 GeV in selected $e\mu b\bar{b}$ events. The data are shown as points with error bars indicating the statistical uncertainty, and are compared to simulation from several NLO $t\bar{t}$ generator configurations. The Wt contribution taken from POWHEG + PYTHIA6 is subtracted from the data. The lower plots show the ratios of the different simulation predictions to data, with the shaded bands including both the statistical and systematic uncertainties of the data.



(a) (b)

Figure 8: Unfolded normalised distributions of particle-level jet p_{T} for the first and second additional jet in selected $e\mu b\bar{b}$ events. The data are shown as points with error bars indicating the statistical uncertainty, and are compared to simulation from several NLO $t\bar{t}$ generator configurations. The Wt contribution taken from POWHEG + PYTHIA6 is subtracted from the data. The lower plots show the ratios of the different simulation predictions to data, with the shaded bands including both the statistical and systematic uncertainties of the data.



(a) (b)

Figure 9: Unfolded normalised distributions of particle-level jet p_{T} for the third and fourth additional jet in selected $e\mu b\bar{b}$ events. The data are shown as points with error bars indicating the statistical uncertainty, and are compared to simulation from several NLO $t\bar{t}$ generator configurations. The Wt contribution taken from POWHEG + PYTHIA6 is subtracted from the data. The lower plots show the ratios of the different simulation predictions to data, with the shaded bands including both the statistical and systematic uncertainties of the data.

Generator	χ^2	p-value
POWHEG+PYTHIA6 $h_{\text{damp}} = \infty$	55.3	6.7×10^{-2}
POWHEG+PYTHIA6 $h_{\text{damp}} = m_t$	57.4	4.6×10^{-2}
POWHEG+PYTHIA8 $h_{\text{damp}} = m_t$	78.0	4.4×10^{-4}
MC@NLO+HERWIG	108.2	5.8×10^{-8}
POWHEG+HERWIG $h_{\text{damp}} = \infty$	51.4	1.3×10^{-1}
ALPGEN+HERWIG	64.0	1.2×10^{-2}
ALPGEN+PYTHIA6	55.5	6.4×10^{-2}
MADGRAPH+PYTHIA6	54.7	7.4×10^{-2}
ACERMC+PYTHIA6 RadHi	138.4	1.8×10^{-12}
ACERMC+PYTHIA6 RadLo	148.1	4.9×10^{-14}
ALPGEN+PYTHIA6 RadHi	104.7	1.8×10^{-7}
ALPGEN+PYTHIA6 RadLo	47.9	2.1×10^{-1}
MADGRAPH+PYTHIA6 q^2 down	50.2	1.5×10^{-1}
MADGRAPH+PYTHIA6 q^2 up	78.7	3.6×10^{-4}

Table 3: Values of χ^2 for the comparison of the full set of additional-jet p_{T} spectra in data with the predictions from various $t\bar{t}$ generator configurations, including both the statistical and systematic uncertainties. The additional jets correspond to the full pseudorapidity range ($|\eta| < 4.5$). The χ^2 and p-values correspond to 41 degrees of freedom.

the baseline tune, agrees best with data. The ACERMC + PYTHIA6 samples do not reproduce the data well, regardless of parameter choice.

7 Gap fraction measurements

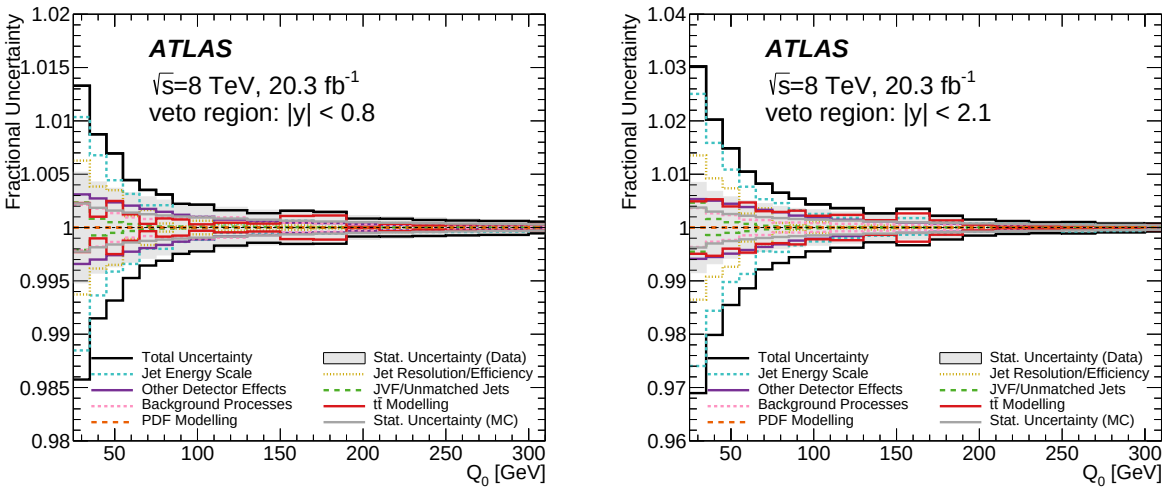
The gap fraction $f(Q_0)$ as defined in Equation (2) was measured by using the analogous definition for reconstructed jets, counting the number of selected $e\mu b\bar{b}$ events N and the number $n(Q_0)$ of them that have no additional jets with $p_{\text{T}} > Q_0$ within the rapidity interval Δy:

$$f^{\text{reco}}(Q_0) \equiv \frac{n(Q_0)}{N} \tag{7}$$

and similarly for the gap fraction based on Q_{sum}. The values of N and n were first corrected to remove the background contributions estimated from simulation, including the Wt contribution, as this study focuses on the comparison of measured gap fractions with the predictions from the $t\bar{t}$ generators discussed in Section 3. The measured gap fraction $f^{\text{reco}}(Q_0)$ was then multiplied by a correction factor $C(Q_0)$ to obtain the particle-level gap fraction $f^{\text{part}}(Q_0)$ defined as in Equation (2) using the particle-level definitions given in Section 4.1. The correction factor was evaluated using the values of $f^{\text{reco}}(Q_0)$ and $f^{\text{part}}(Q_0)$ obtained from the baseline POWHEG + PYTHIA6 $t\bar{t}$ simulation sample:

$$C(Q_0) \equiv \frac{f^{\text{part}}(Q_0)}{f^{\text{reco}}(Q_0)}. \tag{8}$$

Systematic uncertainties arise in this procedure from the uncertainties in $C(Q_0)$ and the backgrounds subtracted before the calculation of N and n.



(a) (b)

Figure 10: Envelope of fractional uncertainties $\Delta f/f$ in the gap fraction $f(Q_0)$ for (a) $|y| < 0.8$ and (b) $|y| < 2.1$. The statistical uncertainty is shown by the hatched area, and the total uncertainty by the solid black line. The systematic uncertainty is shown broken down into several groups, each of which includes various individual components (see text).

The gap fractions $f(Q_0)$ and $f(Q_{\text{sum}})$ were measured for the same rapidity regions as used in Ref. [2], namely $|y| < 0.8$, $0.8 < |y| < 1.5$, $1.5 < |y| < 2.1$ and the inclusive region $|y| < 2.1$. The sets of Q_0 and Q_{sum} threshold values chosen also correspond to those in Ref. [2], and the steps correspond approximately to one standard deviation of the jet energy resolution. The values of the correction factor $C(Q_0)$ (and similarly for Q_{sum}) deviate by at most 5 % from unity at low Q_0 and Q_{sum}, and approach unity at higher threshold values. The small corrections reflect the high selection efficiency and high purity of the event samples; at each threshold Q_0, the baseline simulation predicts that around 80 % of the selected reconstructed events that do not have a jet with $p_{\text{T}} > Q_0$ also have no particle-level jet with $p_{\text{T}} > Q_0$. Therefore, a simple bin-by-bin correction method is adequate, rather than a full unfolding as used for the differential jet cross-section measurement.

The systematic uncertainties in the gap fraction measurements were evaluated as discussed in Section 5, and the uncertainties from different sources added in quadrature. The results are shown in Figure 10 as relative uncertainties $\Delta f/f$ in the measured gap fraction for two illustrative rapidity intervals, $|y| < 0.8$ and $|y| < 2.1$.

7.1 Gap fraction results in rapidity regions

Figures 11 and 12 show the resulting measurements of the gap fraction $f(Q_0)$ in data, corrected to the particle level. Figure 13 shows the analogous results for $f(Q_{\text{sum}})$, for the $|y| < 0.8$ and $|y| < 2.1$ regions only. The gap fraction plots and the first sets of ratio plots compare the data to the same NLO generator configurations as studied in Section 6.3. The middle ratio plots compare the data to the predictions of the leading-order multi-leg generators Alpgen + Pythia6, Alpgen + Herwig and MadGraph + Pythia6. The lower ratio plots compare the data to AcerMC + Pythia6, Alpgen + Pythia6 and MadGraph + Pythia6

Q_0 [GeV]	$f(Q_0)$ [%] Data ±(stat.)±(syst.)	Powheg +Pythia6 $h_{\text{damp}} = \infty$	Powheg +Pythia6 $h_{\text{damp}} = m_t$	Powheg +Pythia8 $h_{\text{damp}} = m_t$	MC@NLO +Herwig	Powheg +Herwig $h_{\text{damp}} = \infty$	ρ^i_j (stat.+syst.)
veto region: $\lvert y\rvert < 0.8$							
25	76.5±0.4±1.1	76.0±0.2	78.1±0.2	76.1±0.2	79.1±0.2	74.6±0.2	$\rho^{25}_{75} = 0.65$
75	93.2±0.2±0.3	92.3±0.1	93.8±0.1	93.0±0.1	94.3±0.1	92.3±0.1	$\rho^{75}_{150} = 0.56$
150	97.8±0.1±0.2	97.3±0.1	98.0±0.1	97.8±0.1	98.3±0.1	97.4±0.1	$\rho^{150}_{25} = 0.31$
veto region: $0.8 < \lvert y\rvert < 1.5$							
25	79.8±0.4±1.1	79.7±0.2	81.6±0.2	80.1±0.2	81.8±0.2	79.2±0.2	$\rho^{25}_{75} = 0.59$
75	94.5±0.2±0.3	93.5±0.1	94.7±0.1	94.3±0.1	94.7±0.1	93.7±0.1	$\rho^{75}_{150} = 0.77$
150	98.2±0.1±0.2	97.8±0.1	98.3±0.1	98.3±0.1	98.3±0.1	97.9±0.1	$\rho^{150}_{25} = 0.39$
veto region: $1.5 < \lvert y\rvert < 2.1$							
25	85.3±0.3±0.9	84.9±0.2	86.1±0.2	85.4±0.2	85.5±0.2	84.7±0.2	$\rho^{25}_{75} = 0.77$
75	96.0±0.2±0.4	95.5±0.1	96.2±0.1	96.0±0.1	95.5±0.1	95.5±0.1	$\rho^{75}_{150} = 0.89$
150	98.7±0.1±0.2	98.6±0.1	98.9±0.0	98.9±0.0	98.6±0.1	98.6±0.1	$\rho^{150}_{25} = 0.64$
veto region: $\lvert y\rvert < 2.1$							
25	53.9±0.5±1.7	53.6±0.2	56.7±0.2	54.5±0.2	56.2±0.2	52.0±0.2	$\rho^{25}_{75} = 0.66$
75	84.8±0.3±0.6	82.9±0.2	85.8±0.2	85.0±0.2	85.3±0.2	83.0±0.2	$\rho^{75}_{150} = 0.74$
150	94.9±0.2±0.3	93.8±0.1	95.4±0.1	95.2±0.1	95.3±0.1	94.1±0.1	$\rho^{150}_{25} = 0.34$

Table 4: The measured gap fraction values $f(Q_0)$ for different veto-region rapidity intervals and Q_0 values of 25, 75 and 150 GeV in data compared to the predictions from various $t\bar{t}$ simulation samples. The combination of statistical and systematic correlations between measurements at $Q_0 = i$ and $Q_0 = j$ is given as ρ^i_j.

samples with increased and decreased levels of parton shower radiation. The numerical values of the gap fraction measurements are presented as a function of Q_0 in Table 4 and as a function of Q_{sum} in Table 5, together with the values predicted by the generators shown in the upper plots of Figures 11, 12 and 13. The matrix of statistical and systematic correlations is shown in Figure 14 for the gap fraction measurement at different values of Q_0 for the full central $|y| < 2.1$ rapidity region. Nearby points in Q_0 are highly correlated, while well-separated Q_0 points are less correlated. The full covariance matrix including correlations was used to calculate a χ^2 value for the consistency of each of the NLO generator predictions with the data in each veto region. The results are shown in Tables 6 and 7.

All the NLO generators provide a reasonable description of the $f(Q_0)$ distribution in the regions $|y| < 0.8$ and $0.8 < |y| < 1.5$. All these generators are also consistent with the data in the most forward region ($1.5 < |y| < 2.1$), whereas at $\sqrt{s} = 7$ TeV, they tended to lie below the data [2]. However, the current measurements are significantly more precise in this region, thanks in particular to improvements in the jet energy scale calibration. Over the full rapidity range ($|y| < 2.1$), Powheg + Pythia8 provides the best description of the data, whilst Powheg + Pythia6 with $h_{\text{damp}} = m_t$ and MC@NLO + Herwig predict slightly less radiation, and Powheg + Pythia6 with $h_{\text{damp}} = \infty$ and Powheg + Herwig predict slightly more. Powheg + Pythia8 also provides the best description across the individual $|y|$ regions. The results for $f(Q_{\text{sum}})$, which are sensitive to all the additional jets within the rapidity interval, show somewhat larger differences between the generators than those for $f(Q_0)$. Over the rapidity region $|y| < 2.1$, Powheg + Pythia6 with $h_{\text{damp}} = m_t$ and MC@NLO + Herwig are disfavoured. The latter generator combination also performs poorly for the differential cross-section measurements discussed in Section 6.

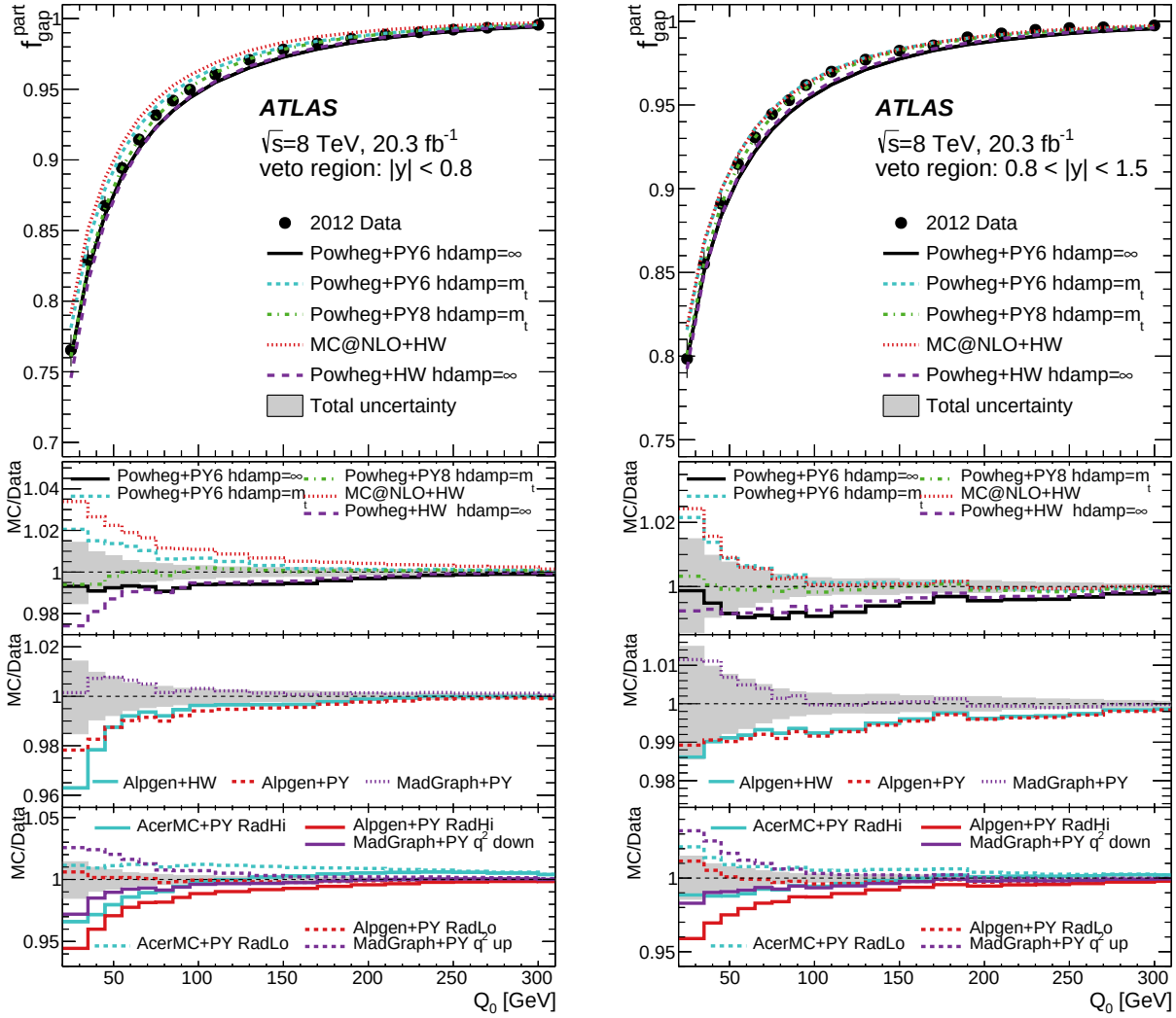
The leading-order generators Alpgen + Pythia6, Alpgen + Herwig and MadGraph +Pythia6 also provide a reasonable description of the gap fraction as a function of Q_0 and Q_{sum}. The pairs of samples with

Q_{sum} [GeV]	$f(Q_{\text{sum}})$ [%] Data ±(stat.)±(syst.)	Powheg +Pythia6 $h_{\text{damp}} = \infty$	Powheg +Pythia6 $h_{\text{damp}} = m_t$	Powheg +Pythia8 $h_{\text{damp}} = m_t$	MC@NLO +Herwig	Powheg +Herwig $h_{\text{damp}} = \infty$	ρ^i_j (stat.+syst.)
veto region: $\|y\| < 0.8$							
55	88.1±0.3±0.5	87.7±0.2	89.5±0.1	88.1±0.2	90.2±0.1	87.2±0.2	$\rho^{55}_{150} = 0.70$
150	97.0±0.2±0.2	96.4±0.1	97.3±0.1	96.9±0.1	97.9±0.1	96.5±0.1	$\rho^{150}_{300} = 0.57$
300	99.4±0.1±0.1	99.1±0.0	99.4±0.0	99.3±0.0	99.6±0.0	99.2±0.0	$\rho^{300}_{55} = 0.47$
veto region: $0.8 < \|y\| < 1.5$							
55	90.5±0.3±0.6	89.8±0.1	91.3±0.1	90.5±0.1	91.4±0.1	89.9±0.1	$\rho^{55}_{150} = 0.68$
150	97.8±0.1±0.2	97.2±0.1	97.9±0.1	97.7±0.1	98.0±0.1	97.4±0.1	$\rho^{150}_{300} = 0.42$
300	99.6±0.1±0.1	99.4±0.0	99.6±0.0	99.5±0.0	99.7±0.0	99.5±0.0	$\rho^{300}_{55} = 0.31$
veto region: $1.5 < \|y\| < 2.1$							
55	93.1±0.2±0.8	92.8±0.1	93.8±0.1	93.4±0.1	93.2±0.1	92.8±0.1	$\rho^{55}_{150} = 0.89$
150	98.5±0.1±0.3	98.3±0.1	98.7±0.1	98.6±0.1	98.5±0.1	98.3±0.1	$\rho^{150}_{300} = 0.64$
300	99.8±0.0±0.1	99.7±0.0	99.8±0.0	99.8±0.0	99.8±0.0	99.7±0.0	$\rho^{300}_{55} = 0.60$
veto region: $\|y\| < 2.1$							
55	72.7±0.4±1.3	71.8±0.2	75.2±0.2	73.3±0.2	74.7±0.2	71.1±0.2	$\rho^{55}_{150} = 0.89$
150	91.3±0.3±0.5	89.9±0.1	92.2±0.1	91.2±0.1	92.6±0.1	90.1±0.1	$\rho^{150}_{300} = 0.79$
300	98.0±0.1±0.2	97.3±0.1	98.1±0.1	97.7±0.1	98.6±0.1	97.5±0.1	$\rho^{300}_{55} = 0.73$

Table 5: The measured gap fraction values $f(Q_{\text{sum}})$ for different veto-region rapidity intervals and Q_{sum} values of 55, 150 and 300 GeV in data compared to the predictions from various $t\bar{t}$ simulation samples. The combination of statistical and systematic correlations between measurements at $Q_{\text{sum}} = i$ and $Q_{\text{sum}} = j$ is given as ρ^i_j.

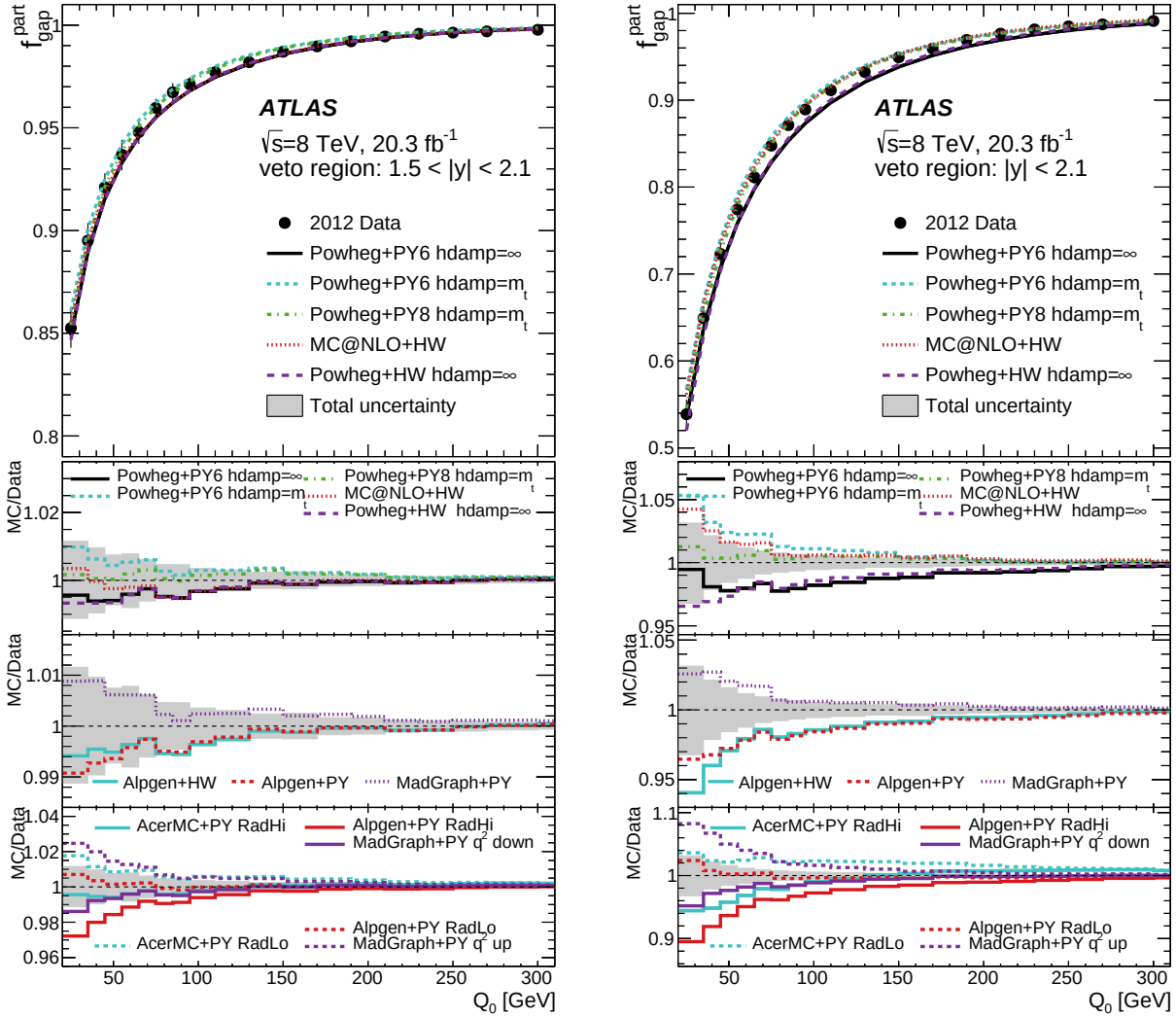
Q_0	$\|y\| < 0.8$		$0.8 < \|y\| < 1.5$		$1.5 < \|y\| < 2.1$		$\|y\| < 2.1$	
Generator	χ^2	p-value	χ^2	p-value	χ^2	p-value	χ^2	p-value
Powheg+Pythia6 $h_{\text{damp}} = \infty$	15.6	6.2×10^{-1}	29.8	3.9×10^{-2}	26.3	9.3×10^{-2}	31.1	2.8×10^{-2}
Powheg+Pythia6 $h_{\text{damp}} = m_t$	17.3	5.0×10^{-1}	20.4	3.1×10^{-1}	28.6	5.4×10^{-2}	25.6	1.1×10^{-1}
Powheg+Pythia8 $h_{\text{damp}} = m_t$	11.1	8.9×10^{-1}	16.8	5.4×10^{-1}	23.2	1.8×10^{-1}	16.6	5.5×10^{-1}
MC@NLO+Herwig	22.9	2.0×10^{-1}	17.9	4.7×10^{-1}	29.9	3.9×10^{-2}	18.5	4.3×10^{-1}
Powheg+Herwig $h_{\text{damp}} = \infty$	16.7	5.5×10^{-1}	24.1	1.5×10^{-1}	29.4	4.4×10^{-2}	21.5	2.5×10^{-1}
Alpgen+Herwig	21.8	2.4×10^{-1}	27.0	8.0×10^{-2}	35.3	8.8×10^{-3}	21.9	2.4×10^{-1}
Alpgen+Pythia6	13.2	7.8×10^{-1}	27.4	7.2×10^{-2}	29.0	4.8×10^{-2}	24.8	1.3×10^{-1}
MadGraph+Pythia6	12.3	8.3×10^{-1}	19.7	3.5×10^{-1}	28.9	5.0×10^{-2}	16.3	5.7×10^{-1}
AcerMC+Pythia6 RadHi	81.0	5.8×10^{-10}	44.6	4.7×10^{-4}	40.2	2.0×10^{-3}	112.5	1.1×10^{-15}
AcerMC+Pythia6 RadLo	55.5	1.1×10^{-5}	38.4	3.4×10^{-3}	41.5	1.3×10^{-3}	93.9	2.9×10^{-12}
Alpgen+Pythia6 RadHi	35.1	9.2×10^{-3}	47.0	2.1×10^{-4}	38.8	3.0×10^{-3}	40.7	1.7×10^{-3}
Alpgen+Pythia6 RadLo	11.2	8.9×10^{-1}	19.0	4.0×10^{-1}	25.2	1.2×10^{-1}	18.8	4.1×10^{-1}
MadGraph+Pythia6 q^2 down	17.8	4.7×10^{-1}	25.2	1.2×10^{-1}	33.7	1.4×10^{-2}	21.1	2.8×10^{-1}
MadGraph+Pythia6 q^2 up	21.0	2.8×10^{-1}	25.3	1.2×10^{-1}	32.4	1.9×10^{-2}	28.0	6.2×10^{-2}

Table 6: Values of χ^2 for the comparison of the measured gap fraction distributions with the predictions from various $t\bar{t}$ generator configurations, for the four rapidity regions as a function of Q_0. The χ^2 and p-values correspond to 18 degrees of freedom.



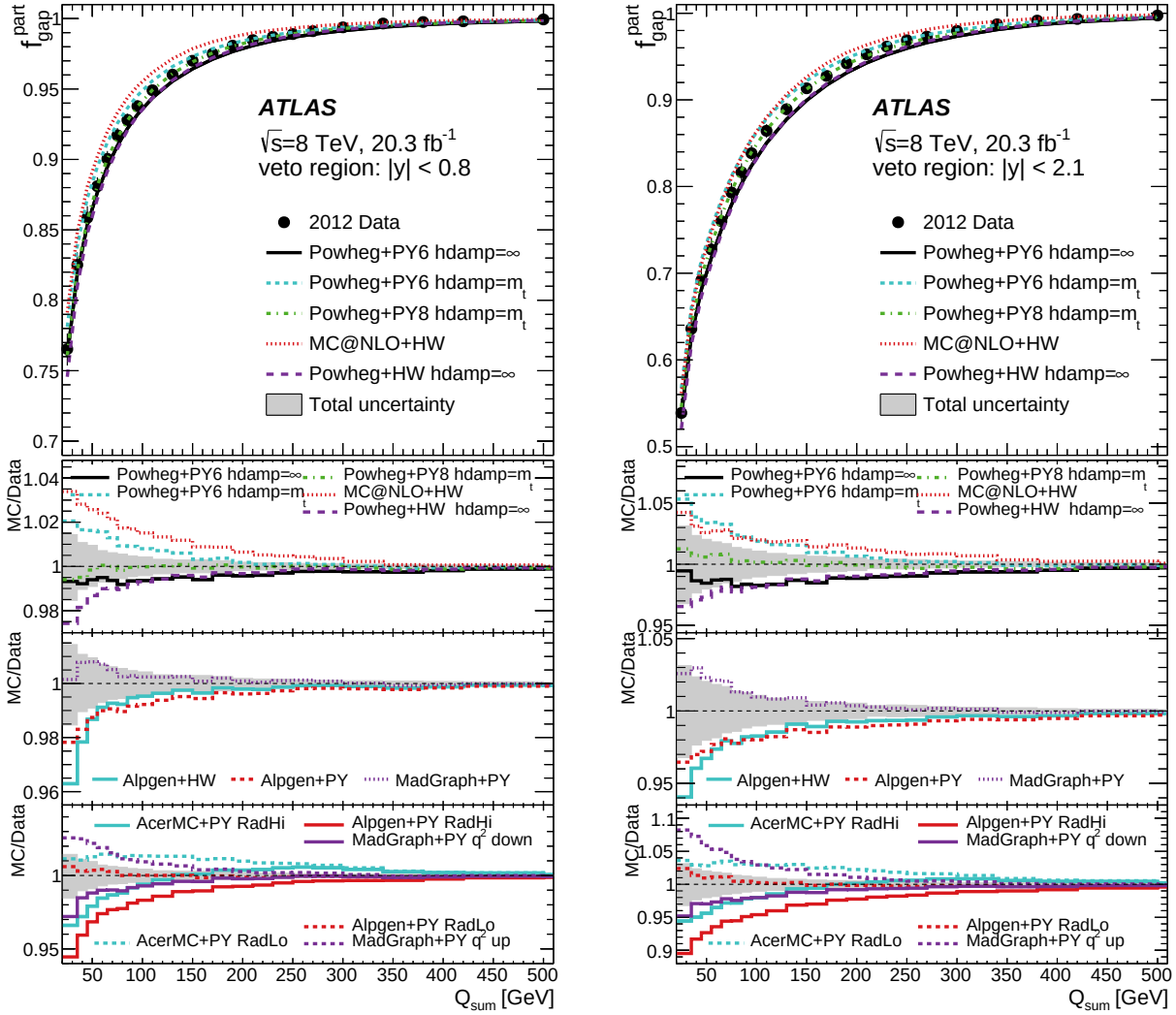
(a) (b)

Figure 11: The measured gap fraction $f(Q_0)$ as a function of Q_0 in different veto-region rapidity intervals Δy, for (a) $|y| < 0.8$ and (b) $0.8 < |y| < 1.5$. The data are shown by the points with error bars indicating the total uncertainty, and compared to the predictions from various $t\bar{t}$ simulation samples (see text) shown as smooth curves. The lower plots show the ratio of predictions to data, with the data uncertainty being indicated by the shaded band, and the Q_0 thresholds corresponding to the left edges of the histogram bins, except for the first bin.



(a) (b)

Figure 12: The measured gap fraction $f(Q_0)$ as a function of Q_0 in different veto-region rapidity intervals Δy, for (a) $1.5 < |y| < 2.1$ and (b) $|y| < 2.1$. The data are shown by the points with error bars indicating the total uncertainty, and compared to the predictions from various $t\bar{t}$ simulation samples (see text) shown as smooth curves. The lower plots show the ratio of predictions to data, with the data uncertainty being indicated by the shaded band, and the Q_0 thresholds corresponding to the left edges of the histogram bins, except for the first bin.



(a) (b)

Figure 13: The measured gap fraction $f(Q_{\text{sum}})$ as a function of Q_{sum} in different veto-region rapidity intervals Δy, for (a) $|y| < 0.8$ and (b) $|y| < 2.1$. The data are shown by the points with error bars indicating the total uncertainty, and compared to the predictions from various $t\bar{t}$ simulation samples (see text) shown as smooth curves. The lower plots show the ratio of predictions to data, with the data uncertainty being indicated by the shaded band, and the Q_{sum} thresholds corresponding to the left edges of the histogram bins, except for the first bin.

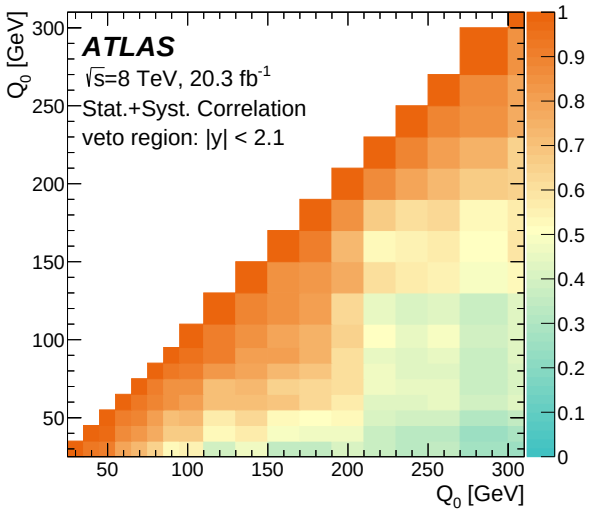


Figure 14: The correlation matrix (including statistical and systematic correlations) for the gap fraction measurement at different values of Q_0 for the full central rapidity region $|y| < 2.1$.

Q_{sum}	$\lvert y\rvert < 0.8$		$0.8 < \lvert y\rvert < 1.5$		$1.5 < \lvert y\rvert < 2.1$		$\lvert y\rvert < 2.1$	
Generator	χ^2	p-value	χ^2	p-value	χ^2	p-value	χ^2	p-value
Powheg+Pythia6 $h_{\text{damp}} = \infty$	22.3	4.4×10^{-1}	41.9	6.5×10^{-3}	25.8	2.6×10^{-1}	39.1	1.4×10^{-2}
Powheg+Pythia6 $h_{\text{damp}} = m_t$	25.6	2.7×10^{-1}	33.8	5.2×10^{-2}	27.8	1.8×10^{-1}	47.0	1.5×10^{-3}
Powheg+Pythia8 $h_{\text{damp}} = m_t$	18.3	6.9×10^{-1}	27.3	2.0×10^{-1}	21.9	4.6×10^{-1}	34.3	4.6×10^{-2}
MC@NLO+Herwig	32.2	7.4×10^{-2}	28.5	1.6×10^{-1}	32.1	7.5×10^{-2}	44.6	3.0×10^{-3}
Powheg+Herwig $h_{\text{damp}} = \infty$	21.4	5.0×10^{-1}	37.7	2.0×10^{-2}	29.6	1.3×10^{-1}	29.9	1.2×10^{-1}
Alpgen+Herwig	33.1	6.1×10^{-2}	37.7	2.0×10^{-2}	32.4	7.1×10^{-2}	31.4	8.8×10^{-2}
Alpgen+Pythia6	23.0	4.0×10^{-1}	39.7	1.2×10^{-2}	28.8	1.5×10^{-1}	37.0	2.4×10^{-2}
MadGraph+Pythia6	20.1	5.7×10^{-1}	30.3	1.1×10^{-1}	28.1	1.7×10^{-1}	31.9	7.9×10^{-2}
AcerMC+Pythia6 RadHi	75.0	1.1×10^{-7}	48.0	1.1×10^{-3}	35.5	3.4×10^{-2}	91.1	2.2×10^{-10}
AcerMC+Pythia6 RadLo	62.4	9.9×10^{-6}	46.4	1.8×10^{-3}	35.6	3.4×10^{-2}	94.8	5.2×10^{-11}
Alpgen+Pythia6 RadHi	44.3	3.3×10^{-3}	62.3	1.0×10^{-5}	42.2	5.9×10^{-3}	61.3	1.4×10^{-5}
Alpgen+Pythia6 RadLo	17.4	7.4×10^{-1}	34.6	4.2×10^{-2}	26.8	2.2×10^{-1}	34.6	4.2×10^{-2}
MadGraph+Pythia6 q^2 down	22.5	4.3×10^{-1}	35.3	3.6×10^{-2}	31.1	9.5×10^{-2}	29.3	1.4×10^{-1}
MadGraph+Pythia6 q^2 up	25.0	3.0×10^{-1}	38.4	1.7×10^{-2}	34.3	4.6×10^{-2}	50.8	4.6×10^{-4}

Table 7: Values of χ^2 for the comparison of the measured gap fraction distributions with the predictions from various $t\bar{t}$ generator configurations, for the four rapidity regions as a function of Q_{sum}. The χ^2 and p-values correspond to 22 degrees of freedom.

increased/decreased radiation also bracket the data in all rapidity regions, except for AcerMC + Pythia6, which always predicts higher gap fractions than observed at high Q_0 and Q_{sum}. As in the differential cross-section measurements, the data show a clear preference for the 'RadLo' variation for Alpgen + Pythia6 and the 'q^2 down' variation for MadGraph+Pythia6, across all rapidity regions. These data should therefore allow the uncertainties due to radiation modelling in $t\bar{t}$ events to be significantly reduced, once the models are tuned to these more precise $\sqrt{s} = 8\,\text{TeV}$ results rather than the $\sqrt{s} = 7\,\text{TeV}$ results used previously [2].

7.2 Gap fraction results in $e\mu b\bar{b}$ mass regions

The gap fraction was also measured over the full rapidity veto region $|y| < 2.1$ after dividing the data sample into four regions of $m_{e\mu b\bar{b}}$. The distribution of reconstructed $m_{e\mu b\bar{b}}$ in the selected $e\mu b\bar{b}$ events is shown in Figure 15, and is reasonably well-reproduced by the baseline $t\bar{t}$ simulation sample. The distribution was divided into four regions at both reconstruction and particle level: $m_{e\mu b\bar{b}} < 300\,\text{GeV}$, $300 < m_{e\mu b\bar{b}} < 425\,\text{GeV}$, $425 < m_{e\mu b\bar{b}} < 600\,\text{GeV}$ and $m_{e\mu b\bar{b}} > 600\,\text{GeV}$. These boundaries were chosen to minimise migration between the regions; in the baseline simulation, around 85 % of the reconstructed events in each $m_{e\mu b\bar{b}}$ region come from the corresponding region at particle level. The corresponding correction factors $C_m(Q_0)$ which translate the measured gap fraction in the reconstruction-level $m_{e\mu b\bar{b}}$ region to the corresponding particle-level gap fractions $f_m(Q_0)$ and $f_m(Q_{\text{sum}})$, are of similar size to $C(Q_0)$, with the exception of the highest $m_{e\mu b\bar{b}}$ region, where they reach about 1.1 at low Q_0. The systematic uncertainties in the gap fraction measurement in two $m_{e\mu b\bar{b}}$ regions are shown in Figure 16. The magnitudes of the systematic uncertainties are comparable to those in the full $m_{e\mu b\bar{b}}$ range, except for the highest $m_{e\mu b\bar{b}}$ region where they are significantly larger.

Figures 17 and 18 show the resulting measurements of the gap fractions as a function of Q_0 in the four $m_{e\mu b\bar{b}}$ regions in data, compared to the same set of predictions as shown in Figures 11, 12 and 13. Tables 8 and 9 show the gap fractions at selected Q_0 and Q_{sum} values in each invariant mass region, again compared to predictions from the first set of generators. Figure 19 gives an alternative presentation of the gap fraction $f_m(Q_0)$ as a function of $m_{e\mu b\bar{b}}$ for four different Q_0 values. The χ^2 values for the consistency of the prediction from each NLO generator with data in the four mass regions are given in Tables 10 and 11.

In general, the different generator configurations provide a good model of the evolution of the gap fraction distributions with $m_{e\mu b\bar{b}}$, and similar trends in the predictions of individual generators are seen as for the inclusive $|y| < 2.1$ results discussed in Section 7.1. However, it can be seen from Figures 18 and 19 that in the $425 < m_{e\mu b\bar{b}} < 600\,\text{GeV}$ region, the NLO generator predictions split into two groups, with Powheg + Herwig and Powheg + Pythia6 with $h_{\text{damp}} = \infty$ being consistent with the data, and Powheg + Pythia6 with $h_{\text{damp}} = m_t$, Powheg + Pythia8 and MC@NLO + Herwig predicting a slightly larger gap fraction (and hence less radiation). In the region with $m_{e\mu b\bar{b}} > 600\,\text{GeV}$, the measurement uncertainties are too large to discriminate between the predictions.

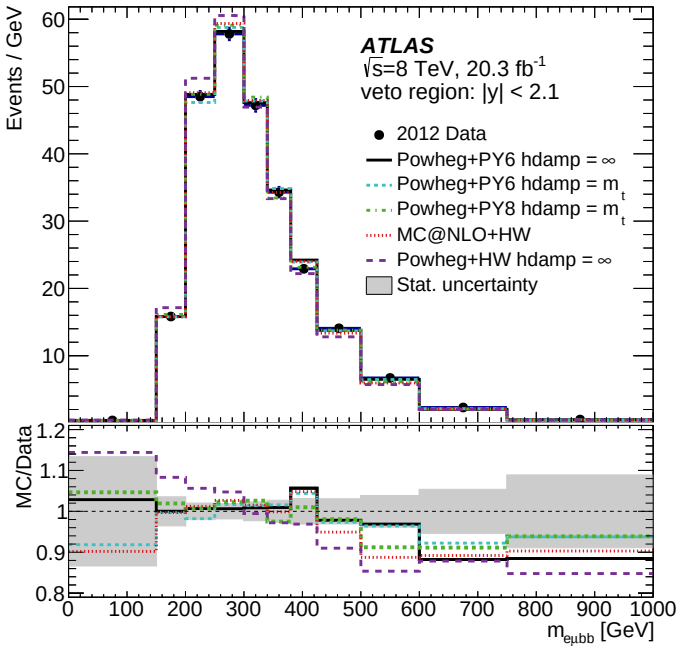


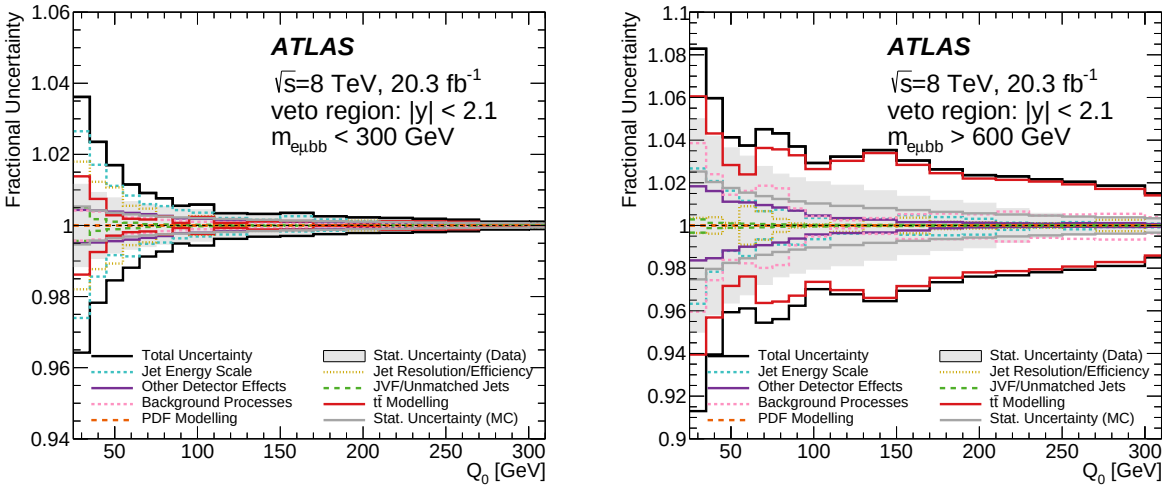
Figure 15: Distribution of the reconstructed invariant mass of the $e\mu b\bar{b}$ system $m_{e\mu b\bar{b}}$ in data, compared to simulation using various $t\bar{t}$ generators. The shaded band represents the statistical uncertainty in data. The lower plot shows the ratio of the distribution of invariant mass in data to that in each of the simulation samples.

	$f_m(Q_0)$ [%]						
Q_0 [GeV]	Data ±(stat.)±(syst.)	Powheg +Pythia6 $h_{\text{damp}} = \infty$	Powheg +Pythia6 $h_{\text{damp}} = m_t$	Powheg +Pythia8 $h_{\text{damp}} = m_t$	MC@NLO +Herwig	Powheg +Herwig $h_{\text{damp}} = \infty$	ρ^i_j (stat.+syst.)
veto region: $\|y\| < 2.1$, $m_{e\mu b\bar{b}} < 300$ GeV							
25	56.0±0.6±2.0	55.1±0.3	57.8±0.3	56.0±0.3	57.3±0.3	53.5±0.3	$\rho^{25}_{75} = 0.60$
75	86.7±0.5±0.7	84.3±0.3	86.9±0.2	86.2±0.2	86.4±0.2	84.4±0.2	$\rho^{75}_{150} = 0.80$
150	95.7±0.3±0.3	94.5±0.2	95.9±0.1	95.7±0.1	95.9±0.1	94.7±0.2	$\rho^{150}_{25} = 0.50$
veto region: $\|y\| < 2.1$, $300 < m_{e\mu b\bar{b}} < 425$ GeV							
25	54.4±0.8±1.8	53.5±0.4	57.0±0.4	54.6±0.4	56.2±0.4	52.2±0.4	$\rho^{25}_{75} = 0.63$
75	84.7±0.6±0.7	82.7±0.3	85.8±0.3	84.9±0.3	85.4±0.3	83.0±0.3	$\rho^{75}_{150} = 0.48$
150	95.0±0.4±0.6	93.8±0.2	95.4±0.2	95.2±0.2	95.4±0.2	94.1±0.2	$\rho^{150}_{25} = 0.52$
veto region: $\|y\| < 2.1$, $425 < m_{e\mu b\bar{b}} < 600$ GeV							
25	47.6±1.3±1.7	51.0±0.7	54.2±0.7	51.6±0.6	53.4±0.6	48.1±0.7	$\rho^{25}_{75} = 0.63$
75	79.0±1.0±1.0	80.3±0.5	83.7±0.5	82.9±0.5	82.5±0.5	80.0±0.5	$\rho^{75}_{150} = 0.52$
150	92.7±0.7±0.8	92.6±0.3	94.4±0.3	94.2±0.3	94.0±0.3	92.6±0.3	$\rho^{150}_{25} = 0.11$
veto region: $\|y\| < 2.1$, $m_{e\mu b\bar{b}} > 600$ GeV							
25	45.9±2.3±3.9	45.2±1.2	49.8±1.2	46.8±1.2	51.0±1.2	43.9±1.2	$\rho^{25}_{75} = 0.82$
75	81.7±2.0±3.6	75.7±1.0	80.3±1.0	78.8±1.0	79.8±1.0	75.9±1.1	$\rho^{75}_{150} = 0.85$
150	92.4±1.3±2.8	89.7±0.7	92.6±0.6	92.3±0.6	91.5±0.7	90.5±0.7	$\rho^{150}_{25} = 0.72$

Table 8: The measured gap fraction values $f_m(Q_0)$ for the veto region $|y| < 2.1$ and four invariant mass regions, for Q_0 values of 25, 75 and 150 GeV in data compared to the predictions from various $t\bar{t}$ simulation samples. The combination of statistical and systematic correlations between measurements at $Q_0 = i$ and $Q_0 = j$ is given as ρ^i_j.

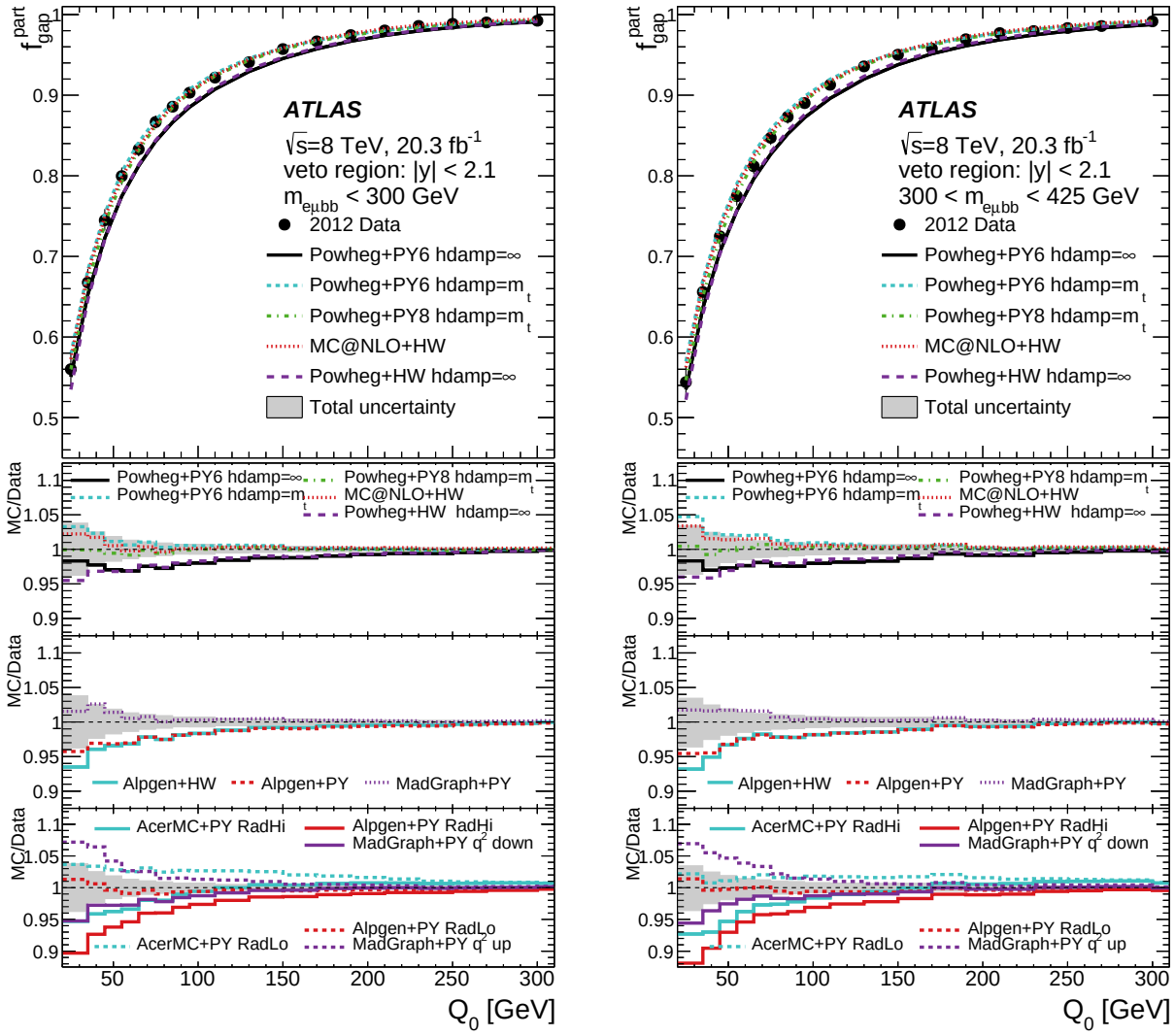
Q_{sum} [GeV]	$f_m(Q_{\text{sum}})$ [%] Data ±(stat.)±(syst.)	Powheg +Pythia6 $h_{\text{damp}} = \infty$	Powheg +Pythia6 $h_{\text{damp}} = m_t$	Powheg +Pythia8 $h_{\text{damp}} = m_t$	MC@NLO +Herwig	Powheg +Herwig $h_{\text{damp}} = \infty$	ρ^i_j (stat.+syst.)
veto region: $\|y\| < 2.1$, $m_{e\mu b\bar{b}} < 300$ GeV							
55	75.0±0.6±1.4	73.5±0.3	76.7±0.3	74.9±0.3	76.1±0.3	72.8±0.3	$\rho^{55}_{150} = 0.80$
150	92.5±0.4±0.5	91.0±0.2	93.0±0.2	92.2±0.2	93.5±0.2	91.1±0.2	$\rho^{150}_{300} = 0.71$
300	98.3±0.2±0.2	97.8±0.1	98.4±0.1	98.1±0.1	98.9±0.1	97.9±0.1	$\rho^{300}_{55} = 0.71$
veto region: $\|y\| < 2.1$, $300 < m_{e\mu b\bar{b}} < 425$ GeV							
55	72.8±0.7±1.3	71.7±0.4	75.2±0.4	73.2±0.4	74.8±0.3	71.1±0.4	$\rho^{55}_{150} = 0.78$
150	91.4±0.5±0.8	90.0±0.2	92.2±0.2	91.2±0.2	92.8±0.2	90.1±0.2	$\rho^{150}_{300} = 0.65$
300	98.1±0.2±0.2	97.3±0.1	98.1±0.1	97.7±0.1	98.6±0.1	97.5±0.1	$\rho^{300}_{55} = 0.62$
veto region: $\|y\| < 2.1$, $425 < m_{e\mu b\bar{b}} < 600$ GeV							
55	67.4±1.2±2.2	68.7±0.6	72.5±0.6	70.3±0.6	71.5±0.6	67.3±0.6	$\rho^{55}_{150} = 0.61$
150	87.9±0.8±0.8	87.9±0.4	90.6±0.4	89.5±0.4	90.6±0.4	87.7±0.4	$\rho^{150}_{300} = 0.61$
300	96.4±0.5±0.3	96.4±0.2	97.4±0.2	97.1±0.2	98.0±0.2	96.6±0.2	$\rho^{300}_{55} = 0.31$
veto region: $\|y\| < 2.1$, $m_{e\mu b\bar{b}} > 600$ GeV							
55	63.2±2.3±4.2	62.6±1.2	67.6±1.1	65.0±1.1	67.9±1.1	61.9±1.2	$\rho^{55}_{150} = 0.82$
150	87.3±1.7±3.0	83.6±0.9	87.6±0.8	85.4±0.8	87.3±0.8	84.1±0.9	$\rho^{150}_{300} = 0.80$
300	97.3±0.8±2.3	94.5±0.6	96.3±0.5	95.7±0.5	96.5±0.5	95.1±0.5	$\rho^{300}_{55} = 0.74$

Table 9: The measured gap fraction values $f_m(Q_{\text{sum}})$ for the veto region $|y| < 2.1$ and four invariant mass regions, for Q_{sum} values of 55, 150 and 300 GeV in data compared to the predictions from various $t\bar{t}$ simulation samples. The combination of statistical and systematic correlations between measurements at $Q_{\text{sum}} = i$ and $Q_{\text{sum}} = j$ is given as ρ^i_j.



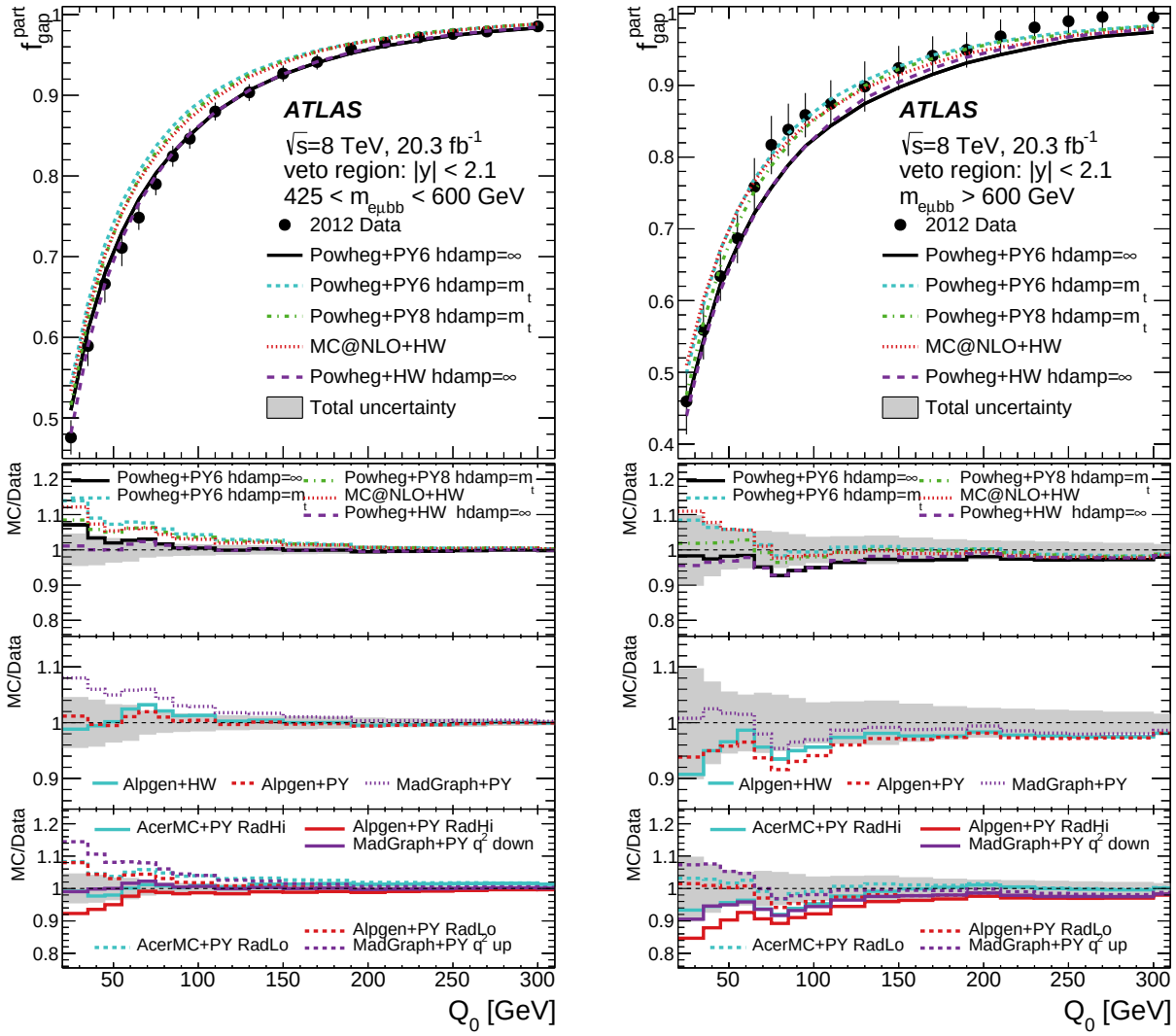
(a) (b)

Figure 16: Envelope of fractional uncertainties $\Delta f/f$ in the gap fraction $f_m(Q_0)$ for (a) $m_{e\mu b\bar{b}} < 300$ GeV and (b) $m_{e\mu b\bar{b}} > 600$ GeV. The statistical uncertainty is shown by the hatched area, and the total systematic uncertainty by the solid black line. The systematic uncertainty is also shown broken down into several groups, each of which includes various individual components (see text).



(a) (b)

Figure 17: The measured gap fraction $f_m(Q_0)$ as a function of Q_0 in the veto region $|y| < 2.1$ for the invariant mass regions (a) $m_{e\mu b\bar{b}} < 300\,\text{GeV}$ and (b) $300 < m_{e\mu b\bar{b}} < 425\,\text{GeV}$. The data are shown by the points with error bars indicating the total uncertainty, and compared to the predictions from various $t\bar{t}$ simulation samples (see text) shown as smooth curves. The lower plots show the ratio of predictions to data, with the data uncertainty being indicated by the shaded band, and the Q_0 thresholds corresponding to the left edges of the histogram bins, except for the first bin.



(a) (b)

Figure 18: The measured gap fraction $f_m(Q_0)$ as a function of Q_0 in the veto region $|y| < 2.1$ for the invariant mass regions (a) $425 < m_{e\mu b\bar{b}} < 600\,\text{GeV}$ and (b) $m_{e\mu b\bar{b}} > 600\,\text{GeV}$. The data are shown by the points with error bars indicating the total uncertainty, and compared to the predictions from various $t\bar{t}$ simulation samples (see text) shown as smooth curves. The lower plots show the ratio of predictions to data, with the data uncertainty being indicated by the shaded band, and the Q_0 thresholds corresponding to the left edges of the histogram bins, except for the first bin.

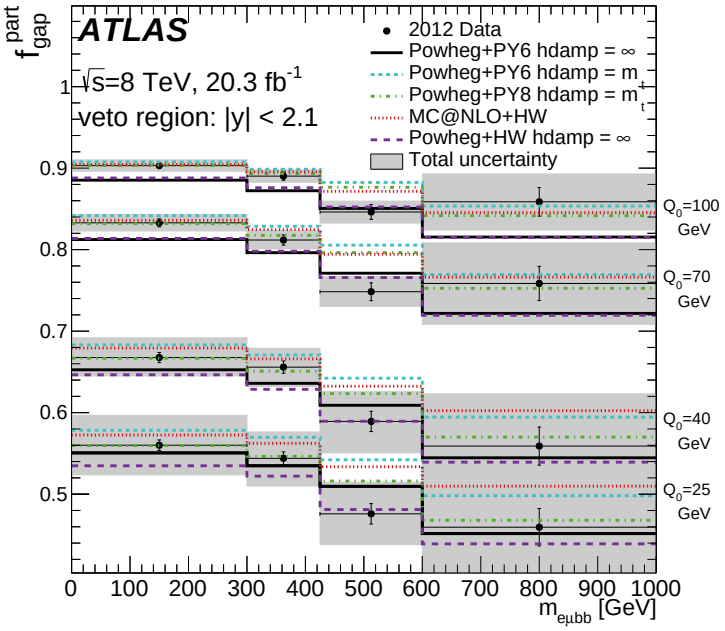


Figure 19: The gap fraction measurement $f_m(Q_0)$ as a function of the invariant mass $m_{e\mu b\bar{b}}$, for several different values of Q_0. The data are shown as points with error bars indicating the statistical uncertainties and shaded boxes the total uncertainties. The data are compared to the predictions from various $t\bar{t}$ simulation samples.

Q_0	$m < 300$ GeV		$300 < m < 425$ GeV		$425 < m < 600$ GeV		$m > 600$ GeV	
Generator	χ^2	p-value	χ^2	p-value	χ^2	p-value	χ^2	p-value
Powheg+Pythia6 $h_{\text{damp}} = \infty$	25.5	1.1×10^{-1}	27.8	6.5×10^{-2}	17.4	5.0×10^{-1}	14.0	7.3×10^{-1}
Powheg+Pythia6 $h_{\text{damp}} = m_t$	18.3	4.4×10^{-1}	22.2	2.2×10^{-1}	34.8	1.0×10^{-2}	20.0	3.3×10^{-1}
Powheg+Pythia8 $h_{\text{damp}} = m_t$	14.1	7.2×10^{-1}	18.9	4.0×10^{-1}	22.6	2.1×10^{-1}	16.0	5.9×10^{-1}
MC@NLO+Herwig	13.9	7.4×10^{-1}	18.6	4.2×10^{-1}	25.7	1.1×10^{-1}	21.9	2.4×10^{-1}
Powheg+Herwig $h_{\text{damp}} = \infty$	22.5	2.1×10^{-1}	23.5	1.7×10^{-1}	13.3	7.7×10^{-1}	14.9	6.7×10^{-1}
Alpgen+Herwig	24.6	1.4×10^{-1}	28.0	6.2×10^{-2}	19.2	3.8×10^{-1}	13.7	7.5×10^{-1}
Alpgen+Pythia6	21.6	2.5×10^{-1}	24.6	1.4×10^{-1}	13.5	7.6×10^{-1}	16.7	5.4×10^{-1}
MadGraph+Pythia6	20.2	3.2×10^{-1}	19.1	3.9×10^{-1}	20.1	3.3×10^{-1}	14.6	6.9×10^{-1}
AcerMC+Pythia6 RadHi	58.8	3.2×10^{-6}	68.7	7.4×10^{-8}	23.4	1.8×10^{-1}	21.1	2.7×10^{-1}
AcerMC+Pythia6 RadLo	52.6	3.0×10^{-5}	49.7	8.3×10^{-5}	30.3	3.5×10^{-2}	16.4	5.6×10^{-1}
Alpgen+Pythia6 RadHi	32.7	1.8×10^{-2}	39.2	2.7×10^{-3}	14.1	7.2×10^{-1}	17.8	4.7×10^{-1}
Alpgen+Pythia6 RadLo	18.7	4.1×10^{-1}	23.1	1.9×10^{-1}	20.5	3.1×10^{-1}	18.8	4.1×10^{-1}
MadGraph+Pythia6 q^2 down	24.1	1.5×10^{-1}	24.5	1.4×10^{-1}	12.6	8.1×10^{-1}	14.2	7.2×10^{-1}
MadGraph+Pythia6 q^2 up	27.6	6.9×10^{-2}	22.5	2.1×10^{-1}	30.7	3.1×10^{-2}	20.5	3.1×10^{-1}

Table 10: Values of χ^2 for the comparison of the measured gap fraction distributions with the predictions from various $t\bar{t}$ generator configurations, for the four invariant mass $m_{e\mu b\bar{b}}$ regions as a function of Q_0. The χ^2 and p-values correspond to 18 degrees of freedom.

Q_{sum}	$m < 300$ GeV		$300 < m < 425$ GeV		$425 < m < 600$ GeV		$m > 600$ GeV	
Generator	χ^2	p-value	χ^2	p-value	χ^2	p-value	χ^2	p-value
Powheg+Pythia6 $h_{\text{damp}} = \infty$	35.8	3.2×10^{-2}	26.4	2.3×10^{-1}	13.1	9.3×10^{-1}	31.1	9.4×10^{-2}
Powheg+Pythia6 $h_{\text{damp}} = m_t$	34.7	4.1×10^{-2}	24.7	3.1×10^{-1}	26.8	2.2×10^{-1}	31.1	9.5×10^{-2}
Powheg+Pythia8 $h_{\text{damp}} = m_t$	31.2	9.3×10^{-2}	21.7	4.8×10^{-1}	13.6	9.1×10^{-1}	29.7	1.3×10^{-1}
MC@NLO+Herwig	33.5	5.5×10^{-2}	20.8	5.3×10^{-1}	24.0	3.5×10^{-1}	20.5	5.5×10^{-1}
Powheg+Herwig $h_{\text{damp}} = \infty$	35.4	3.5×10^{-2}	23.6	3.7×10^{-1}	9.8	9.9×10^{-1}	30.7	1.0×10^{-1}
Alpgen+Herwig	42.6	5.3×10^{-3}	25.3	2.8×10^{-1}	12.8	9.4×10^{-1}	30.8	9.9×10^{-2}
Alpgen+Pythia6	39.0	1.4×10^{-2}	25.9	2.6×10^{-1}	12.1	9.6×10^{-1}	31.8	8.1×10^{-2}
MadGraph+Pythia6	32.0	7.8×10^{-2}	16.7	7.8×10^{-1}	15.7	8.3×10^{-1}	29.3	1.4×10^{-1}
AcerMC+Pythia6 RadHi	64.6	4.6×10^{-6}	44.9	2.8×10^{-3}	29.4	1.4×10^{-1}	27.8	1.8×10^{-1}
AcerMC+Pythia6 RadLo	64.5	4.7×10^{-6}	30.6	1.0×10^{-1}	31.2	9.2×10^{-2}	23.3	3.8×10^{-1}
Alpgen+Pythia6 RadHi	60.5	1.9×10^{-5}	44.8	2.8×10^{-3}	15.5	8.4×10^{-1}	38.9	1.5×10^{-2}
Alpgen+Pythia6 RadLo	31.5	8.7×10^{-2}	22.6	4.3×10^{-1}	14.9	8.7×10^{-1}	25.8	2.6×10^{-1}
MadGraph+Pythia6 q^2 down	37.2	2.3×10^{-2}	18.0	7.1×10^{-1}	11.7	9.6×10^{-1}	29.3	1.4×10^{-1}
MadGraph+Pythia6 q^2 up	40.2	1.0×10^{-2}	22.3	4.4×10^{-1}	26.6	2.3×10^{-1}	27.8	1.8×10^{-1}

Table 11: Values of χ^2 for the comparison of the measured gap fraction distributions with the predictions from various $t\bar{t}$ generator configurations, for the four invariant mass $m_{e\mu b\bar{b}}$ regions as a function of Q_{sum}. The χ^2 and p-values correspond to 22 degrees of freedom.

8 Conclusions

Studies of the additional jet activity in dileptonic $t\bar{t}$ events with an opposite-sign $e\mu$ pair and two b-tagged jets have been presented, using 20.3 fb^{-1} of $\sqrt{s} = 8$ TeV pp collision data collected by the ATLAS detector at the LHC. The measurements were corrected to the particle level and defined in a fiducial region corresponding closely to the experimental acceptance, facilitating comparisons with the predictions of different Monte Carlo $t\bar{t}$ event generators. The additional-jet multiplicity for various jet p_{T} thresholds has been measured in the pseudorapidity region $|\eta| < 4.5$, together with the normalised differential cross-sections as a function of the first to the fourth jet p_{T}. The gap fraction, the fraction of events with no additional jet above a certain p_{T} threshold, has also been measured in the central rapidity region $|y| < 2.1$, for subsets of this y region, and as a function of the invariant mass of the $e\mu b\bar{b}$ system. Taken together, these measurements can help to characterise the production of additional jets in $t\bar{t}$ events, an important test of QCD and a significant source of systematic uncertainty in many measurements and searches for new physics at the LHC. The results will be made available in the HepData repository and through the Rivet analysis framework.

The measurements are generally well-described by the predictions of the next-to-leading-order generators used in ATLAS physics analyses. Both Powheg (interfaced to Pythia6, Pythia8 or Herwig) and MC@NLO + Herwig give good descriptions of the p_{T} spectrum of the first additional jet, although MC@NLO + Herwig does not describe higher jet multiplicities, or the gap fraction as a function of a threshold on the sum of the p_{T} of all additional jets. The leading-order multi-leg generators Alpgen, interfaced to Pythia6 or Herwig, and MadGraph interfaced to Pythia6, are also generally compatible with the data. The predictions of these generators are sensitive to the choice of QCD scale and parton shower parameters, and tuning to the precise measurements presented here offers considerable scope for reducing the range of parameter variations which need to be considered when evaluating $t\bar{t}$ modelling uncertainties, compared to the ranges derived from previous analyses based on smaller $\sqrt{s} = 7$ TeV ATLAS data samples.

Acknowledgements

We thank CERN for the very successful operation of the LHC, as well as the support staff from our institutions without whom ATLAS could not be operated efficiently.

We acknowledge the support of ANPCyT, Argentina; YerPhI, Armenia; ARC, Australia; BMWFW and FWF, Austria; ANAS, Azerbaijan; SSTC, Belarus; CNPq and FAPESP, Brazil; NSERC, NRC and CFI, Canada; CERN; CONICYT, Chile; CAS, MOST and NSFC, China; COLCIENCIAS, Colombia; MSMT CR, MPO CR and VSC CR, Czech Republic; DNRF and DNSRC, Denmark; IN2P3-CNRS, CEA-DSM/IRFU, France; GNSF, Georgia; BMBF, HGF, and MPG, Germany; GSRT, Greece; RGC, Hong Kong SAR, China; ISF, I-CORE and Benoziyo Center, Israel; INFN, Italy; MEXT and JSPS, Japan; CNRST, Morocco; FOM and NWO, Netherlands; RCN, Norway; MNiSW and NCN, Poland; FCT, Portugal; MNE/IFA, Romania; MES of Russia and NRC KI, Russian Federation; JINR; MESTD, Serbia; MSSR, Slovakia; ARRS and MIZŠ, Slovenia; DST/NRF, South Africa; MINECO, Spain; SRC and Wallenberg Foundation, Sweden; SERI, SNSF and Cantons of Bern and Geneva, Switzerland; MOST, Taiwan; TAEK, Turkey; STFC, United Kingdom; DOE and NSF, United States of America. In addition, individual groups and members have received support from BCKDF, the Canada Council, CANARIE, CRC, Compute Canada, FQRNT, and the Ontario Innovation Trust, Canada; EPLANET, ERC, FP7, Horizon 2020 and Marie Skłodowska-Curie Actions, European Union; Investissements d'Avenir Labex and Idex, ANR, Région Auvergne and Fondation Partager le Savoir, France; DFG and AvH Foundation, Germany; Herakleitos, Thales and Aristeia programmes co-financed by EU-ESF and the Greek NSRF; BSF, GIF and Minerva, Israel; BRF, Norway; Generalitat de Catalunya, Generalitat Valenciana, Spain; the Royal Society and Leverhulme Trust, United Kingdom.

The crucial computing support from all WLCG partners is acknowledged gratefully, in particular from CERN and the ATLAS Tier-1 facilities at TRIUMF (Canada), NDGF (Denmark, Norway, Sweden), CC-IN2P3 (France), KIT/GridKA (Germany), INFN-CNAF (Italy), NL-T1 (Netherlands), PIC (Spain), ASGC (Taiwan), RAL (UK) and BNL (USA) and in the Tier-2 facilities worldwide.

References

[1] ATLAS Collaboration, *Measurement of the $t\bar{t}$ production cross-section using $e\mu$ events with b-tagged jets in pp collisions at $\sqrt{s} = 7$ and 8 TeV with the ATLAS detector*, Eur. Phys. J. C **74** (2014) 3109, arXiv:1406.5375 [hep-ex].

[2] ATLAS Collaboration, *Measurement of $t\bar{t}$ production with a veto on additional central jet activity in pp collisions at $\sqrt{s} = 7$ TeV using the ATLAS detector*, Eur. Phys. J. C **72** (2012) 2043, arXiv:1203.5015 [hep-ex].

[3] ATLAS Collaboration, *Measurement of the $t\bar{t}$ production cross-section as a function of jet multiplicity and jet transverse momentum in 7 TeV proton–proton collisions with the ATLAS detector*, JHEP **01** (2015) 020, arXiv:1407.0891 [hep-ex].

[4] CMS Collaboration, *Measurement of jet multiplicity distributions in $t\bar{t}$ production in pp collisions at $\sqrt{s} = 7$ TeV*, Eur. Phys. J. C **74** (2015) 3014, arXiv:1404.3171 [hep-ex].

[5] CMS Collaboration, *Measurement of $t\bar{t}$ production with additional jet activity, including b quark jets, in the dilepton decay channel using pp collisions at $\sqrt{s}$ = 8 TeV*, (2015), arXiv:1510.03072 [hep-ex].

[6] A. Buckley et al., *Rivet user manual*, Comput. Phys. Commun. **184** (2013) 2803, arXiv:1003.0694 [hep-ph].

[7] ATLAS Collaboration, *Comparison of Monte Carlo generator predictions for gap fraction and jet multiplicity observables in $t\bar{t}$ events*, ATL-PHYS-PUB-2014-005, 2014, URL: http://cdsweb.cern.ch/record/1703034.

[8] ATLAS Collaboration, *Comparison of Monte Carlo generator predictions to ATLAS measurements of top pair production at 7 TeV*, ATL-PHYS-PUB-2015-002, 2015, URL: http://cdsweb.cern.ch/record/1981319.

[9] ATLAS Collaboration, *A study of the sensitivity to the* Pythia8 *parton shower parameters of $t\bar{t}$ production measurements in pp collisions at $\sqrt{s}$ = 7 TeV with the ATLAS experiment at the LHC*, ATL-PHYS-PUB-2015-007, 2015, URL: http://cdsweb.cern.ch/record/2004362.

[10] ATLAS Collaboration, *Comparison of Monte Carlo generator predictions from Powheg and Sherpa to ATLAS measurements of top pair production at 7 TeV*, ATL-PHYS-PUB-2015-011, 2015, URL: https://cds.cern.ch/record/2020602.

[11] ATLAS Collaboration, *Simulation of top-quark production for the ATLAS experiment at $\sqrt{s}$ = 13 TeV*, ATL-PHYS-PUB-2016-004, 2016, URL: http://cdsweb.cern.ch/record/2120417.

[12] ATLAS Collaboration, *The ATLAS Experiment at the CERN Large Hadron Collider*, JINST **3** (2008) S08003.

[13] ATLAS Collaboration, *Improved luminosity determination in pp collisions at $\sqrt{s}$ = 7 TeV using the ATLAS detector at the LHC*, Eur. Phys. J. C **73** (2013) 2518, arXiv:1302.4393 [hep-ex].

[14] ATLAS Collaboration, *The ATLAS Simulation Infrastructure*, Eur. Phys. J. C **70** (2010) 823, arXiv:1005.4568 [hep-ex].

[15] S. Agostinelli et al., *GEANT4: A Simulation toolkit*, Nucl. Instrum. Meth. A **506** (2003) 250.

[16] ATLAS Collaboration, *The simulation principle and performance of the ATLAS fast calorimeter simulation FastCaloSim*, ATL-PHYS-PUB-2010-013, 2010, URL: http://cds.cern.ch/record/1300517.

[17] T. Sjostrand, S. Mrenna and P. Z. Skands, *A Brief Introduction to PYTHIA 8.1*, Comput. Phys. Commun. **178** (2008) 852, arXiv:0710.3820 [hep-ph].

[18] A. D. Martin et al., *Parton distributions for the LHC*, Eur. Phys. J. C **63** (2009) 189, arXiv:0901.0002 [hep-ph].

[19] ATLAS Collaboration, *Summary of ATLAS Pythia 8 tunes*, ATL-PHYS-PUB-2012-003, 2012, URL: http://cds.cern.ch/record/1474107.

[20] P. Nason, *A new method for combining NLO QCD with shower Monte Carlo algorithms*, JHEP **0411** (2004) 040, arXiv:hep-ph/0409146.

[21] S. Frixione, P. Nason and C. Oleari, *Matching NLO QCD computations with Parton Shower simulations: the POWHEG method*, JHEP **0711** (2007) 070, arXiv:0709.2092 [hep-ph].

[22] S. Alioli et al., *A general framework for implementing NLO calculations in shower Monte Carlo programs: the POWHEG BOX*, JHEP **1006** (2010) 043, arXiv:1002.2581 [hep-ph].

[23] H.-L. Lai et al., *New parton distributions for collider physics*, Phys. Rev. D **82** (2010) 074024, arXiv:1007.2241 [hep-ph].

[24] T. Sjöstrand, S. Mrenna and P. Skands, *Pythia 6.4 Physics and Manual*, JHEP **0605** (2006) 026, arXiv:hep-ph/0603175.

[25] J. Pumplin et al., *New generation of parton distributions with uncertainties from global QCD analysis*, JHEP **0207** (2002) 012, arXiv:hep-ph/0201195.

[26] P. Z. Skands, *Tuning Monte Carlo Generators: The Perugia Tunes*, Phys. Rev. D **82** (2010) 074018, arXiv:1005.3457 [hep-ph].

[27] M. Cacciari et al., *Top-pair production at hadron colliders with next-to-next-to-leading logarithmic soft-gluon resummation*, Phys. Lett. B **710** (2012) 612, arXiv:1111.5869 [hep-ph].

[28] P. Barnreuther et al., *Percent Level Precision Physics at the Tevatron: First Genuine NNLO QCD Corrections to $q\bar{q} \to t\bar{t} + X$*, Phys. Rev. Lett. **109** (2012) 132001, arXiv:1204.5201 [hep-ph].

[29] M. Czakon and A. Mitov, *NNLO corrections to top-pair production at hadron colliders: the all-fermionic scattering channels*, JHEP **1212** (2012) 054, arXiv:1207.0236 [hep-ph].

[30] M. Czakon and A. Mitov, *NNLO corrections to top pair production at hadron colliders: the quark-gluon reaction*, JHEP **1301** (2013) 080, arXiv:1210.6832 [hep-ph].

[31] M. Czakon, P. Fiedler and A. Mitov, *The total top quark pair production cross-section at hadron colliders through $O(\alpha_S^4)$*, Phys. Rev. Lett. **110** (2013) 252004, arXiv:1303.6254 [hep-ph].

[32] M. Czakon and A. Mitov, *Top++: A Program for the Calculation of the Top-Pair Cross-Section at Hadron Colliders*, Comput. Phys. Commun. **185** (2014) 2930, arXiv:1112.5675 [hep-ph].

[33] M Botje et al., *The PDF4LHC Working Group Interim Recommendations*, (2011), arXiv:1101.0538 [hep-ph].

[34] A. D. Martin et al., *Uncertainties on α_S in global PDF analyses and implications for predicted hadronic cross sections*, Eur. Phys. J. C **64** (2009) 653, arXiv:0905.3531 [hep-ph].

[35] J. Gao et al., *The CT10 next-to-next-to-leading order global analysis of QCD*, Phys. Rev. D **89** (2014) 033009, arXiv:1302.6246 [hep-ph].

[36] R. D. Ball et al., *Parton distributions with LHC data*, Nucl. Phys. B **867** (2013) 244, arXiv:1207.1303 [hep-ph].

[37] G. Marchesini et al., *HERWIG 5.1 - a Monte Carlo event generator for simulating hadron emission reactions with interfering gluons*, Compt. Phys. Commun. **67** (1992) 465.

[38] G. Corcella et al., *HERWIG 6: An Event generator for hadron emission reactions with interfering gluons (including supersymmetric processes)*, JHEP **0101** (2001) 010, arXiv:hep-ph/0011363 [hep-ph].

[39] ATLAS Collaboration, *New ATLAS event generator tunes to 2010 data*, ATL-PHYS-PUB-2011-008, 2011, URL: http://cds.cern.ch/record/1345343.

[40] J. M. Butterworth, J. R. Forshaw and M. H. Seymour,
Multiparton interactions in photoproduction at HERA, Z. Phys. C **72** (1996) 637,
arXiv:hep-ph/9601371 [hep-ph].

[41] ATLAS Collaboration, *ATLAS Pythia 8 tunes to 7 TeV data*, ATL-PHYS-PUB-2014-021, 2014,
URL: http://cdsweb.cern.ch/record/1966419.

[42] S. Frixione and B. R. Webber, *Matching NLO QCD computations and parton shower simulations*,
JHEP **0206** (2002) 029, arXiv:hep-ph/0204244 [hep-ph].

[43] S. Frixione, P. Nason and B. R. Webber,
Matching NLO QCD and parton showers in heavy flavor production, JHEP **0308** (2003) 007,
arXiv:hep-ph/0305252 [hep-ph].

[44] M. L. Mangano et al.,
ALPGEN, a generator for hard multiparton processes in hadronic collisions,
JHEP **0307** (2003) 001, arXiv:hep-ph/0206293 [hep-ph].

[45] J. Alwall et al., *MadGraph 5 : Going Beyond*, JHEP **1106** (2011) 128,
arXiv:1106.0522 [hep-ph].

[46] B. P. Kersevan and E. Richter-Was, *The Monte Carlo event generator AcerMC versions 2.0 to 3.8 with interfaces to PYTHIA 6.4, HERWIG 6.5 and ARIADNE 4.1*,
Comput. Phys. Commun. **184** (2013) 919, arXiv:hep-ph/0405247 [hep-ph].

[47] E. Re,
Single-top Wt-channel production matched with parton showers using the POWHEG method,
Eur. Phys. J. C **71** (2011) 1547, arXiv:1009.2450 [hep-ph].

[48] C. D. White et al., *Isolating Wt production at the LHC*, JHEP **0911** (2009) 074,
arXiv:0908.0631 [hep-ph].

[49] N. Kidonakis,
Two-loop soft anomalous dimensions for single top quark associated production with a W^- or H^-,
Phys. Rev. D **82** (2010) 054018, arXiv:1005.4451 [hep-ph].

[50] J. M. Campbell and R. K. Ellis, *MCFM for the Tevatron and the LHC*,
Nucl. Phys. Proc. Suppl. **205-206** (2010) 10, arXiv:1007.3492 [hep-ph].

[51] ATLAS Collaboration, *Electron reconstruction and identification efficiency measurements with the ATLAS detector using the 2011 LHC proton–proton collision data*,
Eur. Phys. J. C **74** (2014) 2941, arXiv:1404.2240 [hep-ex].

[52] ATLAS Collaboration, *Muon reconstruction efficiency and momentum resolution of the ATLAS experiment in proton–proton collisions at $\sqrt{s} = 7$ TeV in 2010*, Eur. Phys. J. C **74** (2014) 3034,
arXiv:1404.4562 [hep-ex].

[53] M. Cacciari, G. P. Salam and G. Soyez, *The anti-k_t jet clustering algorithm*,
JHEP **0804** (2008) 063, arXiv:0802.1189 [hep-ph].

[54] M. Cacciari and G. P. Salam, *Dispelling the N^3 myth for the k_t jet-finder*,
Phys. Lett. B **641** (2006) 57, arXiv:hep-ph/0512210.

[55] ATLAS Collaboration,
Jet energy measurement with the ATLAS detector in proton–proton collisions at $\sqrt{s} = 7$ TeV,
Eur. Phys. J. C **73** (2013) 2304, arXiv:1112.6426 [hep-ex].

[56] ATLAS Collaboration, *Pile-up subtraction and suppression for jets in ATLAS*, ATLAS-CONF-2013-083, 2013, URL: http://cdsweb.cern.ch/record/1570994.

[57] ATLAS Collaboration, *Jet energy measurement and its systematic uncertainty in proton–proton collisions at $\sqrt{s}$ = 7 TeV with the ATLAS detector*, Eur. Phys. J. C **75** (2015) 17, arXiv:1406.0076 [hep-ex].

[58] ATLAS Collaboration, *Performance of pile-up mitigation techniques for jets in pp collisions with the ATLAS detector*, Nucl. Instrum. Meth. **A824** (2016) 367, arXiv:1510.03823 [hep-ex].

[59] ATLAS Collaboration, *Performance of b-Jet Identification in the ATLAS Experiment*, JINST **11** (2016) P04008, arXiv:1512.01094 [hep-ex].

[60] M. Cacciari, G. P. Salam and G. Soyez, *The Catchment Area of Jets*, JHEP **0804** (2008) 005, arXiv:0802.1188 [hep-ph].

[61] ATLAS Collaboration, *Jet energy resolution in proton–proton collisions at $\sqrt{s}$ = 7 TeV recorded in 2010 with the ATLAS detector*, Eur. Phys. J. C **73** (2013) 2306, arXiv:1210.6210 [hep-ex].

[62] ATLAS Collaboration, *Electron and photon energy calibration with the ATLAS detector using LHC Run 1 data*, Eur. Phys. J. C **74** (2014) 3071, arXiv:1407.5063 [hep-ex].

[63] ATLAS Collaboration, *Measurement of the muon reconstruction performance of the ATLAS detector using 2011 and 2012 LHC proton–proton collision data*, Eur. Phys. J. C **74** (2014) 3130, arXiv:1407.3935 [hep-ex].

[64] G. D'Agostini, *A Multidimensional unfolding method based on Bayes' theorem*, Nucl. Instrum. Meth. A **362** (1995) 487.

[65] T. Adye, *Unfolding algorithms and tests using RooUnfold*, Proceedings of the PHYSTAT 2011 workshop, (2011) 313, arXiv:1105.1160 [physics.data-an].

The ATLAS Collaboration

M. Aaboud[135d], G. Aad[86], B. Abbott[113], J. Abdallah[64], O. Abdinov[12], B. Abeloos[117], R. Aben[107], O.S. AbouZeid[137], N.L. Abraham[149], H. Abramowicz[153], H. Abreu[152], R. Abreu[116], Y. Abulaiti[146a,146b], B.S. Acharya[163a,163b,a], L. Adamczyk[40a], D.L. Adams[27], J. Adelman[108], S. Adomeit[100], T. Adye[131], A.A. Affolder[75], T. Agatonovic-Jovin[14], J. Agricola[56], J.A. Aguilar-Saavedra[126a,126f], S.P. Ahlen[24], F. Ahmadov[66,b], G. Aielli[133a,133b], H. Akerstedt[146a,146b], T.P.A. Åkesson[82], A.V. Akimov[96], G.L. Alberghi[22a,22b], J. Albert[168], S. Albrand[57], M.J. Alconada Verzini[72], M. Aleksa[32], I.N. Aleksandrov[66], C. Alexa[28b], G. Alexander[153], T. Alexopoulos[10], M. Alhroob[113], B. Ali[128], M. Aliev[74a,74b], G. Alimonti[92a], J. Alison[33], S.P. Alkire[37], B.M.M. Allbrooke[149], B.W. Allen[116], P.P. Allport[19], A. Aloisio[104a,104b], A. Alonso[38], F. Alonso[72], C. Alpigiani[138], M. Alstaty[86], B. Alvarez Gonzalez[32], D. Álvarez Piqueras[166], M.G. Alviggi[104a,104b], B.T. Amadio[16], K. Amako[67], Y. Amaral Coutinho[26a], C. Amelung[25], D. Amidei[90], S.P. Amor Dos Santos[126a,126c], A. Amorim[126a,126b], S. Amoroso[32], G. Amundsen[25], C. Anastopoulos[139], L.S. Ancu[51], N. Andari[108], T. Andeen[11], C.F. Anders[59b], G. Anders[32], J.K. Anders[75], K.J. Anderson[33], A. Andreazza[92a,92b], V. Andrei[59a], S. Angelidakis[9], I. Angelozzi[107], P. Anger[46], A. Angerami[37], F. Anghinolfi[32], A.V. Anisenkov[109,c], N. Anjos[13], A. Annovi[124a,124b], C. Antel[59a], M. Antonelli[49], A. Antonov[98,*], F. Anulli[132a], M. Aoki[67], L. Aperio Bella[19], G. Arabidze[91], Y. Arai[67], J.P. Araque[126a], A.T.H. Arce[47], F.A. Arduh[72], J-F. Arguin[95], S. Argyropoulos[64], M. Arik[20a], A.J. Armbruster[143], L.J. Armitage[77], O. Arnaez[32], H. Arnold[50], M. Arratia[30], O. Arslan[23], A. Artamonov[97], G. Artoni[120], S. Artz[84], S. Asai[155], N. Asbah[44], A. Ashkenazi[153], B. Åsman[146a,146b], L. Asquith[149], K. Assamagan[27], R. Astalos[144a], M. Atkinson[165], N.B. Atlay[141], K. Augsten[128], G. Avolio[32], B. Axen[16], M.K. Ayoub[117], G. Azuelos[95,d], M.A. Baak[32], A.E. Baas[59a], M.J. Baca[19], H. Bachacou[136], K. Bachas[74a,74b], M. Backes[32], M. Backhaus[32], P. Bagiacchi[132a,132b], P. Bagnaia[132a,132b], Y. Bai[35a], J.T. Baines[131], O.K. Baker[175], E.M. Baldin[109,c], P. Balek[171], T. Balestri[148], F. Balli[136], W.K. Balunas[122], E. Banas[41], Sw. Banerjee[172,e], A.A.E. Bannoura[174], L. Barak[32], E.L. Barberio[89], D. Barberis[52a,52b], M. Barbero[86], T. Barillari[101], M-S Barisits[32], T. Barklow[143], N. Barlow[30], S.L. Barnes[85], B.M. Barnett[131], R.M. Barnett[16], Z. Barnovska[5], A. Baroncelli[134a], G. Barone[25], A.J. Barr[120], L. Barranco Navarro[166], F. Barreiro[83], J. Barreiro Guimarães da Costa[35a], R. Bartoldus[143], A.E. Barton[73], P. Bartos[144a], A. Basalaev[123], A. Bassalat[117], R.L. Bates[55], S.J. Batista[158], J.R. Batley[30], M. Battaglia[137], M. Bauce[132a,132b], F. Bauer[136], H.S. Bawa[143,f], J.B. Beacham[111], M.D. Beattie[73], T. Beau[81], P.H. Beauchemin[161], P. Bechtle[23], H.P. Beck[18,g], K. Becker[120], M. Becker[84], M. Beckingham[169], C. Becot[110], A.J. Beddall[20e], A. Beddall[20b], V.A. Bednyakov[66], M. Bedognetti[107], C.P. Bee[148], L.J. Beemster[107], T.A. Beermann[32], M. Begel[27], J.K. Behr[44], C. Belanger-Champagne[88], A.S. Bell[79], G. Bella[153], L. Bellagamba[22a], A. Bellerive[31], M. Bellomo[87], K. Belotskiy[98], O. Beltramello[32], N.L. Belyaev[98], O. Benary[153], D. Benchekroun[135a], M. Bender[100], K. Bendtz[146a,146b], N. Benekos[10], Y. Benhammou[153], E. Benhar Noccioli[175], J. Benitez[64], D.P. Benjamin[47], J.R. Bensinger[25], S. Bentvelsen[107], L. Beresford[120], M. Beretta[49], D. Berge[107], E. Bergeaas Kuutmann[164], N. Berger[5], J. Beringer[16], S. Berlendis[57], N.R. Bernard[87], C. Bernius[110], F.U. Bernlochner[23], T. Berry[78], P. Berta[129], C. Bertella[84], G. Bertoli[146a,146b], F. Bertolucci[124a,124b], I.A. Bertram[73], C. Bertsche[44], D. Bertsche[113], G.J. Besjes[38], O. Bessidskaia Bylund[146a,146b], M. Bessner[44], N. Besson[136], C. Betancourt[50], S. Bethke[101], A.J. Bevan[77], R.M. Bianchi[125], L. Bianchini[25], M. Bianco[32], O. Biebel[100], D. Biedermann[17], R. Bielski[85], N.V. Biesuz[124a,124b], M. Biglietti[134a], J. Bilbao De Mendizabal[51], T.R.V. Billoud[95], H. Bilokon[49], M. Bindi[56], S. Binet[117], A. Bingul[20b], C. Bini[132a,132b], S. Biondi[22a,22b], D.M. Bjergaard[47], C.W. Black[150], J.E. Black[143], K.M. Black[24], D. Blackburn[138], R.E. Blair[6], J.-B. Blanchard[136], J.E. Blanco[78], T. Blazek[144a], I. Bloch[44], C. Blocker[25], W. Blum[84,*], U. Blumenschein[56], S. Blunier[34a],

G.J. Bobbink[107], V.S. Bobrovnikov[109,c], S.S. Bocchetta[82], A. Bocci[47], C. Bock[100], M. Boehler[50], D. Boerner[174], J.A. Bogaerts[32], D. Bogavac[14], A.G. Bogdanchikov[109], C. Bohm[146a], V. Boisvert[78], P. Bokan[14], T. Bold[40a], A.S. Boldyrev[163a,163c], M. Bomben[81], M. Bona[77], M. Boonekamp[136], A. Borisov[130], G. Borissov[73], J. Bortfeldt[32], D. Bortoletto[120], V. Bortolotto[61a,61b,61c], K. Bos[107], D. Boscherini[22a], M. Bosman[13], J.D. Bossio Sola[29], J. Boudreau[125], J. Bouffard[2], E.V. Bouhova-Thacker[73], D. Boumediene[36], C. Bourdarios[117], S.K. Boutle[55], A. Boveia[32], J. Boyd[32], I.R. Boyko[66], J. Bracinik[19], A. Brandt[8], G. Brandt[56], O. Brandt[59a], U. Bratzler[156], B. Brau[87], J.E. Brau[116], H.M. Braun[174,*], W.D. Breaden Madden[55], K. Brendlinger[122], A.J. Brennan[89], L. Brenner[107], R. Brenner[164], S. Bressler[171], T.M. Bristow[48], D. Britton[55], D. Britzger[44], F.M. Brochu[30], I. Brock[23], R. Brock[91], G. Brooijmans[37], T. Brooks[78], W.K. Brooks[34b], J. Brosamer[16], E. Brost[108], J.H Broughton[19], P.A. Bruckman de Renstrom[41], D. Bruncko[144b], R. Bruneliere[50], A. Bruni[22a], G. Bruni[22a], L.S. Bruni[107], BH Brunt[30], M. Bruschi[22a], N. Bruscino[23], P. Bryant[33], L. Bryngemark[82], T. Buanes[15], Q. Buat[142], P. Buchholz[141], A.G. Buckley[55], I.A. Budagov[66], F. Buehrer[50], M.K. Bugge[119], O. Bulekov[98], D. Bullock[8], H. Burckhart[32], S. Burdin[75], C.D. Burgard[50], B. Burghgrave[108], K. Burka[41], S. Burke[131], I. Burmeister[45], J.T.P. Burr[120], E. Busato[36], D. Büscher[50], V. Büscher[84], P. Bussey[55], J.M. Butler[24], C.M. Buttar[55], J.M. Butterworth[79], P. Butti[107], W. Buttinger[27], A. Buzatu[55], A.R. Buzykaev[109,c], S. Cabrera Urbán[166], D. Caforio[128], V.M. Cairo[39a,39b], O. Cakir[4a], N. Calace[51], P. Calafiura[16], A. Calandri[86], G. Calderini[81], P. Calfayan[100], G. Callea[39a,39b], L.P. Caloba[26a], S. Calvente Lopez[83], D. Calvet[36], S. Calvet[36], T.P. Calvet[86], R. Camacho Toro[33], S. Camarda[32], P. Camarri[133a,133b], D. Cameron[119], R. Caminal Armadans[165], C. Camincher[57], S. Campana[32], M. Campanelli[79], A. Camplani[92a,92b], A. Campoverde[141], V. Canale[104a,104b], A. Canepa[159a], M. Cano Bret[35e], J. Cantero[114], R. Cantrill[126a], T. Cao[42], M.D.M. Capeans Garrido[32], I. Caprini[28b], M. Caprini[28b], M. Capua[39a,39b], R. Caputo[84], R.M. Carbone[37], R. Cardarelli[133a], F. Cardillo[50], I. Carli[129], T. Carli[32], G. Carlino[104a], L. Carminati[92a,92b], S. Caron[106], E. Carquin[34b], G.D. Carrillo-Montoya[32], J.R. Carter[30], J. Carvalho[126a,126c], D. Casadei[19], M.P. Casado[13,h], M. Casolino[13], D.W. Casper[162], E. Castaneda-Miranda[145a], R. Castelijn[107], A. Castelli[107], V. Castillo Gimenez[166], N.F. Castro[126a,i], A. Catinaccio[32], J.R. Catmore[119], A. Cattai[32], J. Caudron[84], V. Cavaliere[165], E. Cavallaro[13], D. Cavalli[92a], M. Cavalli-Sforza[13], V. Cavasinni[124a,124b], F. Ceradini[134a,134b], L. Cerda Alberich[166], B.C. Cerio[47], A.S. Cerqueira[26b], A. Cerri[149], L. Cerrito[77], F. Cerutti[16], M. Cerv[32], A. Cervelli[18], S.A. Cetin[20d], A. Chafaq[135a], D. Chakraborty[108], S.K. Chan[58], Y.L. Chan[61a], P. Chang[165], J.D. Chapman[30], D.G. Charlton[19], A. Chatterjee[51], C.C. Chau[158], C.A. Chavez Barajas[149], S. Che[111], S. Cheatham[73], A. Chegwidden[91], S. Chekanov[6], S.V. Chekulaev[159a], G.A. Chelkov[66,j], M.A. Chelstowska[90], C. Chen[65], H. Chen[27], K. Chen[148], S. Chen[35c], S. Chen[155], X. Chen[35f], Y. Chen[68], H.C. Cheng[90], H.J Cheng[35a], Y. Cheng[33], A. Cheplakov[66], E. Cheremushkina[130], R. Cherkaoui El Moursli[135e], V. Chernyatin[27,*], E. Cheu[7], L. Chevalier[136], V. Chiarella[49], G. Chiarelli[124a,124b], G. Chiodini[74a], A.S. Chisholm[19], A. Chitan[28b], M.V. Chizhov[66], K. Choi[62], A.R. Chomont[36], S. Chouridou[9], B.K.B. Chow[100], V. Christodoulou[79], D. Chromek-Burckhart[32], J. Chudoba[127], A.J. Chuinard[88], J.J. Chwastowski[41], L. Chytka[115], G. Ciapetti[132a,132b], A.K. Ciftci[4a], D. Cinca[45], V. Cindro[76], I.A. Cioara[23], C. Ciocca[22a,22b], A. Ciocio[16], F. Cirotto[104a,104b], Z.H. Citron[171], M. Citterio[92a], M. Ciubancan[28b], A. Clark[51], B.L. Clark[58], M.R. Clark[37], P.J. Clark[48], R.N. Clarke[16], C. Clement[146a,146b], Y. Coadou[86], M. Cobal[163a,163c], A. Coccaro[51], J. Cochran[65], L. Coffey[25], L. Colasurdo[106], B. Cole[37], A.P. Colijn[107], J. Collot[57], T. Colombo[32], G. Compostella[101], P. Conde Muiño[126a,126b], E. Coniavitis[50], S.H. Connell[145b], I.A. Connelly[78], V. Consorti[50], S. Constantinescu[28b], G. Conti[32], F. Conventi[104a,k], M. Cooke[16], B.D. Cooper[79], A.M. Cooper-Sarkar[120], K.J.R. Cormier[158], T. Cornelissen[174], M. Corradi[132a,132b], F. Corriveau[88,l], A. Corso-Radu[162], A. Cortes-Gonzalez[13], G. Cortiana[101], G. Costa[92a], M.J. Costa[166], D. Costanzo[139], G. Cottin[30], G. Cowan[78], B.E. Cox[85], K. Cranmer[110], S.J. Crawley[55], G. Cree[31],

S. Crépé-Renaudin[57], F. Crescioli[81], W.A. Cribbs[146a,146b], M. Crispin Ortuzar[120], M. Cristinziani[23], V. Croft[106], G. Crosetti[39a,39b], A. Cueto[83], T. Cuhadar Donszelmann[139], J. Cummings[175], M. Curatolo[49], J. Cúth[84], C. Cuthbert[150], H. Czirr[141], P. Czodrowski[3], G. D'amen[22a,22b], S. D'Auria[55], M. D'Onofrio[75], M.J. Da Cunha Sargedas De Sousa[126a,126b], C. Da Via[85], W. Dabrowski[40a], T. Dado[144a], T. Dai[90], O. Dale[15], F. Dallaire[95], C. Dallapiccola[87], M. Dam[38], J.R. Dandoy[33], N.P. Dang[50], A.C. Daniells[19], N.S. Dann[85], M. Danninger[167], M. Dano Hoffmann[136], V. Dao[50], G. Darbo[52a], S. Darmora[8], J. Dassoulas[3], A. Dattagupta[62], W. Davey[23], C. David[168], T. Davidek[129], M. Davies[153], P. Davison[79], E. Dawe[89], I. Dawson[139], R.K. Daya-Ishmukhametova[87], K. De[8], R. de Asmundis[104a], A. De Benedetti[113], S. De Castro[22a,22b], S. De Cecco[81], N. De Groot[106], P. de Jong[107], H. De la Torre[83], F. De Lorenzi[65], A. De Maria[56], D. De Pedis[132a], A. De Salvo[132a], U. De Sanctis[149], A. De Santo[149], J.B. De Vivie De Regie[117], W.J. Dearnaley[73], R. Debbe[27], C. Debenedetti[137], D.V. Dedovich[66], N. Dehghanian[3], I. Deigaard[107], M. Del Gaudio[39a,39b], J. Del Peso[83], T. Del Prete[124a,124b], D. Delgove[117], F. Deliot[136], C.M. Delitzsch[51], M. Deliyergiyev[76], A. Dell'Acqua[32], L. Dell'Asta[24], M. Dell'Orso[124a,124b], M. Della Pietra[104a,k], D. della Volpe[51], M. Delmastro[5], P.A. Delsart[57], D.A. DeMarco[158], S. Demers[175], M. Demichev[66], A. Demilly[81], S.P. Denisov[130], D. Denysiuk[136], D. Derendarz[41], J.E. Derkaoui[135d], F. Derue[81], P. Dervan[75], K. Desch[23], C. Deterre[44], K. Dette[45], P.O. Deviveiros[32], A. Dewhurst[131], S. Dhaliwal[25], A. Di Ciaccio[133a,133b], L. Di Ciaccio[5], W.K. Di Clemente[122], C. Di Donato[132a,132b], A. Di Girolamo[32], B. Di Girolamo[32], B. Di Micco[134a,134b], R. Di Nardo[32], A. Di Simone[50], R. Di Sipio[158], D. Di Valentino[31], C. Diaconu[86], M. Diamond[158], F.A. Dias[48], M.A. Diaz[34a], E.B. Diehl[90], J. Dietrich[17], S. Diglio[86], A. Dimitrievska[14], J. Dingfelder[23], P. Dita[28b], S. Dita[28b], F. Dittus[32], F. Djama[86], T. Djobava[53b], J.I. Djuvsland[59a], M.A.B. do Vale[26c], D. Dobos[32], M. Dobre[28b], C. Doglioni[82], T. Dohmae[155], J. Dolejsi[129], Z. Dolezal[129], B.A. Dolgoshein[98,*], M. Donadelli[26d], S. Donati[124a,124b], P. Dondero[121a,121b], J. Donini[36], J. Dopke[131], A. Doria[104a], M.T. Dova[72], A.T. Doyle[55], E. Drechsler[56], M. Dris[10], Y. Du[35d], J. Duarte-Campderros[153], E. Duchovni[171], G. Duckeck[100], O.A. Ducu[95,m], D. Duda[107], A. Dudarev[32], E.M. Duffield[16], L. Duflot[117], L. Duguid[78], M. Dührssen[32], M. Dumancic[171], M. Dunford[59a], H. Duran Yildiz[4a], M. Düren[54], A. Durglishvili[53b], D. Duschinger[46], B. Dutta[44], M. Dyndal[44], C. Eckardt[44], K.M. Ecker[101], R.C. Edgar[90], N.C. Edwards[48], T. Eifert[32], G. Eigen[15], K. Einsweiler[16], T. Ekelof[164], M. El Kacimi[135c], V. Ellajosyula[86], M. Ellert[164], S. Elles[5], F. Ellinghaus[174], A.A. Elliot[168], N. Ellis[32], J. Elmsheuser[27], M. Elsing[32], D. Emeliyanov[131], Y. Enari[155], O.C. Endner[84], M. Endo[118], J.S. Ennis[169], J. Erdmann[45], A. Ereditato[18], G. Ernis[174], J. Ernst[2], M. Ernst[27], S. Errede[165], E. Ertel[84], M. Escalier[117], H. Esch[45], C. Escobar[125], B. Esposito[49], A.I. Etienvre[136], E. Etzion[153], H. Evans[62], A. Ezhilov[123], F. Fabbri[22a,22b], L. Fabbri[22a,22b], G. Facini[33], R.M. Fakhrutdinov[130], S. Falciano[132a], R.J. Falla[79], J. Faltova[32], Y. Fang[35a], M. Fanti[92a,92b], A. Farbin[8], A. Farilla[134a], C. Farina[125], E.M. Farina[121a,121b], T. Farooque[13], S. Farrell[16], S.M. Farrington[169], P. Farthouat[32], F. Fassi[135e], P. Fassnacht[32], D. Fassouliotis[9], M. Faucci Giannelli[78], A. Favareto[52a,52b], W.J. Fawcett[120], L. Fayard[117], O.L. Fedin[123,n], W. Fedorko[167], S. Feigl[119], L. Feligioni[86], C. Feng[35d], E.J. Feng[32], H. Feng[90], A.B. Fenyuk[130], L. Feremenga[8], P. Fernandez Martinez[166], S. Fernandez Perez[13], J. Ferrando[55], A. Ferrari[164], P. Ferrari[107], R. Ferrari[121a], D.E. Ferreira de Lima[59b], A. Ferrer[166], D. Ferrere[51], C. Ferretti[90], A. Ferretto Parodi[52a,52b], F. Fiedler[84], A. Filipčič[76], M. Filipuzzi[44], F. Filthaut[106], M. Fincke-Keeler[168], K.D. Finelli[150], M.C.N. Fiolhais[126a,126c], L. Fiorini[166], A. Firan[42], A. Fischer[2], C. Fischer[13], J. Fischer[174], W.C. Fisher[91], N. Flaschel[44], I. Fleck[141], P. Fleischmann[90], G.T. Fletcher[139], R.R.M. Fletcher[122], T. Flick[174], A. Floderus[82], L.R. Flores Castillo[61a], M.J. Flowerdew[101], G.T. Forcolin[85], A. Formica[136], A. Forti[85], A.G. Foster[19], D. Fournier[117], H. Fox[73], S. Fracchia[13], P. Francavilla[81], M. Franchini[22a,22b], D. Francis[32], L. Franconi[119], M. Franklin[58], M. Frate[162], M. Fraternali[121a,121b], D. Freeborn[79], S.M. Fressard-Batraneanu[32], F. Friedrich[46], D. Froidevaux[32], J.A. Frost[120], C. Fukunaga[156], E. Fullana Torregrosa[84], T. Fusayasu[102], J. Fuster[166], C. Gabaldon[57], O. Gabizon[174], A. Gabrielli[22a,22b],

A. Gabrielli[16], G.P. Gach[40a], S. Gadatsch[32], S. Gadomski[51], G. Gagliardi[52a,52b], L.G. Gagnon[95], P. Gagnon[62], C. Galea[106], B. Galhardo[126a,126c], E.J. Gallas[120], B.J. Gallop[131], P. Gallus[128], G. Galster[38], K.K. Gan[111], J. Gao[35b,86], Y. Gao[48], Y.S. Gao[143,f], F.M. Garay Walls[48], C. García[166], J.E. García Navarro[166], M. Garcia-Sciveres[16], R.W. Gardner[33], N. Garelli[143], V. Garonne[119], A. Gascon Bravo[44], C. Gatti[49], A. Gaudiello[52a,52b], G. Gaudio[121a], B. Gaur[141], L. Gauthier[95], I.L. Gavrilenko[96], C. Gay[167], G. Gaycken[23], E.N. Gazis[10], Z. Gecse[167], C.N.P. Gee[131], Ch. Geich-Gimbel[23], M. Geisen[84], M.P. Geisler[59a], C. Gemme[52a], M.H. Genest[57], C. Geng[35b,o], S. Gentile[132a,132b], C. Gentsos[154], S. George[78], D. Gerbaudo[13], A. Gershon[153], S. Ghasemi[141], H. Ghazlane[135b], M. Ghneimat[23], B. Giacobbe[22a], S. Giagu[132a,132b], P. Giannetti[124a,124b], B. Gibbard[27], S.M. Gibson[78], M. Gignac[167], M. Gilchriese[16], T.P.S. Gillam[30], D. Gillberg[31], G. Gilles[174], D.M. Gingrich[3,d], N. Giokaris[9], M.P. Giordani[163a,163c], F.M. Giorgi[22a], F.M. Giorgi[17], P.F. Giraud[136], P. Giromini[58], D. Giugni[92a], F. Giuli[120], C. Giuliani[101], M. Giulini[59b], B.K. Gjelsten[119], S. Gkaitatzis[154], I. Gkialas[154], E.L. Gkougkousis[117], L.K. Gladilin[99], C. Glasman[83], J. Glatzer[50], P.C.F. Glaysher[48], A. Glazov[44], M. Goblirsch-Kolb[25], J. Godlewski[41], S. Goldfarb[89], T. Golling[51], D. Golubkov[130], A. Gomes[126a,126b,126d], R. Gonçalo[126a], J. Goncalves Pinto Firmino Da Costa[136], G. Gonella[50], L. Gonella[19], A. Gongadze[66], S. González de la Hoz[166], G. Gonzalez Parra[13], S. Gonzalez-Sevilla[51], L. Goossens[32], P.A. Gorbounov[97], H.A. Gordon[27], I. Gorelov[105], B. Gorini[32], E. Gorini[74a,74b], A. Gorišek[76], E. Gornicki[41], A.T. Goshaw[47], C. Gössling[45], M.I. Gostkin[66], C.R. Goudet[117], D. Goujdami[135c], A.G. Goussiou[138], N. Govender[145b,p], E. Gozani[152], L. Graber[56], I. Grabowska-Bold[40a], P.O.J. Gradin[57], P. Grafström[22a,22b], J. Gramling[51], E. Gramstad[119], S. Grancagnolo[17], V. Gratchev[123], P.M. Gravila[28e], H.M. Gray[32], E. Graziani[134a], Z.D. Greenwood[80,q], C. Grefe[23], K. Gregersen[79], I.M. Gregor[44], P. Grenier[143], K. Grevtsov[5], J. Griffiths[8], A.A. Grillo[137], K. Grimm[73], S. Grinstein[13,r], Ph. Gris[36], J.-F. Grivaz[117], S. Groh[84], J.P. Grohs[46], E. Gross[171], J. Grosse-Knetter[56], G.C. Grossi[80], Z.J. Grout[149], L. Guan[90], W. Guan[172], J. Guenther[63], F. Guescini[51], D. Guest[162], O. Gueta[153], E. Guido[52a,52b], T. Guillemin[5], S. Guindon[2], U. Gul[55], C. Gumpert[32], J. Guo[35e], Y. Guo[35b,o], R. Gupta[42], S. Gupta[120], G. Gustavino[132a,132b], P. Gutierrez[113], N.G. Gutierrez Ortiz[79], C. Gutschow[46], C. Guyot[136], C. Gwenlan[120], C.B. Gwilliam[75], A. Haas[110], C. Haber[16], H.K. Hadavand[8], N. Haddad[135e], A. Hadef[86], P. Haefner[23], S. Hageböck[23], Z. Hajduk[41], H. Hakobyan[176,*], M. Haleem[44], J. Haley[114], G. Halladjian[91], G.D. Hallewell[86], K. Hamacher[174], P. Hamal[115], K. Hamano[168], A. Hamilton[145a], G.N. Hamity[139], P.G. Hamnett[44], L. Han[35b], K. Hanagaki[67,s], K. Hanawa[155], M. Hance[137], B. Haney[122], S. Hanisch[32], P. Hanke[59a], R. Hanna[136], J.B. Hansen[38], J.D. Hansen[38], M.C. Hansen[23], P.H. Hansen[38], K. Hara[160], A.S. Hard[172], T. Harenberg[174], F. Hariri[117], S. Harkusha[93], R.D. Harrington[48], P.F. Harrison[169], F. Hartjes[107], N.M. Hartmann[100], M. Hasegawa[68], Y. Hasegawa[140], A. Hasib[113], S. Hassani[136], S. Haug[18], R. Hauser[91], L. Hauswald[46], M. Havranek[127], C.M. Hawkes[19], R.J. Hawkings[32], D. Hayden[91], C.P. Hays[120], J.M. Hays[77], H.S. Hayward[75], S.J. Haywood[131], S.J. Head[19], T. Heck[84], V. Hedberg[82], L. Heelan[8], S. Heim[122], T. Heim[16], B. Heinemann[16], J.J. Heinrich[100], L. Heinrich[110], C. Heinz[54], J. Hejbal[127], L. Helary[24], S. Hellman[146a,146b], C. Helsens[32], J. Henderson[120], R.C.W. Henderson[73], Y. Heng[172], S. Henkelmann[167], A.M. Henriques Correia[32], S. Henrot-Versille[117], G.H. Herbert[17], Y. Hernández Jiménez[166], G. Herten[50], R. Hertenberger[100], L. Hervas[32], G.G. Hesketh[79], N.P. Hessey[107], J.W. Hetherly[42], R. Hickling[77], E. Higón-Rodriguez[166], E. Hill[168], J.C. Hill[30], K.H. Hiller[44], S.J. Hillier[19], I. Hinchliffe[16], E. Hines[122], R.R. Hinman[16], M. Hirose[50], D. Hirschbuehl[174], J. Hobbs[148], N. Hod[159a], M.C. Hodgkinson[139], P. Hodgson[139], A. Hoecker[32], M.R. Hoeferkamp[105], F. Hoenig[100], D. Hohn[23], T.R. Holmes[16], M. Homann[45], T.M. Hong[125], B.H. Hooberman[165], W.H. Hopkins[116], Y. Horii[103], A.J. Horton[142], J-Y. Hostachy[57], S. Hou[151], A. Hoummada[135a], J. Howarth[44], M. Hrabovsky[115], I. Hristova[17], J. Hrivnac[117], T. Hryn'ova[5], A. Hrynevich[94], C. Hsu[145c], P.J. Hsu[151,t], S.-C. Hsu[138], D. Hu[37], Q. Hu[35b], Y. Huang[44], Z. Hubacek[128], F. Hubaut[86], F. Huegging[23],

T.B. Huffman[120], E.W. Hughes[37], G. Hughes[73], M. Huhtinen[32], P. Huo[148], N. Huseynov[66,b], J. Huston[91], J. Huth[58], G. Iacobucci[51], G. Iakovidis[27], I. Ibragimov[141], L. Iconomidou-Fayard[117], E. Ideal[175], Z. Idrissi[135e], P. Iengo[32], O. Igonkina[107,u], T. Iizawa[170], Y. Ikegami[67], M. Ikeno[67], Y. Ilchenko[11,v], D. Iliadis[154], N. Ilic[143], T. Ince[101], G. Introzzi[121a,121b], P. Ioannou[9,*], M. Iodice[134a], K. Iordanidou[37], V. Ippolito[58], N. Ishijima[118], M. Ishino[69], M. Ishitsuka[157], R. Ishmukhametov[111], C. Issever[120], S. Istin[20a], F. Ito[160], J.M. Iturbe Ponce[85], R. Iuppa[133a,133b], W. Iwanski[41], H. Iwasaki[67], J.M. Izen[43], V. Izzo[104a], S. Jabbar[3], B. Jackson[122], M. Jackson[75], P. Jackson[1], V. Jain[2], K.B. Jakobi[84], K. Jakobs[50], S. Jakobsen[32], T. Jakoubek[127], D.O. Jamin[114], D.K. Jana[80], E. Jansen[79], R. Jansky[63], J. Janssen[23], M. Janus[56], G. Jarlskog[82], N. Javadov[66,b], T. Javůrek[50], F. Jeanneau[136], L. Jeanty[16], J. Jejelava[53a,w], G.-Y. Jeng[150], D. Jennens[89], P. Jenni[50,x], J. Jentzsch[45], C. Jeske[169], S. Jézéquel[5], H. Ji[172], J. Jia[148], H. Jiang[65], Y. Jiang[35b], S. Jiggins[79], J. Jimenez Pena[166], S. Jin[35a], A. Jinaru[28b], O. Jinnouchi[157], P. Johansson[139], K.A. Johns[7], W.J. Johnson[138], K. Jon-And[146a,146b], G. Jones[169], R.W.L. Jones[73], S. Jones[7], T.J. Jones[75], J. Jongmanns[59a], P.M. Jorge[126a,126b], J. Jovicevic[159a], X. Ju[172], A. Juste Rozas[13,r], M.K. Köhler[171], A. Kaczmarska[41], M. Kado[117], H. Kagan[111], M. Kagan[143], S.J. Kahn[86], E. Kajomovitz[47], C.W. Kalderon[120], A. Kaluza[84], S. Kama[42], A. Kamenshchikov[130], N. Kanaya[155], S. Kaneti[30], L. Kanjir[76], V.A. Kantserov[98], J. Kanzaki[67], B. Kaplan[110], L.S. Kaplan[172], A. Kapliy[33], D. Kar[145c], K. Karakostas[10], A. Karamaoun[3], N. Karastathis[10], M.J. Kareem[56], E. Karentzos[10], M. Karnevskiy[84], S.N. Karpov[66], Z.M. Karpova[66], K. Karthik[110], V. Kartvelishvili[73], A.N. Karyukhin[130], K. Kasahara[160], L. Kashif[172], R.D. Kass[111], A. Kastanas[15], Y. Kataoka[155], C. Kato[155], A. Katre[51], J. Katzy[44], K. Kawagoe[71], T. Kawamoto[155], G. Kawamura[56], S. Kazama[155], V.F. Kazanin[109,c], R. Keeler[168], R. Kehoe[42], J.S. Keller[44], J.J. Kempster[78], K Kentaro[103], H. Keoshkerian[158], O. Kepka[127], B.P. Kerševan[76], S. Kersten[174], R.A. Keyes[88], M. Khader[165], F. Khalil-zada[12], A. Khanov[114], A.G. Kharlamov[109,c], T.J. Khoo[51], V. Khovanskiy[97], E. Khramov[66], J. Khubua[53b,y], S. Kido[68], H.Y. Kim[8], S.H. Kim[160], Y.K. Kim[33], N. Kimura[154], O.M. Kind[17], B.T. King[75], M. King[166], S.B. King[167], J. Kirk[131], A.E. Kiryunin[101], T. Kishimoto[68], D. Kisielewska[40a], F. Kiss[50], K. Kiuchi[160], O. Kivernyk[136], E. Kladiva[144b], M.H. Klein[37], M. Klein[75], U. Klein[75], K. Kleinknecht[84], P. Klimek[108], A. Klimentov[27], R. Klingenberg[45], J.A. Klinger[139], T. Klioutchnikova[32], E.-E. Kluge[59a], P. Kluit[107], S. Kluth[101], J. Knapik[41], E. Kneringer[63], E.B.F.G. Knoops[86], A. Knue[55], A. Kobayashi[155], D. Kobayashi[157], T. Kobayashi[155], M. Kobel[46], M. Kocian[143], P. Kodys[129], T. Koffas[31], E. Koffeman[107], T. Koi[143], H. Kolanoski[17], M. Kolb[59b], I. Koletsou[5], A.A. Komar[96,*], Y. Komori[155], T. Kondo[67], N. Kondrashova[44], K. Köneke[50], A.C. König[106], T. Kono[67,z], R. Konoplich[110,aa], N. Konstantinidis[79], R. Kopeliansky[62], S. Koperny[40a], L. Köpke[84], A.K. Kopp[50], K. Korcyl[41], K. Kordas[154], A. Korn[79], A.A. Korol[109,c], I. Korolkov[13], E.V. Korolkova[139], O. Kortner[101], S. Kortner[101], T. Kosek[129], V.V. Kostyukhin[23], A. Kotwal[47], A. Kourkoumeli-Charalampidi[154], C. Kourkoumelis[9], V. Kouskoura[27], A.B. Kowalewska[41], R. Kowalewski[168], T.Z. Kowalski[40a], C. Kozakai[155], W. Kozanecki[136], A.S. Kozhin[130], V.A. Kramarenko[99], G. Kramberger[76], D. Krasnopevtsev[98], M.W. Krasny[81], A. Krasznahorkay[32], J.K. Kraus[23], A. Kravchenko[27], M. Kretz[59c], J. Kretzschmar[75], K. Kreutzfeldt[54], P. Krieger[158], K. Krizka[33], K. Kroeninger[45], H. Kroha[101], J. Kroll[122], J. Kroseberg[23], J. Krstic[14], U. Kruchonak[66], H. Krüger[23], N. Krumnack[65], A. Kruse[172], M.C. Kruse[47], M. Kruskal[24], T. Kubota[89], H. Kucuk[79], S. Kuday[4b], J.T. Kuechler[174], S. Kuehn[50], A. Kugel[59c], F. Kuger[173], A. Kuhl[137], T. Kuhl[44], V. Kukhtin[66], R. Kukla[136], Y. Kulchitsky[93], S. Kuleshov[34b], M. Kuna[132a,132b], T. Kunigo[69], A. Kupco[127], H. Kurashige[68], Y.A. Kurochkin[93], V. Kus[127], E.S. Kuwertz[168], M. Kuze[157], J. Kvita[115], T. Kwan[168], D. Kyriazopoulos[139], A. La Rosa[101], J.L. La Rosa Navarro[26d], L. La Rotonda[39a,39b], C. Lacasta[166], F. Lacava[132a,132b], J. Lacey[31], H. Lacker[17], D. Lacour[81], V.R. Lacuesta[166], E. Ladygin[66], R. Lafaye[5], B. Laforge[81], T. Lagouri[175], S. Lai[56], S. Lammers[62], W. Lampl[7], E. Lançon[136], U. Landgraf[50], M.P.J. Landon[77], M.C. Lanfermann[51], V.S. Lang[59a], J.C. Lange[13], A.J. Lankford[162], F. Lanni[27], K. Lantzsch[23], A. Lanza[121a], S. Laplace[81],

C. Lapoire[32], J.F. Laporte[136], T. Lari[92a], F. Lasagni Manghi[22a,22b], M. Lassnig[32], P. Laurelli[49], W. Lavrijsen[16], A.T. Law[137], P. Laycock[75], T. Lazovich[58], M. Lazzaroni[92a,92b], B. Le[89], O. Le Dortz[81], E. Le Guirriec[86], E.P. Le Quilleuc[136], M. LeBlanc[168], T. LeCompte[6], F. Ledroit-Guillon[57], C.A. Lee[27], S.C. Lee[151], L. Lee[1], G. Lefebvre[81], M. Lefebvre[168], F. Legger[100], C. Leggett[16], A. Lehan[75], G. Lehmann Miotto[32], X. Lei[7], W.A. Leight[31], A. Leisos[154,*ab*], A.G. Leister[175], M.A.L. Leite[26d], R. Leitner[129], D. Lellouch[171], B. Lemmer[56], K.J.C. Leney[79], T. Lenz[23], B. Lenzi[32], R. Leone[7], S. Leone[124a,124b], C. Leonidopoulos[48], S. Leontsinis[10], G. Lerner[149], C. Leroy[95], A.A.J. Lesage[136], C.G. Lester[30], M. Levchenko[123], J. Levêque[5], D. Levin[90], L.J. Levinson[171], M. Levy[19], D. Lewis[77], A.M. Leyko[23], M. Leyton[43], B. Li[35b,*o*], H. Li[148], H.L. Li[33], L. Li[47], L. Li[35e], Q. Li[35a], S. Li[47], X. Li[85], Y. Li[141], Z. Liang[35a], B. Liberti[133a], A. Liblong[158], P. Lichard[32], K. Lie[165], J. Liebal[23], W. Liebig[15], A. Limosani[150], S.C. Lin[151,*ac*], T.H. Lin[84], B.E. Lindquist[148], A.E. Lionti[51], E. Lipeles[122], A. Lipniacka[15], M. Lisovyi[59b], T.M. Liss[165], A. Lister[167], A.M. Litke[137], B. Liu[151,*ad*], D. Liu[151], H. Liu[90], H. Liu[27], J. Liu[86], J.B. Liu[35b], K. Liu[86], L. Liu[165], M. Liu[47], M. Liu[35b], Y.L. Liu[35b], Y. Liu[35b], M. Livan[121a,121b], A. Lleres[57], J. Llorente Merino[35a], S.L. Lloyd[77], F. Lo Sterzo[151], E. Lobodzinska[44], P. Loch[7], W.S. Lockman[137], F.K. Loebinger[85], A.E. Loevschall-Jensen[38], K.M. Loew[25], A. Loginov[175,*], T. Lohse[17], K. Lohwasser[44], M. Lokajicek[127], B.A. Long[24], J.D. Long[165], R.E. Long[73], L. Longo[74a,74b], K.A. Looper[111], L. Lopes[126a], D. Lopez Mateos[58], B. Lopez Paredes[139], I. Lopez Paz[13], A. Lopez Solis[81], J. Lorenz[100], N. Lorenzo Martinez[62], M. Losada[21], P.J. Lösel[100], X. Lou[35a], A. Lounis[117], J. Love[6], P.A. Love[73], H. Lu[61a], N. Lu[90], H.J. Lubatti[138], C. Luci[132a,132b], A. Lucotte[57], C. Luedtke[50], F. Luehring[62], W. Lukas[63], L. Luminari[132a], O. Lundberg[146a,146b], B. Lund-Jensen[147], P.M. Luzi[81], D. Lynn[27], R. Lysak[127], E. Lytken[82], V. Lyubushkin[66], H. Ma[27], L.L. Ma[35d], Y. Ma[35d], G. Maccarrone[49], A. Macchiolo[101], C.M. Macdonald[139], B. Maček[76], J. Machado Miguens[122,126b], D. Madaffari[86], R. Madar[36], H.J. Maddocks[164], W.F. Mader[46], A. Madsen[44], J. Maeda[68], S. Maeland[15], T. Maeno[27], A. Maevskiy[99], E. Magradze[56], J. Mahlstedt[107], C. Maiani[117], C. Maidantchik[26a], A.A. Maier[101], T. Maier[100], A. Maio[126a,126b,126d], S. Majewski[116], Y. Makida[67], N. Makovec[117], B. Malaescu[81], Pa. Malecki[41], V.P. Maleev[123], F. Malek[57], U. Mallik[64], D. Malon[6], C. Malone[143], S. Maltezos[10], S. Malyukov[32], J. Mamuzic[166], G. Mancini[49], B. Mandelli[32], L. Mandelli[92a], I. Mandić[76], J. Maneira[126a,126b], L. Manhaes de Andrade Filho[26b], J. Manjarres Ramos[159b], A. Mann[100], A. Manousos[32], B. Mansoulie[136], J.D. Mansour[35a], R. Mantifel[88], M. Mantoani[56], S. Manzoni[92a,92b], L. Mapelli[32], G. Marceca[29], L. March[51], G. Marchiori[81], M. Marcisovsky[127], M. Marjanovic[14], D.E. Marley[90], F. Marroquim[26a], S.P. Marsden[85], Z. Marshall[16], S. Marti-Garcia[166], B. Martin[91], T.A. Martin[169], V.J. Martin[48], B. Martin dit Latour[15], M. Martinez[13,*r*], V.I. Martinez Outschoorn[165], S. Martin-Haugh[131], V.S. Martoiu[28b], A.C. Martyniuk[79], M. Marx[138], A. Marzin[32], L. Masetti[84], T. Mashimo[155], R. Mashinistov[96], J. Masik[85], A.L. Maslennikov[109,*c*], I. Massa[22a,22b], L. Massa[22a,22b], P. Mastrandrea[5], A. Mastroberardino[39a,39b], T. Masubuchi[155], P. Mättig[174], J. Mattmann[84], J. Maurer[28b], S.J. Maxfield[75], D.A. Maximov[109,*c*], R. Mazini[151], S.M. Mazza[92a,92b], N.C. Mc Fadden[105], G. Mc Goldrick[158], S.P. Mc Kee[90], A. McCarn[90], R.L. McCarthy[148], T.G. McCarthy[101], L.I. McClymont[79], E.F. McDonald[89], J.A. Mcfayden[79], G. Mchedlidze[56], S.J. McMahon[131], R.A. McPherson[168,*l*], M. Medinnis[44], S. Meehan[138], S. Mehlhase[100], A. Mehta[75], K. Meier[59a], C. Meineck[100], B. Meirose[43], D. Melini[166], B.R. Mellado Garcia[145c], M. Melo[144a], F. Meloni[18], A. Mengarelli[22a,22b], S. Menke[101], E. Meoni[161], S. Mergelmeyer[17], P. Mermod[51], L. Merola[104a,104b], C. Meroni[92a], F.S. Merritt[33], A. Messina[132a,132b], J. Metcalfe[6], A.S. Mete[162], C. Meyer[84], C. Meyer[122], J-P. Meyer[136], J. Meyer[107], H. Meyer Zu Theenhausen[59a], F. Miano[149], R.P. Middleton[131], S. Miglioranzi[52a,52b], L. Mijović[23], G. Mikenberg[171], M. Mikestikova[127], M. Mikuž[76], M. Milesi[89], A. Milic[63], D.W. Miller[33], C. Mills[48], A. Milov[171], D.A. Milstead[146a,146b], A.A. Minaenko[130], Y. Minami[155], I.A. Minashvili[66], A.I. Mincer[110], B. Mindur[40a], M. Mineev[66], Y. Ming[172], L.M. Mir[13], K.P. Mistry[122], T. Mitani[170], J. Mitrevski[100], V.A. Mitsou[166], A. Miucci[51], P.S. Miyagawa[139],

J.U. Mjörnmark[82], T. Moa[146a,146b], K. Mochizuki[95], S. Mohapatra[37], S. Molander[146a,146b], R. Moles-Valls[23], R. Monden[69], M.C. Mondragon[91], K. Mönig[44], J. Monk[38], E. Monnier[86], A. Montalbano[148], J. Montejo Berlingen[32], F. Monticelli[72], S. Monzani[92a,92b], R.W. Moore[3], N. Morange[117], D. Moreno[21], M. Moreno Llácer[56], P. Morettini[52a], D. Mori[142], T. Mori[155], M. Morii[58], M. Morinaga[155], V. Morisbak[119], S. Moritz[84], A.K. Morley[150], G. Mornacchi[32], J.D. Morris[77], S.S. Mortensen[38], L. Morvaj[148], M. Mosidze[53b], J. Moss[143], K. Motohashi[157], R. Mount[143], E. Mountricha[27], S.V. Mouraviev[96,*], E.J.W. Moyse[87], S. Muanza[86], R.D. Mudd[19], F. Mueller[101], J. Mueller[125], R.S.P. Mueller[100], T. Mueller[30], D. Muenstermann[73], P. Mullen[55], G.A. Mullier[18], F.J. Munoz Sanchez[85], J.A. Murillo Quijada[19], W.J. Murray[169,131], H. Musheghyan[56], M. Muškinja[76], A.G. Myagkov[130,*ae*], M. Myska[128], B.P. Nachman[143], O. Nackenhorst[51], K. Nagai[120], R. Nagai[67,*z*], K. Nagano[67], Y. Nagasaka[60], K. Nagata[160], M. Nagel[50], E. Nagy[86], A.M. Nairz[32], Y. Nakahama[32], K. Nakamura[67], T. Nakamura[155], I. Nakano[112], H. Namasivayam[43], R.F. Naranjo Garcia[44], R. Narayan[11], D.I. Narrias Villar[59a], I. Naryshkin[123], T. Naumann[44], G. Navarro[21], R. Nayyar[7], H.A. Neal[90], P.Yu. Nechaeva[96], T.J. Neep[85], P.D. Nef[143], A. Negri[121a,121b], M. Negrini[22a], S. Nektarijevic[106], C. Nellist[117], A. Nelson[162], S. Nemecek[127], P. Nemethy[110], A.A. Nepomuceno[26a], M. Nessi[32,*af*], M.S. Neubauer[165], M. Neumann[174], R.M. Neves[110], P. Nevski[27], P.R. Newman[19], D.H. Nguyen[6], T. Nguyen Manh[95], R.B. Nickerson[120], R. Nicolaidou[136], J. Nielsen[137], A. Nikiforov[17], V. Nikolaenko[130,*ae*], I. Nikolic-Audit[81], K. Nikolopoulos[19], J.K. Nilsen[119], P. Nilsson[27], Y. Ninomiya[155], A. Nisati[132a], R. Nisius[101], T. Nobe[155], M. Nomachi[118], I. Nomidis[31], T. Nooney[77], S. Norberg[113], M. Nordberg[32], N. Norjoharuddeen[120], O. Novgorodova[46], S. Nowak[101], M. Nozaki[67], L. Nozka[115], K. Ntekas[10], E. Nurse[79], F. Nuti[89], F. O'grady[7], D.C. O'Neil[142], A.A. O'Rourke[44], V. O'Shea[55], F.G. Oakham[31,*d*], H. Oberlack[101], T. Obermann[23], J. Ocariz[81], A. Ochi[68], I. Ochoa[37], J.P. Ochoa-Ricoux[34a], S. Oda[71], S. Odaka[67], H. Ogren[62], A. Oh[85], S.H. Oh[47], C.C. Ohm[16], H. Ohman[164], H. Oide[32], H. Okawa[160], Y. Okumura[33], T. Okuyama[67], A. Olariu[28b], L.F. Oleiro Seabra[126a], S.A. Olivares Pino[48], D. Oliveira Damazio[27], A. Olszewski[41], J. Olszowska[41], A. Onofre[126a,126e], K. Onogi[103], P.U.E. Onyisi[11,*v*], M.J. Oreglia[33], Y. Oren[153], D. Orestano[134a,134b], N. Orlando[61b], R.S. Orr[158], B. Osculati[52a,52b], R. Ospanov[85], G. Otero y Garzon[29], H. Otono[71], M. Ouchrif[135d], F. Ould-Saada[119], A. Ouraou[136], K.P. Oussoren[107], Q. Ouyang[35a], M. Owen[55], R.E. Owen[19], V.E. Ozcan[20a], N. Ozturk[8], K. Pachal[142], A. Pacheco Pages[13], L. Pacheco Rodriguez[136], C. Padilla Aranda[13], M. Pagáčová[50], S. Pagan Griso[16], F. Paige[27], P. Pais[87], K. Pajchel[119], G. Palacino[159b], S. Palestini[32], M. Palka[40b], D. Pallin[36], A. Palma[126a,126b], E.St. Panagiotopoulou[10], C.E. Pandini[81], J.G. Panduro Vazquez[78], P. Pani[146a,146b], S. Panitkin[27], D. Pantea[28b], L. Paolozzi[51], Th.D. Papadopoulou[10], K. Papageorgiou[154], A. Paramonov[6], D. Paredes Hernandez[175], A.J. Parker[73], M.A. Parker[30], K.A. Parker[139], F. Parodi[52a,52b], J.A. Parsons[37], U. Parzefall[50], V.R. Pascuzzi[158], E. Pasqualucci[132a], S. Passaggio[52a], Fr. Pastore[78], G. Pásztor[31,*ag*], S. Pataraia[174], J.R. Pater[85], T. Pauly[32], J. Pearce[168], B. Pearson[113], L.E. Pedersen[38], M. Pedersen[119], S. Pedraza Lopez[166], R. Pedro[126a,126b], S.V. Peleganchuk[109,*c*], D. Pelikan[164], O. Penc[127], C. Peng[35a], H. Peng[35b], J. Penwell[62], B.S. Peralva[26b], M.M. Perego[136], D.V. Perepelitsa[27], E. Perez Codina[159a], L. Perini[92a,92b], H. Pernegger[32], S. Perrella[104a,104b], R. Peschke[44], V.D. Peshekhonov[66], K. Peters[44], R.F.Y. Peters[85], B.A. Petersen[32], T.C. Petersen[38], E. Petit[57], A. Petridis[1], C. Petridou[154], P. Petroff[117], E. Petrolo[132a], M. Petrov[120], F. Petrucci[134a,134b], N.E. Pettersson[87], A. Peyaud[136], R. Pezoa[34b], P.W. Phillips[131], G. Piacquadio[143], E. Pianori[169], A. Picazio[87], E. Piccaro[77], M. Piccinini[22a,22b], M.A. Pickering[120], R. Piegaia[29], J.E. Pilcher[33], A.D. Pilkington[85], A.W.J. Pin[85], M. Pinamonti[163a,163c,*ah*], J.L. Pinfold[3], A. Pingel[38], S. Pires[81], H. Pirumov[44], M. Pitt[171], L. Plazak[144a], M.-A. Pleier[27], V. Pleskot[84], E. Plotnikova[66], P. Plucinski[91], D. Pluth[65], R. Poettgen[146a,146b], L. Poggioli[117], D. Pohl[23], G. Polesello[121a], A. Poley[44], A. Policicchio[39a,39b], R. Polifka[158], A. Polini[22a], C.S. Pollard[55], V. Polychronakos[27], K. Pommès[32], L. Pontecorvo[132a], B.G. Pope[91], G.A. Popeneciu[28c], D.S. Popovic[14], A. Poppleton[32], S. Pospisil[128],

K. Potamianos[16], I.N. Potrap[66], C.J. Potter[30], C.T. Potter[116], G. Poulard[32], J. Poveda[32], V. Pozdnyakov[66], M.E. Pozo Astigarraga[32], P. Pralavorio[86], A. Pranko[16], S. Prell[65], D. Price[85], L.E. Price[6], M. Primavera[74a], S. Prince[88], K. Prokofiev[61c], F. Prokoshin[34b], S. Protopopescu[27], J. Proudfoot[6], M. Przybycien[40a], D. Puddu[134a,134b], M. Purohit[27,ai], P. Puzo[117], J. Qian[90], G. Qin[55], Y. Qin[85], A. Quadt[56], W.B. Quayle[163a,163b], M. Queitsch-Maitland[85], D. Quilty[55], S. Raddum[119], V. Radeka[27], V. Radescu[59b], S.K. Radhakrishnan[148], P. Radloff[116], P. Rados[89], F. Ragusa[92a,92b], G. Rahal[177], J.A. Raine[85], S. Rajagopalan[27], M. Rammensee[32], C. Rangel-Smith[164], M.G. Ratti[92a,92b], F. Rauscher[100], S. Rave[84], T. Ravenscroft[55], I. Ravinovich[171], M. Raymond[32], A.L. Read[119], N.P. Readioff[75], M. Reale[74a,74b], D.M. Rebuzzi[121a,121b], A. Redelbach[173], G. Redlinger[27], R. Reece[137], K. Reeves[43], L. Rehnisch[17], J. Reichert[122], H. Reisin[29], C. Rembser[32], H. Ren[35a], M. Rescigno[132a], S. Resconi[92a], O.L. Rezanova[109,c], P. Reznicek[129], R. Rezvani[95], R. Richter[101], S. Richter[79], E. Richter-Was[40b], O. Ricken[23], M. Ridel[81], P. Rieck[17], C.J. Riegel[174], J. Rieger[56], O. Rifki[113], M. Rijssenbeek[148], A. Rimoldi[121a,121b], M. Rimoldi[18], L. Rinaldi[22a], B. Ristić[51], E. Ritsch[32], I. Riu[13], F. Rizatdinova[114], E. Rizvi[77], C. Rizzi[13], S.H. Robertson[88,l], A. Robichaud-Veronneau[88], D. Robinson[30], J.E.M. Robinson[44], A. Robson[55], C. Roda[124a,124b], Y. Rodina[86], A. Rodriguez Perez[13], D. Rodriguez Rodriguez[166], S. Roe[32], C.S. Rogan[58], O. Røhne[119], A. Romaniouk[98], M. Romano[22a,22b], S.M. Romano Saez[36], E. Romero Adam[166], N. Rompotis[138], M. Ronzani[50], L. Roos[81], E. Ros[166], S. Rosati[132a], K. Rosbach[50], P. Rose[137], O. Rosenthal[141], N.-A. Rosien[56], V. Rossetti[146a,146b], E. Rossi[104a,104b], L.P. Rossi[52a], J.H.N. Rosten[30], R. Rosten[138], M. Rotaru[28b], I. Roth[171], J. Rothberg[138], D. Rousseau[117], C.R. Royon[136], A. Rozanov[86], Y. Rozen[152], X. Ruan[145c], F. Rubbo[143], M.S. Rudolph[158], F. Rühr[50], A. Ruiz-Martinez[31], Z. Rurikova[50], N.A. Rusakovich[66], A. Ruschke[100], H.L. Russell[138], J.P. Rutherfoord[7], N. Ruthmann[32], Y.F. Ryabov[123], M. Rybar[165], G. Rybkin[117], S. Ryu[6], A. Ryzhov[130], G.F. Rzehorz[56], A.F. Saavedra[150], G. Sabato[107], S. Sacerdoti[29], H.F-W. Sadrozinski[137], R. Sadykov[66], F. Safai Tehrani[132a], P. Saha[108], M. Sahinsoy[59a], M. Saimpert[136], T. Saito[155], H. Sakamoto[155], Y. Sakurai[170], G. Salamanna[134a,134b], A. Salamon[133a,133b], J.E. Salazar Loyola[34b], D. Salek[107], P.H. Sales De Bruin[138], D. Salihagic[101], A. Salnikov[143], J. Salt[166], D. Salvatore[39a,39b], F. Salvatore[149], A. Salvucci[61a], A. Salzburger[32], D. Sammel[50], D. Sampsonidis[154], A. Sanchez[104a,104b], J. Sánchez[166], V. Sanchez Martinez[166], H. Sandaker[119], R.L. Sandbach[77], H.G. Sander[84], M. Sandhoff[174], C. Sandoval[21], R. Sandstroem[101], D.P.C. Sankey[131], M. Sannino[52a,52b], A. Sansoni[49], C. Santoni[36], R. Santonico[133a,133b], H. Santos[126a], I. Santoyo Castillo[149], K. Sapp[125], A. Sapronov[66], J.G. Saraiva[126a,126d], B. Sarrazin[23], O. Sasaki[67], Y. Sasaki[155], K. Sato[160], G. Sauvage[5,*], E. Sauvan[5], G. Savage[78], P. Savard[158,d], C. Sawyer[131], L. Sawyer[80,q], J. Saxon[33], C. Sbarra[22a], A. Sbrizzi[22a,22b], T. Scanlon[79], D.A. Scannicchio[162], M. Scarcella[150], V. Scarfone[39a,39b], J. Schaarschmidt[171], P. Schacht[101], B.M. Schachtner[100], D. Schaefer[32], R. Schaefer[44], J. Schaeffer[84], S. Schaepe[23], S. Schaetzel[59b], U. Schäfer[84], A.C. Schaffer[117], D. Schaile[100], R.D. Schamberger[148], V. Scharf[59a], V.A. Schegelsky[123], D. Scheirich[129], M. Schernau[162], C. Schiavi[52a,52b], S. Schier[137], C. Schillo[50], M. Schioppa[39a,39b], S. Schlenker[32], K.R. Schmidt-Sommerfeld[101], K. Schmieden[32], C. Schmitt[84], S. Schmitt[44], S. Schmitz[84], B. Schneider[159a], U. Schnoor[50], L. Schoeffel[136], A. Schoening[59b], B.D. Schoenrock[91], E. Schopf[23], M. Schott[84], J. Schovancova[8], S. Schramm[51], M. Schreyer[173], N. Schuh[84], A. Schulte[84], M.J. Schultens[23], H.-C. Schultz-Coulon[59a], H. Schulz[17], M. Schumacher[50], B.A. Schumm[137], Ph. Schune[136], A. Schwartzman[143], T.A. Schwarz[90], Ph. Schwegler[101], H. Schweiger[85], Ph. Schwemling[136], R. Schwienhorst[91], J. Schwindling[136], T. Schwindt[23], G. Sciolla[25], F. Scuri[124a,124b], F. Scutti[89], J. Searcy[90], P. Seema[23], S.C. Seidel[105], A. Seiden[137], F. Seifert[128], J.M. Seixas[26a], G. Sekhniaidze[104a], K. Sekhon[90], S.J. Sekula[42], D.M. Seliverstov[123,*], N. Semprini-Cesari[22a,22b], C. Serfon[119], L. Serin[117], L. Serkin[163a,163b], M. Sessa[134a,134b], R. Seuster[168], H. Severini[113], T. Sfiligoj[76], F. Sforza[32], A. Sfyrla[51], E. Shabalina[56], N.W. Shaikh[146a,146b], L.Y. Shan[35a], R. Shang[165], J.T. Shank[24], M. Shapiro[16], P.B. Shatalov[97], K. Shaw[163a,163b], S.M. Shaw[85],

A. Shcherbakova[146a,146b], C.Y. Shehu[149], P. Sherwood[79], L. Shi[151,aj], S. Shimizu[68], C.O. Shimmin[162], M. Shimojima[102], M. Shiyakova[66,ak], A. Shmeleva[96], D. Shoaleh Saadi[95], M.J. Shochet[33], S. Shojaii[92a,92b], S. Shrestha[111], E. Shulga[98], M.A. Shupe[7], P. Sicho[127], A.M. Sickles[165], P.E. Sidebo[147], O. Sidiropoulou[173], D. Sidorov[114], A. Sidoti[22a,22b], F. Siegert[46], Dj. Sijacki[14], J. Silva[126a,126d], S.B. Silverstein[146a], V. Simak[128], O. Simard[5], Lj. Simic[14], S. Simion[117], E. Simioni[84], B. Simmons[79], D. Simon[36], M. Simon[84], P. Sinervo[158], N.B. Sinev[116], M. Sioli[22a,22b], G. Siragusa[173], S.Yu. Sivoklokov[99], J. Sjölin[146a,146b], M.B. Skinner[73], H.P. Skottowe[58], P. Skubic[113], M. Slater[19], T. Slavicek[128], M. Slawinska[107], K. Sliwa[161], R. Slovak[129], V. Smakhtin[171], B.H. Smart[5], L. Smestad[15], J. Smiesko[144a], S.Yu. Smirnov[98], Y. Smirnov[98], L.N. Smirnova[99,al], O. Smirnova[82], M.N.K. Smith[37], R.W. Smith[37], M. Smizanska[73], K. Smolek[128], A.A. Snesarev[96], S. Snyder[27], R. Sobie[168,l], F. Socher[46], A. Soffer[153], D.A. Soh[151], G. Sokhrannyi[76], C.A. Solans Sanchez[32], M. Solar[128], E.Yu. Soldatov[98], U. Soldevila[166], A.A. Solodkov[130], A. Soloshenko[66], O.V. Solovyanov[130], V. Solovyev[123], P. Sommer[50], H. Son[161], H.Y. Song[35b,am], A. Sood[16], A. Sopczak[128], V. Sopko[128], V. Sorin[13], D. Sosa[59b], C.L. Sotiropoulou[124a,124b], R. Soualah[163a,163c], A.M. Soukharev[109,c], D. South[44], B.C. Sowden[78], S. Spagnolo[74a,74b], M. Spalla[124a,124b], M. Spangenberg[169], F. Spanò[78], D. Sperlich[17], F. Spettel[101], R. Spighi[22a], G. Spigo[32], L.A. Spiller[89], M. Spousta[129], R.D. St. Denis[55,*], A. Stabile[92a], R. Stamen[59a], S. Stamm[17], E. Stanecka[41], R.W. Stanek[6], C. Stanescu[134a], M. Stanescu-Bellu[44], M.M. Stanitzki[44], S. Stapnes[119], E.A. Starchenko[130], G.H. Stark[33], J. Stark[57], P. Staroba[127], P. Starovoitov[59a], S. Stärz[32], R. Staszewski[41], P. Steinberg[27], B. Stelzer[142], H.J. Stelzer[32], O. Stelzer-Chilton[159a], H. Stenzel[54], G.A. Stewart[55], J.A. Stillings[23], M.C. Stockton[88], M. Stoebe[88], G. Stoicea[28b], P. Stolte[56], S. Stonjek[101], A.R. Stradling[8], A. Straessner[46], M.E. Stramaglia[18], J. Strandberg[147], S. Strandberg[146a,146b], A. Strandlie[119], M. Strauss[113], P. Strizenec[144b], R. Ströhmer[173], D.M. Strom[116], R. Stroynowski[42], A. Strubig[106], S.A. Stucci[18], B. Stugu[15], N.A. Styles[44], D. Su[143], J. Su[125], S. Suchek[59a], Y. Sugaya[118], M. Suk[128], V.V. Sulin[96], S. Sultansoy[4c], T. Sumida[69], S. Sun[58], X. Sun[35a], J.E. Sundermann[50], K. Suruliz[149], G. Susinno[39a,39b], M.R. Sutton[149], S. Suzuki[67], M. Svatos[127], M. Swiatlowski[33], I. Sykora[144a], T. Sykora[129], D. Ta[50], C. Taccini[134a,134b], K. Tackmann[44], J. Taenzer[158], A. Taffard[162], R. Tafirout[159a], N. Taiblum[153], H. Takai[27], R. Takashima[70], T. Takeshita[140], Y. Takubo[67], M. Talby[86], A.A. Talyshev[109,c], K.G. Tan[89], J. Tanaka[155], R. Tanaka[117], S. Tanaka[67], B.B. Tannenwald[111], S. Tapia Araya[34b], S. Tapprogge[84], S. Tarem[152], G.F. Tartarelli[92a], P. Tas[129], M. Tasevsky[127], T. Tashiro[69], E. Tassi[39a,39b], A. Tavares Delgado[126a,126b], Y. Tayalati[135e], A.C. Taylor[105], G.N. Taylor[89], P.T.E. Taylor[89], W. Taylor[159b], F.A. Teischinger[32], P. Teixeira-Dias[78], K.K. Temming[50], D. Temple[142], H. Ten Kate[32], P.K. Teng[151], J.J. Teoh[118], F. Tepel[174], S. Terada[67], K. Terashi[155], J. Terron[83], S. Terzo[101], M. Testa[49], R.J. Teuscher[158,l], T. Theveneaux-Pelzer[86], J.P. Thomas[19], J. Thomas-Wilsker[78], E.N. Thompson[37], P.D. Thompson[19], A.S. Thompson[55], L.A. Thomsen[175], E. Thomson[122], M. Thomson[30], M.J. Tibbetts[16], R.E. Ticse Torres[86], V.O. Tikhomirov[96,an], Yu.A. Tikhonov[109,c], S. Timoshenko[98], P. Tipton[175], S. Tisserant[86], K. Todome[157], T. Todorov[5,*], S. Todorova-Nova[129], J. Tojo[71], S. Tokár[144a], K. Tokushuku[67], E. Tolley[58], L. Tomlinson[85], M. Tomoto[103], L. Tompkins[143,ao], K. Toms[105], B. Tong[58], E. Torrence[116], H. Torres[142], E. Torró Pastor[138], J. Toth[86,ap], F. Touchard[86], D.R. Tovey[139], T. Trefzger[173], A. Tricoli[27], I.M. Trigger[159a], S. Trincaz-Duvoid[81], M.F. Tripiana[13], W. Trischuk[158], B. Trocmé[57], A. Trofymov[44], C. Troncon[92a], M. Trottier-McDonald[16], M. Trovatelli[168], L. Truong[163a,163c], M. Trzebinski[41], A. Trzupek[41], J.C-L. Tseng[120], P.V. Tsiareshka[93], G. Tsipolitis[10], N. Tsirintanis[9], S. Tsiskaridze[13], V. Tsiskaridze[50], E.G. Tskhadadze[53a], K.M. Tsui[61a], I.I. Tsukerman[97], V. Tsulaia[16], S. Tsuno[67], D. Tsybychev[148], A. Tudorache[28b], V. Tudorache[28b], A.N. Tuna[58], S.A. Tupputi[22a,22b], S. Turchikhin[99,al], D. Turecek[128], D. Turgeman[171], R. Turra[92a,92b], A.J. Turvey[42], P.M. Tuts[37], M. Tyndel[131], G. Ucchielli[22a,22b], I. Ueda[155], M. Ughetto[146a,146b], F. Ukegawa[160], G. Unal[32], A. Undrus[27], G. Unel[162], F.C. Ungaro[89], Y. Unno[67], C. Unverdorben[100], J. Urban[144b], P. Urquijo[89], P. Urrejola[84], G. Usai[8], A. Usanova[63], L. Vacavant[86], V. Vacek[128], B. Vachon[88],

C. Valderanis[100], E. Valdes Santurio[146a,146b], N. Valencic[107], S. Valentinetti[22a,22b], A. Valero[166], L. Valery[13], S. Valkar[129], S. Vallecorsa[51], J.A. Valls Ferrer[166], W. Van Den Wollenberg[107], P.C. Van Der Deijl[107], R. van der Geer[107], H. van der Graaf[107], N. van Eldik[152], P. van Gemmeren[6], J. Van Nieuwkoop[142], I. van Vulpen[107], M.C. van Woerden[32], M. Vanadia[132a,132b], W. Vandelli[32], R. Vanguri[122], A. Vaniachine[130], P. Vankov[107], G. Vardanyan[176], R. Vari[132a], E.W. Varnes[7], T. Varol[42], D. Varouchas[81], A. Vartapetian[8], K.E. Varvell[150], J.G. Vasquez[175], F. Vazeille[36], T. Vazquez Schroeder[88], J. Veatch[56], L.M. Veloce[158], F. Veloso[126a,126c], S. Veneziano[132a], A. Ventura[74a,74b], M. Venturi[168], N. Venturi[158], A. Venturini[25], V. Vercesi[121a], M. Verducci[132a,132b], W. Verkerke[107], J.C. Vermeulen[107], A. Vest[46,*aq*], M.C. Vetterli[142,*d*], O. Viazlo[82], I. Vichou[165,*], T. Vickey[139], O.E. Vickey Boeriu[139], G.H.A. Viehhauser[120], S. Viel[16], L. Vigani[120], M. Villa[22a,22b], M. Villaplana Perez[92a,92b], E. Vilucchi[49], M.G. Vincter[31], V.B. Vinogradov[66], C. Vittori[22a,22b], I. Vivarelli[149], S. Vlachos[10], M. Vlasak[128], M. Vogel[174], P. Vokac[128], G. Volpi[124a,124b], M. Volpi[89], H. von der Schmitt[101], E. von Toerne[23], V. Vorobel[129], K. Vorobev[98], M. Vos[166], R. Voss[32], J.H. Vossebeld[75], N. Vranjes[14], M. Vranjes Milosavljevic[14], V. Vrba[127], M. Vreeswijk[107], R. Vuillermet[32], I. Vukotic[33], Z. Vykydal[128], P. Wagner[23], W. Wagner[174], H. Wahlberg[72], S. Wahrmund[46], J. Wakabayashi[103], J. Walder[73], R. Walker[100], W. Walkowiak[141], V. Wallangen[146a,146b], C. Wang[35c], C. Wang[35d,86], F. Wang[172], H. Wang[16], H. Wang[42], J. Wang[44], J. Wang[150], K. Wang[88], R. Wang[6], S.M. Wang[151], T. Wang[23], T. Wang[37], W. Wang[35b], X. Wang[175], C. Wanotayaroj[116], A. Warburton[88], C.P. Ward[30], D.R. Wardrope[79], A. Washbrook[48], P.M. Watkins[19], A.T. Watson[19], M.F. Watson[19], G. Watts[138], S. Watts[85], B.M. Waugh[79], S. Webb[84], M.S. Weber[18], S.W. Weber[173], J.S. Webster[6], A.R. Weidberg[120], B. Weinert[62], J. Weingarten[56], C. Weiser[50], H. Weits[107], P.S. Wells[32], T. Wenaus[27], T. Wengler[32], S. Wenig[32], N. Wermes[23], M. Werner[50], M.D. Werner[65], P. Werner[32], M. Wessels[59a], J. Wetter[161], K. Whalen[116], N.L. Whallon[138], A.M. Wharton[73], A. White[8], M.J. White[1], R. White[34b], D. Whiteson[162], F.J. Wickens[131], W. Wiedenmann[172], M. Wielers[131], P. Wienemann[23], C. Wiglesworth[38], L.A.M. Wiik-Fuchs[23], A. Wildauer[101], F. Wilk[85], H.G. Wilkens[32], H.H. Williams[122], S. Williams[107], C. Willis[91], S. Willocq[87], J.A. Wilson[19], I. Wingerter-Seez[5], F. Winklmeier[116], O.J. Winston[149], B.T. Winter[23], M. Wittgen[143], J. Wittkowski[100], T.M.H. Wolf[107], M.W. Wolter[41], H. Wolters[126a,126c], S.D. Worm[131], B.K. Wosiek[41], J. Wotschack[32], M.J. Woudstra[85], K.W. Wozniak[41], M. Wu[57], M. Wu[33], S.L. Wu[172], X. Wu[51], Y. Wu[90], T.R. Wyatt[85], B.M. Wynne[48], S. Xella[38], D. Xu[35a], L. Xu[27], B. Yabsley[150], S. Yacoob[145a], R. Yakabe[68], D. Yamaguchi[157], Y. Yamaguchi[118], A. Yamamoto[67], S. Yamamoto[155], T. Yamanaka[155], K. Yamauchi[103], Y. Yamazaki[68], Z. Yan[24], H. Yang[35e], H. Yang[172], Y. Yang[151], Z. Yang[15], W-M. Yao[16], Y.C. Yap[81], Y. Yasu[67], E. Yatsenko[5], K.H. Yau Wong[23], J. Ye[42], S. Ye[27], I. Yeletskikh[66], A.L. Yen[58], E. Yildirim[84], K. Yorita[170], R. Yoshida[6], K. Yoshihara[122], C. Young[143], C.J.S. Young[32], S. Youssef[24], D.R. Yu[16], J. Yu[8], J.M. Yu[90], J. Yu[65], L. Yuan[68], S.P.Y. Yuen[23], I. Yusuff[30,*ar*], B. Zabinski[41], R. Zaidan[35d], A.M. Zaitsev[130,*ae*], N. Zakharchuk[44], J. Zalieckas[15], A. Zaman[148], S. Zambito[58], L. Zanello[132a,132b], D. Zanzi[89], C. Zeitnitz[174], M. Zeman[128], A. Zemla[40a], J.C. Zeng[165], Q. Zeng[143], K. Zengel[25], O. Zenin[130], T. Ženiš[144a], D. Zerwas[117], D. Zhang[90], F. Zhang[172], G. Zhang[35b,*am*], H. Zhang[35c], J. Zhang[6], L. Zhang[50], R. Zhang[23], R. Zhang[35b,*as*], X. Zhang[35d], Z. Zhang[117], X. Zhao[42], Y. Zhao[35d], Z. Zhao[35b], A. Zhemchugov[66], J. Zhong[120], B. Zhou[90], C. Zhou[47], L. Zhou[37], L. Zhou[42], M. Zhou[148], N. Zhou[35f], C.G. Zhu[35d], H. Zhu[35a], J. Zhu[90], Y. Zhu[35b], X. Zhuang[35a], K. Zhukov[96], A. Zibell[173], D. Zieminska[62], N.I. Zimine[66], C. Zimmermann[84], S. Zimmermann[50], Z. Zinonos[56], M. Zinser[84], M. Ziolkowski[141], L. Živković[14], G. Zobernig[172], A. Zoccoli[22a,22b], M. zur Nedden[17], L. Zwalinski[32].

[1] Department of Physics, University of Adelaide, Adelaide, Australia
[2] Physics Department, SUNY Albany, Albany NY, United States of America
[3] Department of Physics, University of Alberta, Edmonton AB, Canada

[4] [(a)] Department of Physics, Ankara University, Ankara; [(b)] Istanbul Aydin University, Istanbul; [(c)] Division of Physics, TOBB University of Economics and Technology, Ankara, Turkey
[5] LAPP, CNRS/IN2P3 and Université Savoie Mont Blanc, Annecy-le-Vieux, France
[6] High Energy Physics Division, Argonne National Laboratory, Argonne IL, United States of America
[7] Department of Physics, University of Arizona, Tucson AZ, United States of America
[8] Department of Physics, The University of Texas at Arlington, Arlington TX, United States of America
[9] Physics Department, University of Athens, Athens, Greece
[10] Physics Department, National Technical University of Athens, Zografou, Greece
[11] Department of Physics, The University of Texas at Austin, Austin TX, United States of America
[12] Institute of Physics, Azerbaijan Academy of Sciences, Baku, Azerbaijan
[13] Institut de Física d'Altes Energies (IFAE), The Barcelona Institute of Science and Technology, Barcelona, Spain, Spain
[14] Institute of Physics, University of Belgrade, Belgrade, Serbia
[15] Department for Physics and Technology, University of Bergen, Bergen, Norway
[16] Physics Division, Lawrence Berkeley National Laboratory and University of California, Berkeley CA, United States of America
[17] Department of Physics, Humboldt University, Berlin, Germany
[18] Albert Einstein Center for Fundamental Physics and Laboratory for High Energy Physics, University of Bern, Bern, Switzerland
[19] School of Physics and Astronomy, University of Birmingham, Birmingham, United Kingdom
[20] [(a)] Department of Physics, Bogazici University, Istanbul; [(b)] Department of Physics Engineering, Gaziantep University, Gaziantep; [(d)] Istanbul Bilgi University, Faculty of Engineering and Natural Sciences, Istanbul,Turkey; [(e)] Bahcesehir University, Faculty of Engineering and Natural Sciences, Istanbul, Turkey, Turkey
[21] Centro de Investigaciones, Universidad Antonio Narino, Bogota, Colombia
[22] [(a)] INFN Sezione di Bologna; [(b)] Dipartimento di Fisica e Astronomia, Università di Bologna, Bologna, Italy
[23] Physikalisches Institut, University of Bonn, Bonn, Germany
[24] Department of Physics, Boston University, Boston MA, United States of America
[25] Department of Physics, Brandeis University, Waltham MA, United States of America
[26] [(a)] Universidade Federal do Rio De Janeiro COPPE/EE/IF, Rio de Janeiro; [(b)] Electrical Circuits Department, Federal University of Juiz de Fora (UFJF), Juiz de Fora; [(c)] Federal University of Sao Joao del Rei (UFSJ), Sao Joao del Rei; [(d)] Instituto de Fisica, Universidade de Sao Paulo, Sao Paulo, Brazil
[27] Physics Department, Brookhaven National Laboratory, Upton NY, United States of America
[28] [(a)] Transilvania University of Brasov, Brasov, Romania; [(b)] National Institute of Physics and Nuclear Engineering, Bucharest; [(c)] National Institute for Research and Development of Isotopic and Molecular Technologies, Physics Department, Cluj Napoca; [(d)] University Politehnica Bucharest, Bucharest; [(e)] West University in Timisoara, Timisoara, Romania
[29] Departamento de Física, Universidad de Buenos Aires, Buenos Aires, Argentina
[30] Cavendish Laboratory, University of Cambridge, Cambridge, United Kingdom
[31] Department of Physics, Carleton University, Ottawa ON, Canada
[32] CERN, Geneva, Switzerland
[33] Enrico Fermi Institute, University of Chicago, Chicago IL, United States of America
[34] [(a)] Departamento de Física, Pontificia Universidad Católica de Chile, Santiago; [(b)] Departamento de Física, Universidad Técnica Federico Santa María, Valparaíso, Chile
[35] [(a)] Institute of High Energy Physics, Chinese Academy of Sciences, Beijing; [(b)] Department of Modern Physics, University of Science and Technology of China, Anhui; [(c)] Department of Physics,

Nanjing University, Jiangsu; [d] School of Physics, Shandong University, Shandong; [e] Department of Physics and Astronomy, Shanghai Key Laboratory for Particle Physics and Cosmology, Shanghai Jiao Tong University, Shanghai; (also affiliated with PKU-CHEP); [f] Physics Department, Tsinghua University, Beijing 100084, China
[36] Laboratoire de Physique Corpusculaire, Clermont Université and Université Blaise Pascal and CNRS/IN2P3, Clermont-Ferrand, France
[37] Nevis Laboratory, Columbia University, Irvington NY, United States of America
[38] Niels Bohr Institute, University of Copenhagen, Kobenhavn, Denmark
[39] [a] INFN Gruppo Collegato di Cosenza, Laboratori Nazionali di Frascati; [b] Dipartimento di Fisica, Università della Calabria, Rende, Italy
[40] [a] AGH University of Science and Technology, Faculty of Physics and Applied Computer Science, Krakow; [b] Marian Smoluchowski Institute of Physics, Jagiellonian University, Krakow, Poland
[41] Institute of Nuclear Physics Polish Academy of Sciences, Krakow, Poland
[42] Physics Department, Southern Methodist University, Dallas TX, United States of America
[43] Physics Department, University of Texas at Dallas, Richardson TX, United States of America
[44] DESY, Hamburg and Zeuthen, Germany
[45] Institut für Experimentelle Physik IV, Technische Universität Dortmund, Dortmund, Germany
[46] Institut für Kern- und Teilchenphysik, Technische Universität Dresden, Dresden, Germany
[47] Department of Physics, Duke University, Durham NC, United States of America
[48] SUPA - School of Physics and Astronomy, University of Edinburgh, Edinburgh, United Kingdom
[49] INFN Laboratori Nazionali di Frascati, Frascati, Italy
[50] Fakultät für Mathematik und Physik, Albert-Ludwigs-Universität, Freiburg, Germany
[51] Section de Physique, Université de Genève, Geneva, Switzerland
[52] [a] INFN Sezione di Genova; [b] Dipartimento di Fisica, Università di Genova, Genova, Italy
[53] [a] E. Andronikashvili Institute of Physics, Iv. Javakhishvili Tbilisi State University, Tbilisi; [b] High Energy Physics Institute, Tbilisi State University, Tbilisi, Georgia
[54] II Physikalisches Institut, Justus-Liebig-Universität Giessen, Giessen, Germany
[55] SUPA - School of Physics and Astronomy, University of Glasgow, Glasgow, United Kingdom
[56] II Physikalisches Institut, Georg-August-Universität, Göttingen, Germany
[57] Laboratoire de Physique Subatomique et de Cosmologie, Université Grenoble-Alpes, CNRS/IN2P3, Grenoble, France
[58] Laboratory for Particle Physics and Cosmology, Harvard University, Cambridge MA, United States of America
[59] [a] Kirchhoff-Institut für Physik, Ruprecht-Karls-Universität Heidelberg, Heidelberg; [b] Physikalisches Institut, Ruprecht-Karls-Universität Heidelberg, Heidelberg; [c] ZITI Institut für technische Informatik, Ruprecht-Karls-Universität Heidelberg, Mannheim, Germany
[60] Faculty of Applied Information Science, Hiroshima Institute of Technology, Hiroshima, Japan
[61] [a] Department of Physics, The Chinese University of Hong Kong, Shatin, N.T., Hong Kong; [b] Department of Physics, The University of Hong Kong, Hong Kong; [c] Department of Physics, The Hong Kong University of Science and Technology, Clear Water Bay, Kowloon, Hong Kong, China
[62] Department of Physics, Indiana University, Bloomington IN, United States of America
[63] Institut für Astro- und Teilchenphysik, Leopold-Franzens-Universität, Innsbruck, Austria
[64] University of Iowa, Iowa City IA, United States of America
[65] Department of Physics and Astronomy, Iowa State University, Ames IA, United States of America
[66] Joint Institute for Nuclear Research, JINR Dubna, Dubna, Russia
[67] KEK, High Energy Accelerator Research Organization, Tsukuba, Japan
[68] Graduate School of Science, Kobe University, Kobe, Japan

[69] Faculty of Science, Kyoto University, Kyoto, Japan
[70] Kyoto University of Education, Kyoto, Japan
[71] Department of Physics, Kyushu University, Fukuoka, Japan
[72] Instituto de Física La Plata, Universidad Nacional de La Plata and CONICET, La Plata, Argentina
[73] Physics Department, Lancaster University, Lancaster, United Kingdom
[74] [(a)] INFN Sezione di Lecce; [(b)] Dipartimento di Matematica e Fisica, Università del Salento, Lecce, Italy
[75] Oliver Lodge Laboratory, University of Liverpool, Liverpool, United Kingdom
[76] Department of Physics, Jožef Stefan Institute and University of Ljubljana, Ljubljana, Slovenia
[77] School of Physics and Astronomy, Queen Mary University of London, London, United Kingdom
[78] Department of Physics, Royal Holloway University of London, Surrey, United Kingdom
[79] Department of Physics and Astronomy, University College London, London, United Kingdom
[80] Louisiana Tech University, Ruston LA, United States of America
[81] Laboratoire de Physique Nucléaire et de Hautes Energies, UPMC and Université Paris-Diderot and CNRS/IN2P3, Paris, France
[82] Fysiska institutionen, Lunds universitet, Lund, Sweden
[83] Departamento de Fisica Teorica C-15, Universidad Autonoma de Madrid, Madrid, Spain
[84] Institut für Physik, Universität Mainz, Mainz, Germany
[85] School of Physics and Astronomy, University of Manchester, Manchester, United Kingdom
[86] CPPM, Aix-Marseille Université and CNRS/IN2P3, Marseille, France
[87] Department of Physics, University of Massachusetts, Amherst MA, United States of America
[88] Department of Physics, McGill University, Montreal QC, Canada
[89] School of Physics, University of Melbourne, Victoria, Australia
[90] Department of Physics, The University of Michigan, Ann Arbor MI, United States of America
[91] Department of Physics and Astronomy, Michigan State University, East Lansing MI, United States of America
[92] [(a)] INFN Sezione di Milano; [(b)] Dipartimento di Fisica, Università di Milano, Milano, Italy
[93] B.I. Stepanov Institute of Physics, National Academy of Sciences of Belarus, Minsk, Republic of Belarus
[94] National Scientific and Educational Centre for Particle and High Energy Physics, Minsk, Republic of Belarus
[95] Group of Particle Physics, University of Montreal, Montreal QC, Canada
[96] P.N. Lebedev Physical Institute of the Russian Academy of Sciences, Moscow, Russia
[97] Institute for Theoretical and Experimental Physics (ITEP), Moscow, Russia
[98] National Research Nuclear University MEPhI, Moscow, Russia
[99] D.V. Skobeltsyn Institute of Nuclear Physics, M.V. Lomonosov Moscow State University, Moscow, Russia
[100] Fakultät für Physik, Ludwig-Maximilians-Universität München, München, Germany
[101] Max-Planck-Institut für Physik (Werner-Heisenberg-Institut), München, Germany
[102] Nagasaki Institute of Applied Science, Nagasaki, Japan
[103] Graduate School of Science and Kobayashi-Maskawa Institute, Nagoya University, Nagoya, Japan
[104] [(a)] INFN Sezione di Napoli; [(b)] Dipartimento di Fisica, Università di Napoli, Napoli, Italy
[105] Department of Physics and Astronomy, University of New Mexico, Albuquerque NM, United States of America
[106] Institute for Mathematics, Astrophysics and Particle Physics, Radboud University Nijmegen/Nikhef, Nijmegen, Netherlands
[107] Nikhef National Institute for Subatomic Physics and University of Amsterdam, Amsterdam,

Netherlands
[108] Department of Physics, Northern Illinois University, DeKalb IL, United States of America
[109] Budker Institute of Nuclear Physics, SB RAS, Novosibirsk, Russia
[110] Department of Physics, New York University, New York NY, United States of America
[111] Ohio State University, Columbus OH, United States of America
[112] Faculty of Science, Okayama University, Okayama, Japan
[113] Homer L. Dodge Department of Physics and Astronomy, University of Oklahoma, Norman OK, United States of America
[114] Department of Physics, Oklahoma State University, Stillwater OK, United States of America
[115] Palacký University, RCPTM, Olomouc, Czech Republic
[116] Center for High Energy Physics, University of Oregon, Eugene OR, United States of America
[117] LAL, Univ. Paris-Sud, CNRS/IN2P3, Université Paris-Saclay, Orsay, France
[118] Graduate School of Science, Osaka University, Osaka, Japan
[119] Department of Physics, University of Oslo, Oslo, Norway
[120] Department of Physics, Oxford University, Oxford, United Kingdom
[121] [(a)] INFN Sezione di Pavia; [(b)] Dipartimento di Fisica, Università di Pavia, Pavia, Italy
[122] Department of Physics, University of Pennsylvania, Philadelphia PA, United States of America
[123] National Research Centre "Kurchatov Institute" B.P.Konstantinov Petersburg Nuclear Physics Institute, St. Petersburg, Russia
[124] [(a)] INFN Sezione di Pisa; [(b)] Dipartimento di Fisica E. Fermi, Università di Pisa, Pisa, Italy
[125] Department of Physics and Astronomy, University of Pittsburgh, Pittsburgh PA, United States of America
[126] [(a)] Laboratório de Instrumentação e Física Experimental de Partículas - LIP, Lisboa; [(b)] Faculdade de Ciências, Universidade de Lisboa, Lisboa; [(c)] Department of Physics, University of Coimbra, Coimbra; [(d)] Centro de Física Nuclear da Universidade de Lisboa, Lisboa; [(e)] Departamento de Fisica, Universidade do Minho, Braga; [(f)] Departamento de Fisica Teorica y del Cosmos and CAFPE, Universidad de Granada, Granada (Spain); [(g)] Dep Fisica and CEFITEC of Faculdade de Ciencias e Tecnologia, Universidade Nova de Lisboa, Caparica, Portugal
[127] Institute of Physics, Academy of Sciences of the Czech Republic, Praha, Czech Republic
[128] Czech Technical University in Prague, Praha, Czech Republic
[129] Faculty of Mathematics and Physics, Charles University in Prague, Praha, Czech Republic
[130] State Research Center Institute for High Energy Physics (Protvino), NRC KI, Russia
[131] Particle Physics Department, Rutherford Appleton Laboratory, Didcot, United Kingdom
[132] [(a)] INFN Sezione di Roma; [(b)] Dipartimento di Fisica, Sapienza Università di Roma, Roma, Italy
[133] [(a)] INFN Sezione di Roma Tor Vergata; [(b)] Dipartimento di Fisica, Università di Roma Tor Vergata, Roma, Italy
[134] [(a)] INFN Sezione di Roma Tre; [(b)] Dipartimento di Matematica e Fisica, Università Roma Tre, Roma, Italy
[135] [(a)] Faculté des Sciences Ain Chock, Réseau Universitaire de Physique des Hautes Energies - Université Hassan II, Casablanca; [(b)] Centre National de l'Energie des Sciences Techniques Nucleaires, Rabat; [(c)] Faculté des Sciences Semlalia, Université Cadi Ayyad, LPHEA-Marrakech; [(d)] Faculté des Sciences, Université Mohamed Premier and LPTPM, Oujda; [(e)] Faculté des sciences, Université Mohammed V, Rabat, Morocco
[136] DSM/IRFU (Institut de Recherches sur les Lois Fondamentales de l'Univers), CEA Saclay (Commissariat à l'Energie Atomique et aux Energies Alternatives), Gif-sur-Yvette, France
[137] Santa Cruz Institute for Particle Physics, University of California Santa Cruz, Santa Cruz CA, United States of America

[138] Department of Physics, University of Washington, Seattle WA, United States of America
[139] Department of Physics and Astronomy, University of Sheffield, Sheffield, United Kingdom
[140] Department of Physics, Shinshu University, Nagano, Japan
[141] Fachbereich Physik, Universität Siegen, Siegen, Germany
[142] Department of Physics, Simon Fraser University, Burnaby BC, Canada
[143] SLAC National Accelerator Laboratory, Stanford CA, United States of America
[144] [(a)] Faculty of Mathematics, Physics & Informatics, Comenius University, Bratislava; [(b)] Department of Subnuclear Physics, Institute of Experimental Physics of the Slovak Academy of Sciences, Kosice, Slovak Republic
[145] [(a)] Department of Physics, University of Cape Town, Cape Town; [(b)] Department of Physics, University of Johannesburg, Johannesburg; [(c)] School of Physics, University of the Witwatersrand, Johannesburg, South Africa
[146] [(a)] Department of Physics, Stockholm University; [(b)] The Oskar Klein Centre, Stockholm, Sweden
[147] Physics Department, Royal Institute of Technology, Stockholm, Sweden
[148] Departments of Physics & Astronomy and Chemistry, Stony Brook University, Stony Brook NY, United States of America
[149] Department of Physics and Astronomy, University of Sussex, Brighton, United Kingdom
[150] School of Physics, University of Sydney, Sydney, Australia
[151] Institute of Physics, Academia Sinica, Taipei, Taiwan
[152] Department of Physics, Technion: Israel Institute of Technology, Haifa, Israel
[153] Raymond and Beverly Sackler School of Physics and Astronomy, Tel Aviv University, Tel Aviv, Israel
[154] Department of Physics, Aristotle University of Thessaloniki, Thessaloniki, Greece
[155] International Center for Elementary Particle Physics and Department of Physics, The University of Tokyo, Tokyo, Japan
[156] Graduate School of Science and Technology, Tokyo Metropolitan University, Tokyo, Japan
[157] Department of Physics, Tokyo Institute of Technology, Tokyo, Japan
[158] Department of Physics, University of Toronto, Toronto ON, Canada
[159] [(a)] TRIUMF, Vancouver BC; [(b)] Department of Physics and Astronomy, York University, Toronto ON, Canada
[160] Faculty of Pure and Applied Sciences, and Center for Integrated Research in Fundamental Science and Engineering, University of Tsukuba, Tsukuba, Japan
[161] Department of Physics and Astronomy, Tufts University, Medford MA, United States of America
[162] Department of Physics and Astronomy, University of California Irvine, Irvine CA, United States of America
[163] [(a)] INFN Gruppo Collegato di Udine, Sezione di Trieste, Udine; [(b)] ICTP, Trieste; [(c)] Dipartimento di Chimica, Fisica e Ambiente, Università di Udine, Udine, Italy
[164] Department of Physics and Astronomy, University of Uppsala, Uppsala, Sweden
[165] Department of Physics, University of Illinois, Urbana IL, United States of America
[166] Instituto de Fisica Corpuscular (IFIC) and Departamento de Fisica Atomica, Molecular y Nuclear and Departamento de Ingeniería Electrónica and Instituto de Microelectrónica de Barcelona (IMB-CNM), University of Valencia and CSIC, Valencia, Spain
[167] Department of Physics, University of British Columbia, Vancouver BC, Canada
[168] Department of Physics and Astronomy, University of Victoria, Victoria BC, Canada
[169] Department of Physics, University of Warwick, Coventry, United Kingdom
[170] Waseda University, Tokyo, Japan
[171] Department of Particle Physics, The Weizmann Institute of Science, Rehovot, Israel

[172] Department of Physics, University of Wisconsin, Madison WI, United States of America
[173] Fakultät für Physik und Astronomie, Julius-Maximilians-Universität, Würzburg, Germany
[174] Fakultät für Mathematik und Naturwissenschaften, Fachgruppe Physik, Bergische Universität Wuppertal, Wuppertal, Germany
[175] Department of Physics, Yale University, New Haven CT, United States of America
[176] Yerevan Physics Institute, Yerevan, Armenia
[177] Centre de Calcul de l'Institut National de Physique Nucléaire et de Physique des Particules (IN2P3), Villeurbanne, France
[a] Also at Department of Physics, King's College London, London, United Kingdom
[b] Also at Institute of Physics, Azerbaijan Academy of Sciences, Baku, Azerbaijan
[c] Also at Novosibirsk State University, Novosibirsk, Russia
[d] Also at TRIUMF, Vancouver BC, Canada
[e] Also at Department of Physics & Astronomy, University of Louisville, Louisville, KY, United States of America
[f] Also at Department of Physics, California State University, Fresno CA, United States of America
[g] Also at Department of Physics, University of Fribourg, Fribourg, Switzerland
[h] Also at Departament de Fisica de la Universitat Autonoma de Barcelona, Barcelona, Spain
[i] Also at Departamento de Fisica e Astronomia, Faculdade de Ciencias, Universidade do Porto, Portugal
[j] Also at Tomsk State University, Tomsk, Russia
[k] Also at Universita di Napoli Parthenope, Napoli, Italy
[l] Also at Institute of Particle Physics (IPP), Canada
[m] Also at National Institute of Physics and Nuclear Engineering, Bucharest, Romania
[n] Also at Department of Physics, St. Petersburg State Polytechnical University, St. Petersburg, Russia
[o] Also at Department of Physics, The University of Michigan, Ann Arbor MI, United States of America
[p] Also at Centre for High Performance Computing, CSIR Campus, Rosebank, Cape Town, South Africa
[q] Also at Louisiana Tech University, Ruston LA, United States of America
[r] Also at Institucio Catalana de Recerca i Estudis Avancats, ICREA, Barcelona, Spain
[s] Also at Graduate School of Science, Osaka University, Osaka, Japan
[t] Also at Department of Physics, National Tsing Hua University, Taiwan
[u] Also at Institute for Mathematics, Astrophysics and Particle Physics, Radboud University Nijmegen/Nikhef, Nijmegen, Netherlands
[v] Also at Department of Physics, The University of Texas at Austin, Austin TX, United States of America
[w] Also at Institute of Theoretical Physics, Ilia State University, Tbilisi, Georgia
[x] Also at CERN, Geneva, Switzerland
[y] Also at Georgian Technical University (GTU),Tbilisi, Georgia
[z] Also at Ochadai Academic Production, Ochanomizu University, Tokyo, Japan
[aa] Also at Manhattan College, New York NY, United States of America
[ab] Also at Hellenic Open University, Patras, Greece
[ac] Also at Academia Sinica Grid Computing, Institute of Physics, Academia Sinica, Taipei, Taiwan
[ad] Also at School of Physics, Shandong University, Shandong, China
[ae] Also at Moscow Institute of Physics and Technology State University, Dolgoprudny, Russia
[af] Also at Section de Physique, Université de Genève, Geneva, Switzerland
[ag] Also at Eotvos Lorand University, Budapest, Hungary
[ah] Also at International School for Advanced Studies (SISSA), Trieste, Italy
[ai] Also at Department of Physics and Astronomy, University of South Carolina, Columbia SC, United States of America
[aj] Also at School of Physics and Engineering, Sun Yat-sen University, Guangzhou, China

[ak] Also at Institute for Nuclear Research and Nuclear Energy (INRNE) of the Bulgarian Academy of Sciences, Sofia, Bulgaria
[al] Also at Faculty of Physics, M.V.Lomonosov Moscow State University, Moscow, Russia
[am] Also at Institute of Physics, Academia Sinica, Taipei, Taiwan
[an] Also at National Research Nuclear University MEPhI, Moscow, Russia
[ao] Also at Department of Physics, Stanford University, Stanford CA, United States of America
[ap] Also at Institute for Particle and Nuclear Physics, Wigner Research Centre for Physics, Budapest, Hungary
[aq] Also at Flensburg University of Applied Sciences, Flensburg, Germany
[ar] Also at University of Malaya, Department of Physics, Kuala Lumpur, Malaysia
[as] Also at CPPM, Aix-Marseille Université and CNRS/IN2P3, Marseille, France
[*] Deceased